Master Thesis, Department of Geosciences

Tomographic inversion of Pn waves beneath southern Scandinavia

A study to reveal the upper mantle velocity structure to explain anomalous topography of Scandinavian Mountains

Adnan Latif

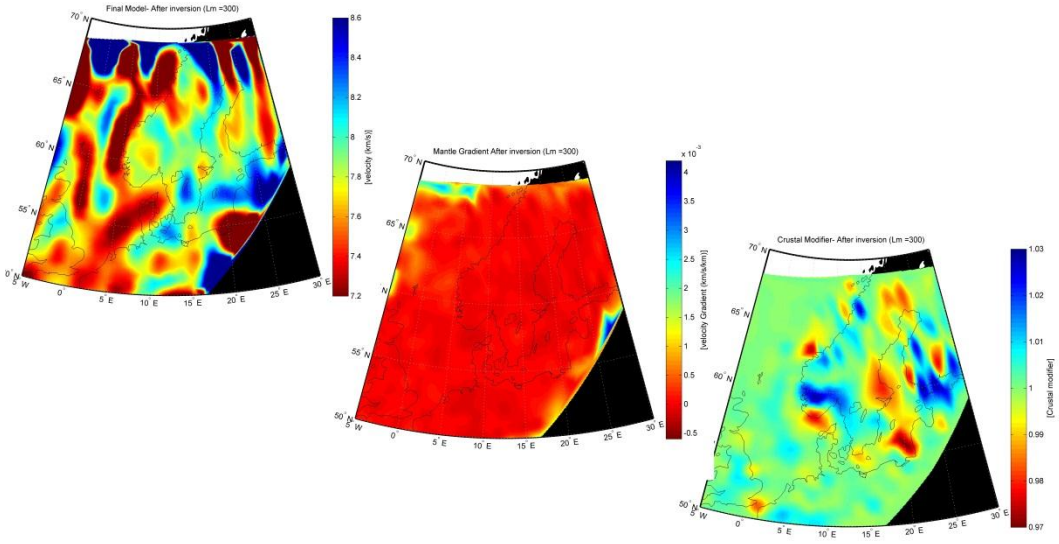

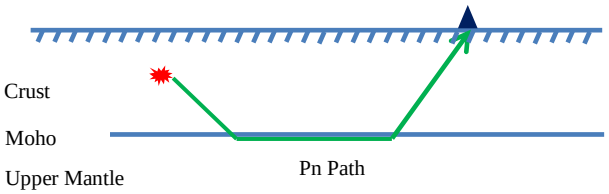

UNIVERSITY OF OSLO

FACULTY OF MATHEMATICS AND NATURAL SCIENCES

Tomographic inversion of Pn waves beneath southern Scandinavia

A study to reveal the upper mantle velocity structure to explain anomalous topography of Scandinavian Mountains

Adnan Latif

Master Thesis in Geosciences

Discipline: Geophysics

Department of Geosciences

Faculty of Mathematics and Natural Sciences

University of Oslo

October, 2012

Tutor(s): Prof. Valerie Maupin (University of Oslo)

This work is published digitally through DUO – Digitale Utgivelser ved UiO

http://www.duo.uio.no

It is also catalogued in BIBSYS (http://www.bibsys.no/english)

ACKNOWLEDGMENTS

First of all I am very thankful to my supervisor Prof. Valerie Maupin at the department of Geoscience, UiO who proposed this thesis. This work was impossible without her support and guidance. I am very thankful for her positive critics and valuable suggestions.

I am also thankful to International Seismological Center (ISC) for providing me the dataset used in this study, especially to Ben Dando (Seismologist /Developer at ISC) for his assistance for data retrieval from ISC bulletins and clarifying quarries about the data content.

I am thankful to Sandia National Laboratories and National Nuclear Security Administration USA for providing me RSTT earth package software. I am thankful to Myers, Stephen C for explaining this software along with discussion on the tomography methodology used in this study.

I want to express my gratitude to all teachers, class fellows and administration staff of Department of Geoscience UiO who always helped me when I ever I turned around them.

In last but not least I am very thankful to Department of Geoscience, University of Oslo for giving me chance to study in this world's leading institute.

ABSTRACT

Scandinavian Mountain Range is located at the continental margin of the Eurasian plate. This area is part of the Baltic shield so topography is expected to be generally low. But this is not the case here. In South western corner of the Baltic shield (Southern Norway) topography is rough and ranges up to 1500 m above sea level forming a NE-SW mountain range. Absence of active tectonics in this area and results from various geophysical studies show that the cause of this topography is merely not a pure crustal phenomenon. There could be some mantle process that caused and sustained this topography.

The objective of this study is to analyze the upper mantle composition and heterogeneities by using the concept of Pn tomography (by imaging P wave velocities in the upper mantle). This could be helpful to explain anomalous topography in terms of velocity anomalies in mantle, if any in this region. The tomographic formulation of Myers et al. (2010) and preconditioned conjugate inversion is employed to invert travel times for model parameters. In addition to the mantle velocity perturbations this tomographic formulation also allows to image mantle vertical velocity gradient and crustal modification in the subsurface.

Results of mantle velocity imaging indicates a general trend of low velocity in the thinner and younger part of Baltic shield (Norway and offshore) whereas high velocity in the thicker and older parts (Sweden and Baltic). Further, as expected, low velocities are observed in the younger part of central Europe. North Sea is observed to have high velocity surrounded by low velocities of southern Scandinavia and central Europe. Velocity structure beneath southern and central Norway is anomalous (having low velocity) with respect to the rest of Baltic shield. These low velocities are probably the connected to Iceland plume in the west by a narrow channel where low velocities are related to hot and shallow mantle beneath the plume. These results are in good agreement with previous studies (Bannister et al. 1991; Bondo et al. 2009; Husebye et al. 1986).

Another important observation is the crustal modifier after inversion. In southern Norway crustal modifier suggests that either the crust in this area has low velocity compared to the rest or that a low velocity anomaly in the mantle is leaked into the crustal part during inversion.

Contents

Chapter 1: Introduction

1.1 Purpose of study

The Scandinavian Mountain Range is located at the continental margin of the Eurasian plate. This area is part of the Baltic shield so topography is expected to be generally low. But this is not the case here. Topographic map of this area is shown in Fig 1.1. It can be seen that in the south western corner of the Baltic shield (Southern Norway), topography is rough and ranges up to 1500 m above sea level forming a NE-SW mountain range (Scandinavian mountains). East west extension of these mountains ranges from 200km (in the northern part) to 400km (in southern part).

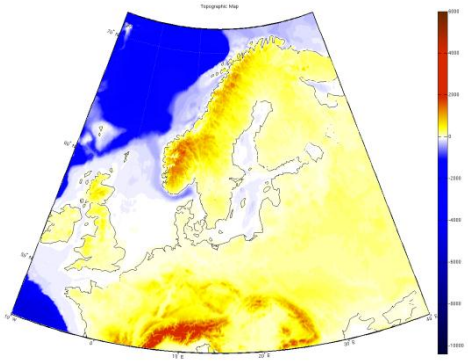

Fig 1.1: Topographic map of study area and surrounding

This type of topography is usually expected to be present in tectonically active regions e.g. at the plate boundaries. Absence of active tectonics in this area and results from various geophysical studies show that the cause of this topography is merely not a crustal phase. There could be some mantle process that caused and sustained this topography.

The objective of this study is to analyze the upper mantle composition and heterogeneities by using the concept of Pn tomography (by imaging P wave velocities in the upper mantle). This could be helpful to explain anomalous topography in terms of velocity anomalies in mantle, if any in this region.

Main goals of the study:

- To understand the structural evolution of the study area by tomographic analysis of Pn data, by mapping P wave velocities in the upper mantle

- To find the location and sharpness of boundary between the normal shield-like structure (southern Sweden) and the platform-like structure (southern Norway) and how this structure extends westwards (North Sea).

1.2 Tectonic Context of Scandinavian Mountains

The tectonic Story of northern Europe begins from Achaean, when Baltic shield was created by accretion of various orogeneses (between 3.1 Ga to 1.5 Ga). This area includes today's Norway, Sweden, Finland, Kola Peninsula and Karelia in USSR (Husebye *et al.* 1986) (Fig 1.2).

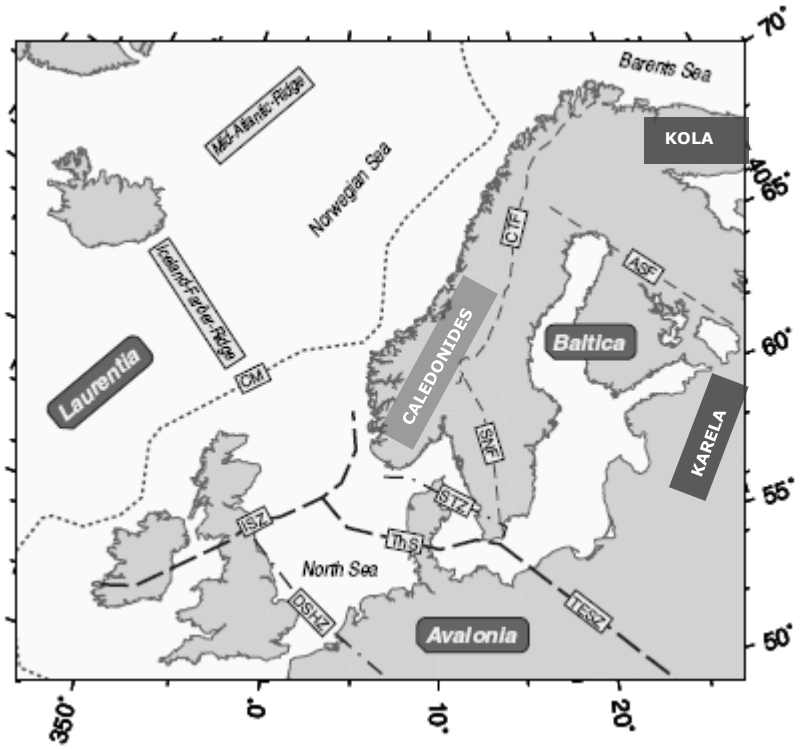

Fig 1.2: Schematic tectonic overview. Thick black dashed lines indicate identified suture zones of Avalonia, namely Iapetus suture (ISZ) to Laurentia and the Trans-European-Suture-Zone (TESZ) and Thor Suture (ThS) to Baltica. Alternative boundaries (thinner dash–dot lines) include the Dowsing-South Hewett Fault Zone (DSHZ) and the Sorgenfrei-Tornquist Zone (STZ). The grey dotted line marks today's continental margin (CM, following 500m bathymetry) and grey dashed lines internal deformation fronts within the Baltica plate related to Archean-Svecofennian (ASF) (2 Ga), Svecofennian–Sveconorwegian (SNF) (1 Ga) and Caledonian (CTF) (450–500 Ma) orogenies.(Edited from Fig 1 in Weidle & Maupin 2008)

The age of the curst generally decreases from East to West. The oldest crust stems in the northeast (Kola Peninsula and northeastern Finland).This part of the crust was created 2+ Ga ago.

Moving towards West, Svecofennides (Western Finland & eastern and southern Sweden) was formed some 1.9 Ga ago. Moving further West, Sveconorwegian sequence (Norway & western Sweden) that forms the southwestern corner of the Baltic shield was created about 1.2 to 1.5 Ga ago. This area was reworked again by metamorphism in 0.9 to 1.2 Ga period (Husebye et al. 1986).

Afterwards there were many tectonic events comprising of complex series of compressions and extensions that shaped this area to the present day configuration. Starting from Ordovician-Silurian (443 Ma) collision between Baltica and Avalonia and soon after (430-410 Ma) collision of western side of Baltica with Laurentia. This collision resulted in the closure of a proto-Atlantic ocean. This continent-continent collision is believed to be the source that gave rise to the formation of Scandinavian Caledonides. Structurally the Scandies are formed with allochthonous units overthrusting Precambrian Baltica crust from West to East (Bondo et al., 2009)

Following this compression period, an important and relatively younger rifting (followed by magmatism and subsidence) event occurred in Carboniferious-Permo-Triasic (305-245 Ma). This event resulted in the formation of Oslo Graben and caused significant thinning of the crust in Oslo region (Svenningsen *et al.* 2007). These events resulted in the formation of two East-West basins i.e. Norwegian-Danish Basin & North German basin (Frederiksen *et al.* 2001).

Afterwards this region has gone through various rifting, extension and uplifting phases e.g. rifting in Jurassic-Triassic and extension that resulted in continental breakup in early Eocene. (Smelror *et al.*, 2007)

A major topographical feature on the Baltic shield is the NE-SW trending Scandinavian Mountains that are located at its western coast (Northern & Southern Norway) (Fig 1.2). These mountains are believed to have Caledonian origin but the extension afterwards (Paleozoic) collapsed this high topography.

Exact origin of this present day topography (Scandinavian mountains) is still unknown. There are two significant hypotheses that have been debated by various authors to explain this anomaly. First hypothesis (Nilsen *et al.* 2009) assumes that the present day topography is the remnant of Caledonian formation and its erosion rate is strongly affected by the climate. Flat regions at high elevations could have been formed by glacial and preglacial processes in equal rates. According to this hypothesis today's topography can be explained by the isocratic response of ex- thick crust and excludes the involvement of tectonic forces that could be responsible of this uplift.

Second hypothesis (Smelror *et al.* 2007) involves tectonic forces to be responsible for this high topography. It believes that the past topography was eroded in Mesozoic followed by tectonic uplift in Neogene and Paleogene then again erosion and uplift due to isostatic response. There are various theories about this uplift mechanism; some of them are explained in next section.

1.3 Previous Geophysical studies in this area

High topography in tectonically inactive area could be thought of an effect of post glacial rebound. But the anomalous uplift rate of 8 mm/yr in the southern Norway cannot be explained only by deglaciation. There must be some tectonic component involved as well that caused and sustained this topography (Fjeldskaar et al., 2000).

Some other geophysical and isostatical studies e.g. Fjeldskaar (1997), Poudjom Djomani *et al.* (1999), Rohrmann *et al.* (1996), Perez-Gussinye *et al.* 2004 , Ebbing & Olsen (2005), shows that in the southern part of the Scandinavian mountains (Southern Norway) this topography is only partially compensated by the flexural rigidity.

Absence of full isostatic compensation form crustal root and absence of active tectonics in this area gave space for the assumption of the presence of some mantle process involved in this uplift. There are many geophysical studies that have been conducted in this region to analyze the upper mantle and results from most of these studies favor this hypothesis. Brief description of some of these studies is as follows:

A tomographic mapping of lithosphere-asthenosphere in this area (Husebye et al. (1986)) was conducted on the observations mainly located in Sweden along with some limited stations in Denmark and Norway. This study reveals that the upper mantle velocity in southern Norway, Oslo Graben and in basin area is low as compared to velocities in the thicker and older part of Baltic shield (southern Sweden) (shown in fig 1.3). Velocity structure in the southern Norway has good resemblance with the velocities found in the Denmark area but the topography of Denmark is entirely different from this region. As this study was conducted on sparse station coverage so resolution issues suggest the need of a new detailed study of upper mantle velocity variations in this area.

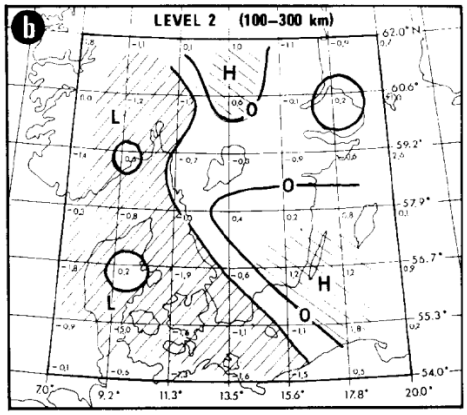

Fig 1.3: Seismic image of 100-300 km, comprising lower lithosphere and/or upper mantle. L: low velocity region & H: high velocity region. (Fig 5.b in Husebye *et al.* 1986)

A Pn & Sn tomography study by Bannister *et al.* 1991 was conducted in this region by using arrivals of uppermost mantle P and S waves that were recorded on permanent seismological stations. This study shows that the upper mantle beneath southern Norway has low velocity and low density (Fig 1.4a & 1.4b). Geologically these low velocity anomaly can be associated with the geodynamic process involved in the opening of the Norwegian-Greenland sea (Bannister et al., 1991).

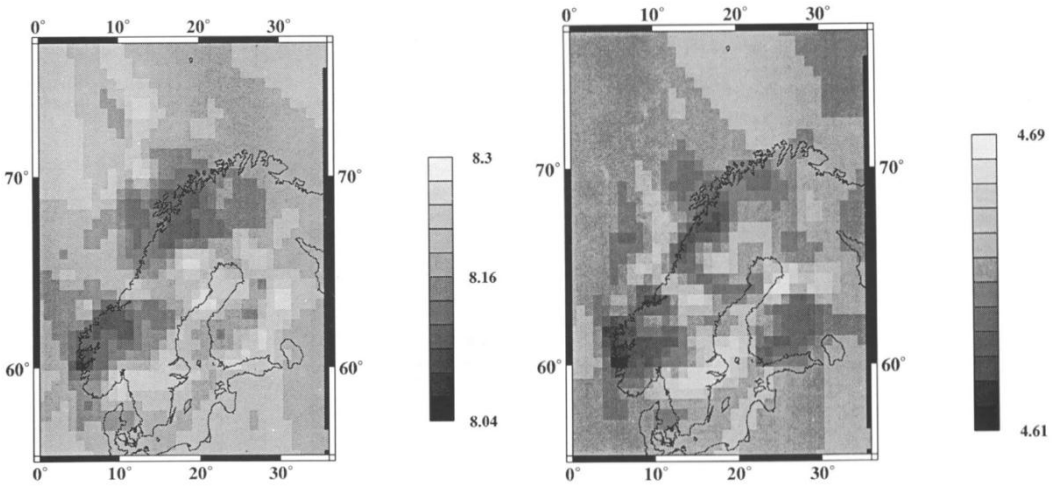

(a) (b)

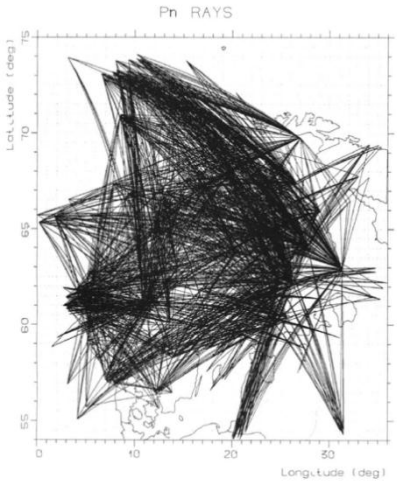

(c)

Fig 1.4: (a) Estimated Pn wave velocities (b) Estimated Sn wave velocities (c) Ray paths (Fig 4, 7 & 8 in Bannister *et al.* 1991)

A relative P wave residual study by Bondo *et al.* (2009) was conducted on 48 temporary and 15 permanent seismological stations; it also shows that arrivals are generally late in southern Norway (Red dots in Fig 1.5) and early in the East (Blue dots in Fig 1.5).

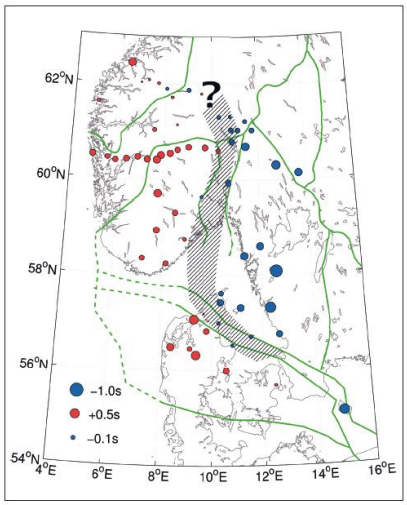

Fig 1.5: Interpreted lithospheric transition zone (hatched), with mean P-residuals after topographic and crustal corrections. Blue and red colors represent early and late arrivals respectively (Fig 7 in Bondo *et al.* 2009)

A surface wave study was conducted in this region by Weidle & Maupin, (2008) to map S-wave velocities. Results from this study indicate that a low velocity anomaly is present in southern Norway area, with the depth range of 70-150 km. Furthermore this velocity anomaly forms a 400km wide channel and seems to extent towards the Iceland plume, beneath the North Atlantic (Fig 1.6a & 1.6b)

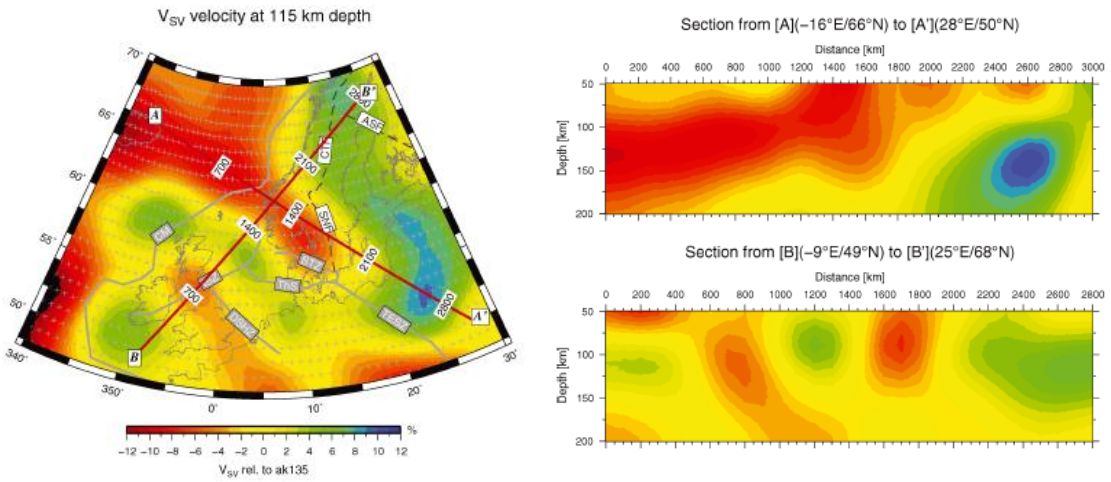

(a) (b)

Fig 1.6: (a) VSV model based on EUCAK at 115 km depth. (b) Cross-sections A-A' & B-B' (Fig 15 in Weidle & Maupin. 2008)

Another similar study by Maupin, (2011) was conducted in this region to map SV-Wave velocity by inverting average phase velocity of the Rayleigh wave fundamental mode.

Results of this study were similar to the results of Weidle & Maupin, (2008), showing a low velocity zone in upper mantle.

A study of teleseismic receiver functions by Svenningsen *et al.* (2007) gives somewhat different results. It shows that in the West of the Oslo rift, Moho depth correlates well with the topography and Bouguer gravity values. Topography in the eastern side of Oslo rift is compensated by ca. 10-12 km of thick Airy-type crustal root (Fig 1.7a & 1.7b). This crustal root is enough for the isostaic compensation. This result contradicts the hypothesis of the presence of buoyancy effects below Moho.

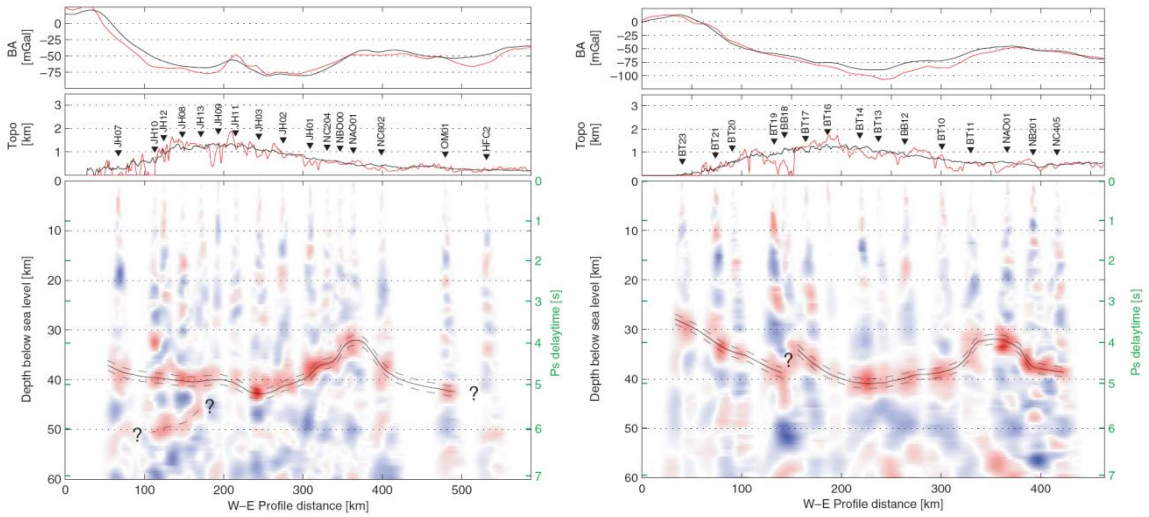

(a) (b)

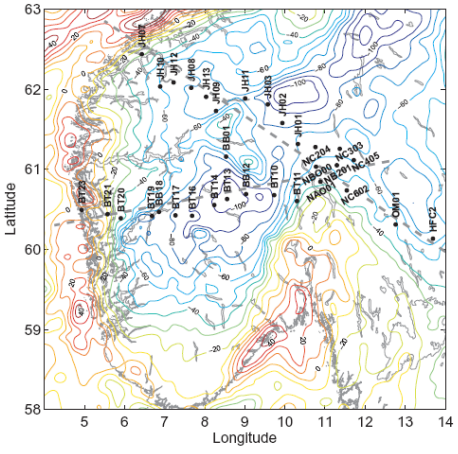

(c)

Fig 1.7: (a) & (b) The depth-migrated receiver functions estimates for the northern (Jotunheimen) and southern (Hardangervidda) profile projected onto a vertical cross-section through the northern profile line. The interpreted Moho is outlined as full black curve. Two

dashed grey curves 1 km above and below the interpreted Moho, respectively, represent the likely uncertainty due to the partly coupled uncertainty in VP and σ used in the migration model on the right-hand side, in green, is shown an equivalent receiver function timescale (Ps delay-time) for a reference slowness of 6.4 s /deg. Above the cross-section are shown variations of topography and the Bouguer gravity anomaly (BA) along the profile. Red curves illustrate variations exactly along the profile line and black curves variations of mean values for an interval of +80 km perpendicular to profile line.(c) location of these two profiles superimposed on bouguer gravity map (Fig 5, 6 &7 in Svenningsen *et al.* 2007)

Refraction studies by Statford *et al.* (2009) gave results somewhat in-between these two hypotheses. This study shows that the Moho is about 38-40 km deep beneath the southern Scandies (as shown in the Fig 1.8b). Moho beneath the highest topography is slightly deep as compared to the other parts of southern Norway, and contributes to the isostaic compensation but this compensation is not sufficient. Other buoyancy forces like anomalous lower crust or upper mantle must be added to keep this system in isostaic equilibrium.

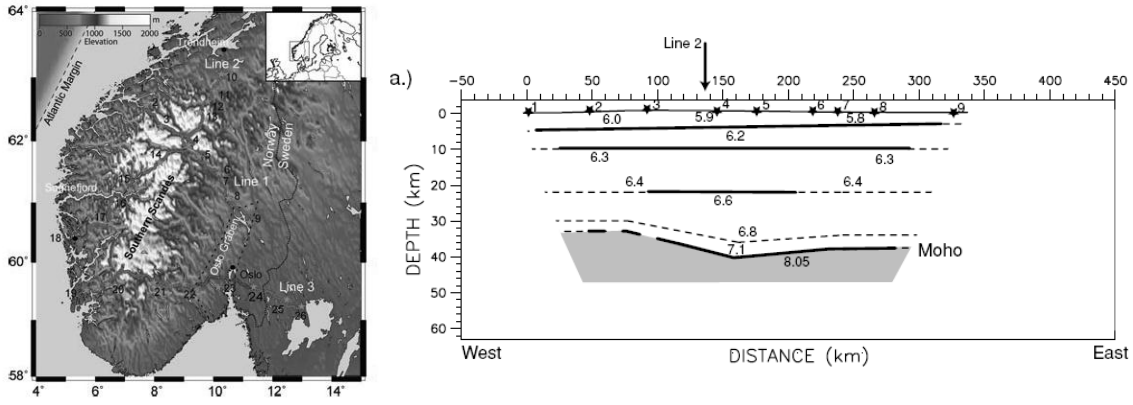

(a) (b)

Fig 1.8: (a) location of refraction profiles. (b) Forward modeling ray tracing solution for line 2 (Northwest–Southeast blue line in (a)). Solid lines- where constraint is available from refractions, Thick dashed lines- where constraint is from PmP reflections only & Thin dashed lines- velocity layers boundaries. (Fig 1 & 4a in Statford *et al.* 2009)

If the presence of a low velocity-low density in the upper mantle, the next question is to find geodynamic processes that can be responsible for the presence of this anomalous mantle. There are various theories that have been extensively debated to explain this phenomena e.g. presence of a low density material in upper mantle (Ebbing & Olsen, 2005), mantle convection along the boundary between a warm oceanic asthenosphere and a colder continental asthenosphere (Bannister *et al.* 1991) and connection of this anomaly to the

Iceland plume in North Atlantic (Weidle & Maupin 2008). But the exact origin of this anomalous mantle is still unknown.

1.4 Outline of this thesis

The main objective of this study is to image P-wave velocity in the upper mantle beneath the southern Scandies. This study could be helpful to analyze the mantle composition and to explain this anomalous topography in terms of mantle velocity anomalies, if any in this region.

This study is different from previous Pn studies conducted for this region with respect to data coverage and methodology. The previous studies were conducted on very sparse data whereas our dataset consists of ~ 100,000 Pn rays.

The majority of the previous tomographic studies were conducted by assuming that the Pn wave is a simple head wave propagating just below Moho. For far-regional distance (>700km), Pn waves dive appreciably into the mantle due to the velocity gradient with depth and Earth sphericity (Myers *et al.* 2010). We used the method described in Myers *et al.* 2011 for this tomographic study. In this method inversion tries to find a best fit model with the observed data by adjusting model parameters for mantle slowness, vertical velocity gradient below Moho and a scalar adjustment to the crustal structure at each node. After inversion 1D model at each node is interpolated to make a 3D velocity model.

1.4.1 Dataset:

Data for this study comprises Pn travel times recorded on various permanent and temporary networks located in Southern Norway, Sweden, Finland, UK, Denmark, Netherlands and Germany. This data is retrieved from International Seismological Center (ISC) bulletin.

1.4.2 Data Processing:

Before inversion, this travel time data is subject to various pre-processing to enhance S/N ratio and remove various discrepancies. This pre-processing includes sorting of phases, identification & removal of outliers, filtering for residual, magnitude & epicenteral limits

and formation of summary rays. A MATLAB script is developed for this for all pre-processing as well as for inversion algorithm.

1.7 Deliverables:

Main deliverables from this study are maps of upper mantle P-wave velocity and velocity gradient below Moho. A MATLAB script has also been developed to be used as a tool for any future tomographic study. Possibly it can also be transformed into software by making a user interface.

CHAPTER 2: THEORETICAL BACKGROUND OF TOMOGRAPHY

2.1 Introduction

The word tomography has a Greek origin and comprises of two words ‘tomos’ and ‘graphy’. ‘’Tomos’’ means section and ‘’graphy’’ refers to drawing. This technique is not limited to seismology. Many other applications exist in material and medicine sciences. The basic idea in all of its applications is to reveal the internal structure of object by imaging the cross section (Padina *et al*. 2006). This principle can be used to image from micro structures (e.g. biological cells) to the very-large scale objects like subsurface of Earth (known as seismic tomography).

2.1.1 Travel time tomography

Travel time tomography is a subclass of seismic tomography. It used to explore the subsurface by analyzing the travel times of waves going down into the subsurface (from natural and artificial sources) and reflecting/refracting back to earth surface. In case of seismic travel time tomography, the source of the seismic wave could be an artificial source like a large explosion / vibration or a natural release of energy from earthquakes. Natural source has the advantage that the released energy is usually very huge so it goes deeper down into subsurface, enabling us to have a large depth of investigation. It is used to image deep structures like lower crust, upper mantle, lower mantle, and even the inner core.

The depth of the source also depends on the type of sources. For artificial sources, source depth ranges from 0 to several meters down whereas in case of natural sources, source depth ranges up to several kilometers from the surface. Receivers of these waves are usually planted on the surface (Geophone, hydrophone, seismometer) or at small depth (borehole Geophones).

Return of seismic energy back to the surface could be either reflection/refraction from the boundaries (having strong impedance contrast) or could be by the continued refraction from layers of increasing impedances.

Travel times of waves (downward and upward) depend on the thickness and velocities of layers encountered in the ray path. Tomographic inversion tries to reveal this information by inverting these travel times.

2.1.2 Forward modeling vs. Inversion

Forward modeling is the procedure of generating predicted data that would be observed if we performed that experiment in real world. It is helpful to setup an a-priori or starting model in inversion. It can also be used periodically in inversion to analyze the misfit of a model. Most important information in forward modeling is the accurate information about subsurface (Model Parameters).

A simple illustration of forward modeling is shown in the following flow chart

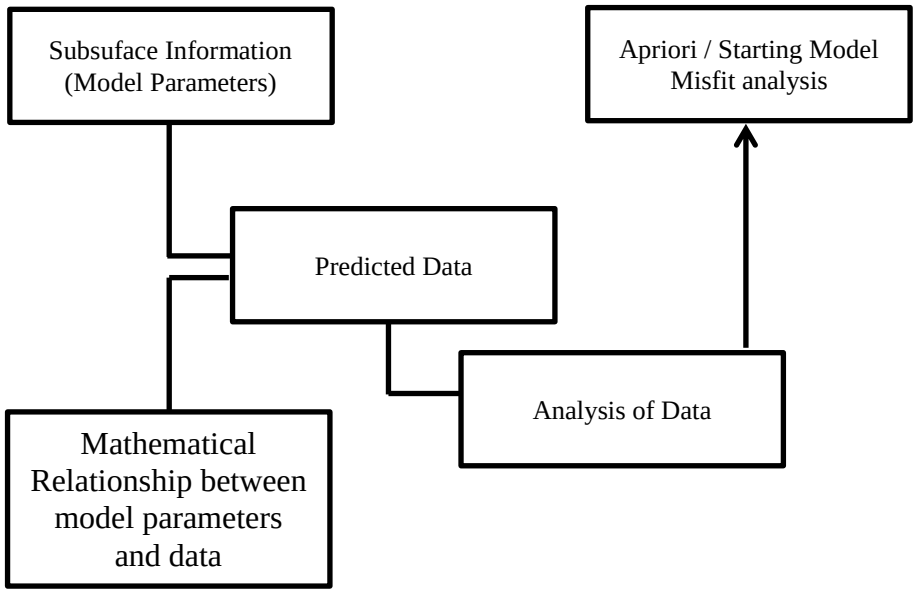

Inversion is opposite to the forward modeling. Here series of mathematical techniques are applied on the data (obtained from the physical experiment) to retrieve model parameters (Subsurface structure and its physical properties)

A simple illustration of Inverse modeling is shown in the following flow chart

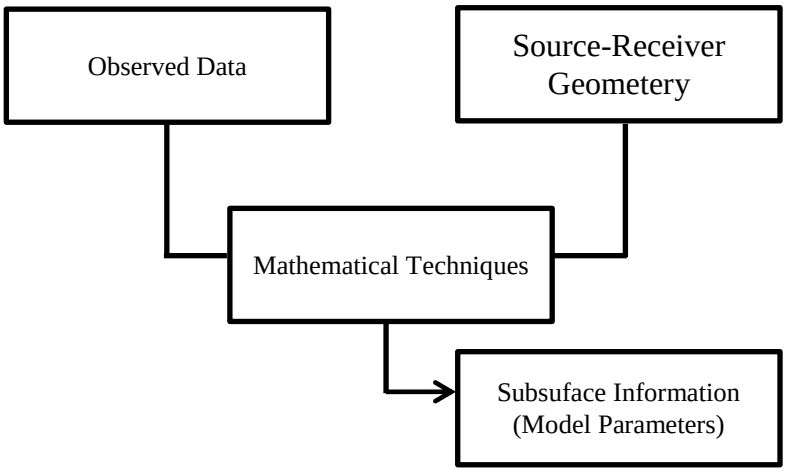

These two modeling techniques can be used in combination by updating each other e.g. model parameters obtained by the inversion can be used as a starting model for the forward modeling and vice versa.

2.2 Tomographic problem breakdown

Over all a tomography problem can be breakdown into a number of steps, starting by choosing a representation of the subsurface, setup of travel time equations and in last inversion of travel times for model parameters.

2.2.1 Choosing a representation of the subsurface

The simplest assumption about subsurface structure is to consider a layered structure, with constant velocity in a particular layer and flat interfaces. If this situation is true, forward modeling is very simple and easy. But this is not the case in the real world. Various studies show that although the subsurface is layers, but these layers are not flat. Further the velocity variations are not only in vertical direction. There are considerable lateral variations as well. So in conclusion, existence of rough interfaces and lateral variation in velocity makes the representation of the subsurface a major element in the inversion procedure

One way to cope with this problem is to divide the subsurface into small units (1D, 2D or 3D). In these small units physical properties are assumed to be constant

.

Fig 2.1 shows an example of 2 layers case (k & j could be thought of lower crust and upper mantle respectively) with velocity variation in vertical (sk & sj) and lateral (sk & sk+1) direction. Consider a refracted ray along this boundary (Pn wave). Actual ray path is along the boundary but for the sake of mathematical treatment we have to consider a horizontal ray path along the boundary (Moho in this case). Further there will be a lateral velocity contrast along this ray path. In conclusion a horizontal ray along Moho, with constant velocity, could not represent the actual ray path of a refracted ray along this boundary.

To deal with this problem, horizontal distance visited by this ray can be divided into small units, considering constant parameters in one unit. This will help to make a better approximation of rough variations in parameters and will also leads to the ease in mathematical calculations.

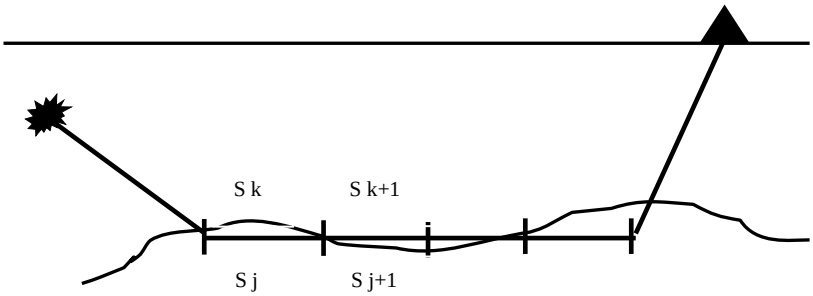

Fig 2.1 Subsurface divisions into small units with constant parameters

It can be seen in the above figure that there is still allot of approximation involved for the ray traveling from source to receiver via refracting interface. This averaging can be reduced by decreasing the cell size which will increase the resolution of the model. This high resolution will ultimately leads to the accuracy of whole system

2.2.2 Travel Time equations

Travel time data and information about ray paths can be jointly used to estimate velocities in each of these small units. Mathematically total travel time of refracted wave along this path can be written as

$$T_i = T_{i,Source} + T_{i,Receiver} + T_{i,Interface}$$

Where T_i is travel time of i[th] ray from source to the receiver, $T_{i,Source}$ is the time taken by i[th] ray from source to the refracting surface and $T_{i,Interface}$ is the travel time along the refracting surface and $T_{i,Receiver}$ is the travel time of i[th] ray from refracting boundary to the receiver. $T_{i,Interface}$ Can be further subdivided

$$T_{i,Interface} = d_{i,1}\, s_1 + d_{i,2}\, s_2 + d_{i,3}\, s_3 + \cdots + d_{i,m}\, s_m \qquad (2.1)$$

$d_{i,j}$ is the distance travel by the i[th] ray in j[th] unit and s_j is the slowness of j[th] unit ($\frac{1}{v_j}$)

In tomography more than one ray is used to image the velocities in these defined units so equation 2.1 can be written in the matrix form as

$$\begin{bmatrix} d_{1,1} & d_{1,2} \ldots & d_{1,m} \\ d_{2,1} & d_{2,2} \cdots & d_{2,m} \\ \vdots & \vdots & \vdots \\ d_{n,1} & d_{n,2} & d_{n,m} \end{bmatrix} \begin{bmatrix} s_1 \\ s_2 \\ \vdots \\ s_m \end{bmatrix} = \begin{bmatrix} t_{1,Interface} \\ t_{2,Interface} \\ \vdots \\ t_{n,Interface} \end{bmatrix} \quad (2.2)$$

Or

$$T_n = D_{n \times m} \times S_m \quad (2.3)$$

n = Number of rays, m = Number of small units along ray, D = $n \times m$ matrix containing distance terms for all cell visited by the rays, S= $m \times 1$ vector contains slowness of all the cells, T= $n \times 1$ vector containing observed travel times for the interface

2.2.3 Solution to the tomographic Problem

Final tomographic problem statement is defined in equation 2.3. To solve this equation, apparently we have two know parameters i.e. Observed Travel times (T) from the recorded data and Distance Matrix (D) (either from the ray tracing or previous tomography studies). In reality both of these parameters (T, the time terms and D, the distance terms) have associated with various types of errors and uncertainties

We have two sets of 3 variables (T, D & S terms). First set belongs to the real world

$$T_{real} = D_{real} \times S_{real} \qquad (2.4)$$

And second belongs to assumptions on the model we took in a priori/ ray tracing step

$$T_{model} = D_{model} \times S_{model} \quad (2.5)$$

This system has more unknowns than known variables so to solve this system it needs some assumptions. An important assumption is the equality of distance matrix D in real and modeled world i.e.

$$D_{real} = D_{model} = D$$

This system of equations can be solved in an iterative way. A simple flow chart for this process is shown below (Padina *et al.* 2006)

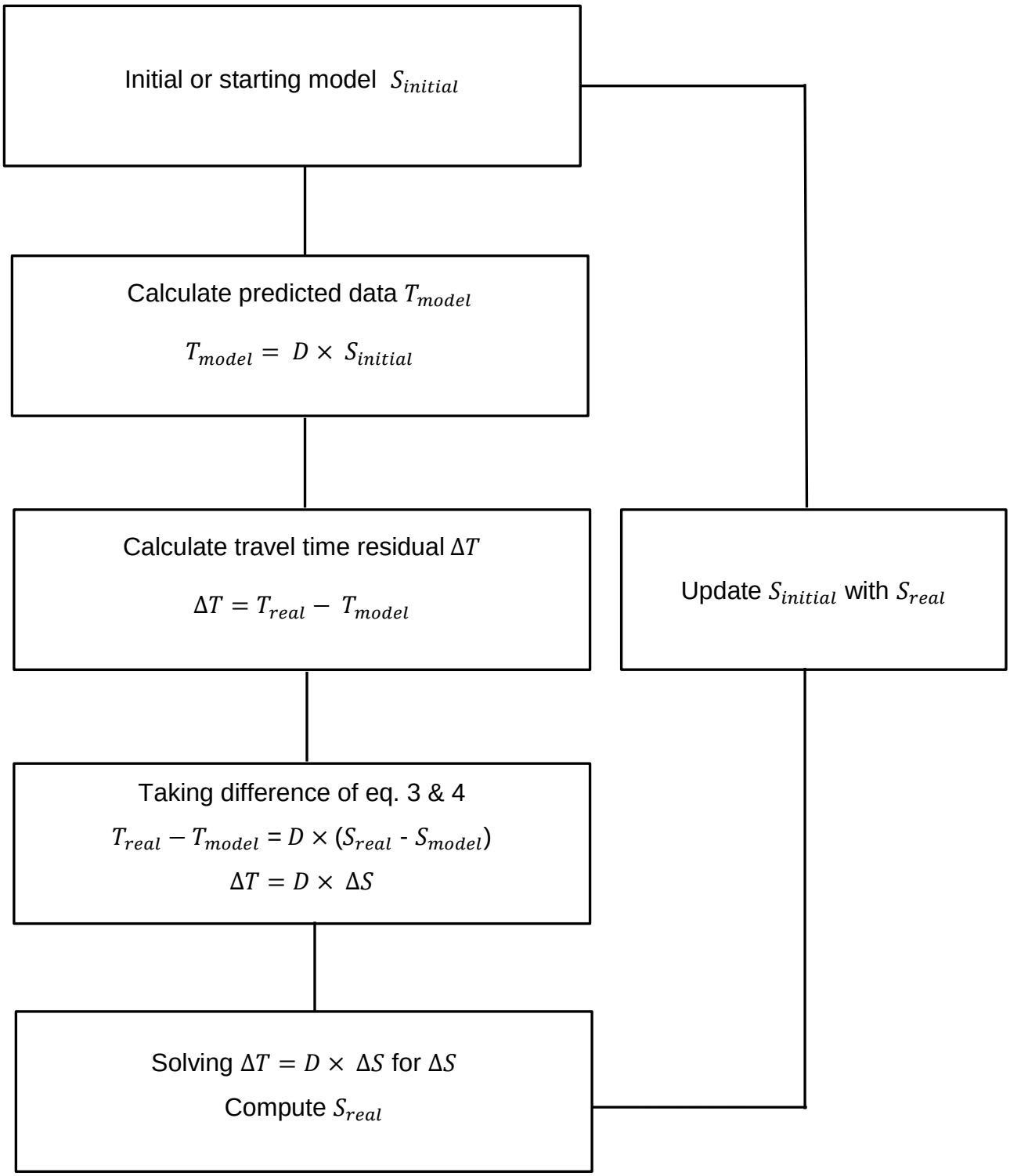

The most important and difficult step in tomography is the step 5 (marked by green box) i.e. solution to $\Delta T = D \times \Delta S$ for ΔS. This procedure is briefly explained in chapter 3 (c.f. Section 3.4)

CHAPTER 3: PN TOMOGRAPHIC INVERSION: METHODOLOGY (CONJUGATE INVERSION SCHEME)

3.1 Pn Phase

Seismic waves from earthquakes are recorded at geographically dispersed stations. These waves can be characterized either on the basis of the epicenteral distance or on the basis of reflecting/refracted surface.

Most of these waves travel through the crust and sub-crustal uppermost mantle. Thickness, composition and internal structure of the crust strongly vary due to folding and faulting which leads to strong heterogeneities in the physical properties of subsurface. These heterogeneities cause scattering of seismic waves so a primary wave is usually followed by signal generated noise (coda waves). Due to this scattering, small discontinuities (intra-crustal) are usually hidden in the recorded data (Lay & Wakkace 1995). Mohorovicic discontinuity (Moho) is a main large scale discontinuity with about 20% velocity contrast at the interface between crust and upper mantle. This contrast produces first or later waves onsets that can be recognizable above noise level. In seismological nomenclature these reflected and refracted waves from Moho are named as PmP/SmS and Pn/Sn phase respectively. Path of these waves are illustrated in Fig: 3.1

Pn/Sn phase is usually more identifiable at regional distances because at these distances, direct P/S waves are more attenuated and scattered due to their entire path in the crust whereas Pn/Sn wave dives down into the mantle so are less attenuated. Pn phase is also the first arrival in this distance range

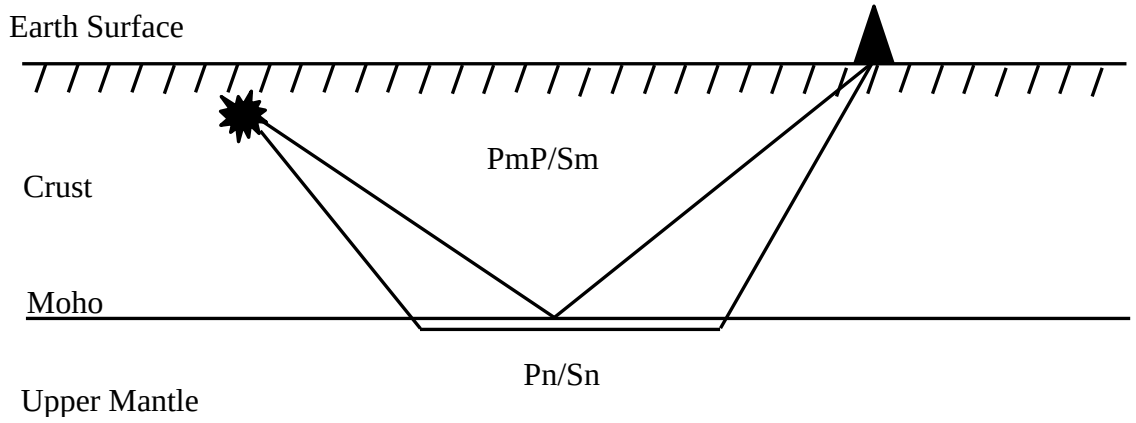

Figure 3. 1 Ray paths for reflected and refracted form Mohorovicic discontinuity

As explained earlier, Pn phase could be very useful for imaging the velocity structure of upper mantle. A widely used procedure for this purpose is to do inversion of these travel times for velocity.

3.2 Data Selection

Data set used in this study is retrieved from International seismological network (ISC) bulletin. It consists of ~ 9,000 events in total with ~ 95,000 Pn waves (waves refracted from Moho) recorded on 351 different stations in the surrounding area. This database contains Information about Station code, Magnitude, Epicenteral distance, Station to event azimuth, Phase, Date of arrival, Time of Arrival, Residual with respect to reference model, Flag showing whether the phase was time-defining (whether it was used in the computation of an ISC location), Amplitude, Period, Origin date, Origin time, Origin Latitude, Origin Longitude and Origin depth. (C.f. Section 4.1)

3.3 Pre Processing of data

In real world these travel time observations are associated with noise and uncertainties. Before starting inversion, this data is processed to increase the S/N ratio and eliminate several discrepancies from the data. Some major processing steps used in this study are listed below.

- Sorting of phases
- Filtering for minimum Magnitude
- Filtering for missing residuals and Origin depth
- Filtering for minimum and maximum epicenteral distance
- Filtering for residual limit
- Forming summary rays
- Calculation and analysis of hit count

All these processing is further described in chapter 4 (c.f. section 4.2)

3.4 Model parameterization

In this study crust and the upper mantle velocity structure is parameterized by their values at geographically distributed nodes in a region ranging between 10 Deg W to 45 Deg E & 45 Deg N to 75 Deg N). Node spacing is of approximately 1 Deg. At each node, we have a

vertical 1D model. Interpolation in between the nodes is used to see the lateral variations in model parameters.

3.4.1 Crustal Model

Following the tomographic procedure described by Myers *et al.* (2010), the crustal model used in this study is the same as described by Pasyanos *et al.* (2004). This model includes mainly 8 layers and then mantle as a half space with a vertical velocity gradient. Summary of this model is shown in table 3.1.

Table 3.1

Entry Number	Model Entity	Representation	Parameter
1	Water	Layer	Velocity
2	Sediment 1	Layer	Velocity
3	Sediment 2	Layer	Velocity
4	Sediment 3	Layer	Velocity
5	Upper crust	Layer	Velocity
6	Middle crust	Layer	Velocity
7	Lower crust	Layer	Velocity
8	Mantle at Moho	Half space	Velocity
9	Mantle Gradient		Velocity Gradient

Table 3.1: Model Entities & their definitions used to construct depth profile at each node (after Myers et al. 2010)

Depths (km) of these layers are calculated from center of earth. All these layers are assumed to be present with a sharp boundary, so the bottom of each layer is the top of underlying layer. Velocities are in km/sec and velocity gradient is (km/sec)/km. Travel time in the crustal part (both for receiver and source side) is defined as (Myers *et al.* 2010)

$$t_{crust} = \sum_{j=1}^{n} \left[\sqrt{\frac{r_j^2}{v_j^2} - p^2} - \sqrt{\frac{r_{j+1}^2}{v_j^2} - p^2} \right] \qquad (3.1)$$

Where t_{crust} is the one way travel time either for source side or for receiver side. r_j is the distance of top of the layer j from the earth center. r_{j+1} is the distance from earth center to the top of overlying layer. v_j is the interval velocity of the particular layer. p is the ray

parameter (reciprocal of mantle velocity). n are the total number of crustal layers encountered in ray path.

Crustal structure could vary laterally e.g. at some places several layers could be missing or with variable thickness. A simple cross section of this scenario is illustrated in fig 3.2. In this study we used 1D crustal structure of RSTT model (Regional Seismic Travel Time Model by Myers *et al.* 2010) on geographically distributed node locations. Further this crustal structure is allowed to vary during inversion in terms of percentage of travel times of the crustal legs of total travel time.

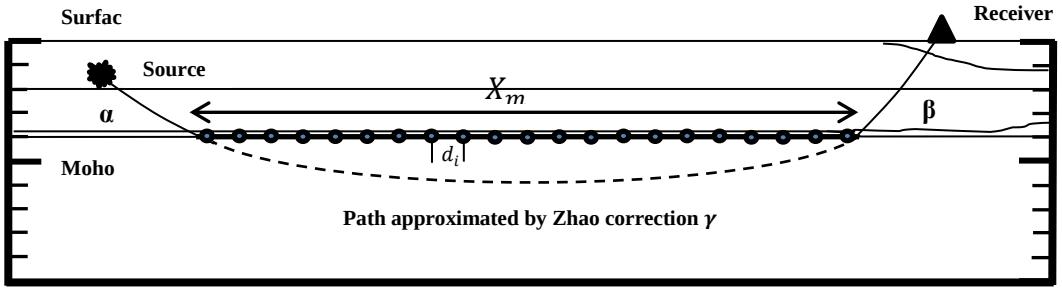

Fig 3.2: Cross section of a possible laterally variable model. Variable depth Moho is shown as a thin black line whereas possible pitchouts in crustal layers are also illustrated as thin grey lines, Thick blue line indicates the horizontal distance travel by the ray along mantle (X_m), diving ray path in mantle is shown by blue dotted line, α & β are the crustal legs of time for source and receiver side respectively (after Myers et al. 2010)

3.4.2 Travel time Equation

An example of a source to receiver path of a Pn wave is shown in fig 3.2. It can be seen that the total travel path of a ray can be subdivided into three parts

1- Source to Moho (crustal part)
2- Head/Diving wave along Moho
3- Moho to the receiver (crustal part)

Further if diving wave concept (Zhao. 1993 and Zhao & Xie 1993) is used, the travel time along Moho can be further divided into two components. First, the travel time along the Moho from source to receiver and 2nd a correction for mantle gradient and the sphericity of the Earth

Summarizing, we can write the travel time equation as (Myers *et al*. 2010)

$$TT = \sum_{i=1}^{N} d_i s_i + \alpha + \beta + \gamma \qquad (3.2)$$

$\sum_{i=1}^{N} d_i s_i$ is sum over the product of horizontal distance travel by the wave and slowness in each of *i* segments comprising great circle path between Moho pierce points near source & station (Myers *et al.* 2010). Example of this division (*i* segments) is shown in figure 3.2 (small segments alongX_m). These small segments are chosen so small that slowness in one segment is considered as constant (c.f. section 2.3.1). Slowness in these small segments are determined from the model at adjacent nodes.

α is the crustal travel time from the source location to the Moho and can be calculated as

$$\alpha = \sum_{j=1}^{M} \left[\sqrt{\frac{r_j^2}{v_j^2} - p^2} - \sqrt{\frac{r_{j+1}^2}{v_j^2} - p^2} \right] \qquad (3.3)$$

v and *r* are the velocity and radius respectively (from the center of earth) for M crustal layers beneath the source. β is the crustal travel time from Moho to the receiver. Similarly to the source side of crustal layers, it is defined as

$$\beta = \sum_{k=1}^{N} \left[\sqrt{\frac{r_k^2}{v_k^2} - p^2} - \sqrt{\frac{r_{k+1}^2}{v_k^2} - p^2} \right] \qquad (3.4)$$

Correction factor applied for the diving wave below Moho (γ) is described as (Zhao *et al.* 1993)

$$\gamma = \frac{c^2 X_m^2}{24\, V_o} \qquad (3.5)$$

Where $X_m$the horizontal distance traveled by Pn wave along Moho, V_o is the average pn velocity, *c* is the vertical velocity gradient, normalized by average velocity in the area corrected for earth sphericity (*r*). Normalized velocity gradient can be converted into real velocity gradient (G_m) by employing following equation (after Myers et al., 2010)

$$G_m = V_o \left(c - \frac{1}{r} \right) \qquad (3.6)$$

3.5 Inversion

In inversion mathematical techniques are used to find model that minimize the difference between the predicted data (d_{prd}) and observed data (d_{obs}). In this study model vector consist of 3 entities i.e. mantle slowness, normalized velocity gradient in mantle and crustal modifier. Observed data consist of travel times obtained after the pre-processing of raw data.

This tomography problem is not perfectly a linear inverse problem. We assumed that the source locations are fixed but in reality it is not. ISC (we used travel time data retrieved form ISC) used Ak135 and JB velocity models to determine hypocenter locations. Travel time residuals suggest that the velocity model in this area is significantly different from the model used by ISC. If velocity model is changed then ultimately hypocenter locations will also be affected. As a regional data is used in this study so we assumed that the small scale variation in velocity model will not affect much to the hypocenter locations therefore we ignored this factor and assumed the linearity of system.

We followed a preconditioned Conjugate Gradient inversion scheme presented by Tarantola (1987). To keep this system within computational limits this conjugate gradient inversion is applied in an iterative way. By assuming a strictly linear problem we find a solution to this system by minimizing the misfit function. Misfit function S is given by (Tarantola 1987).

$$S = \frac{1}{2}\left[(Gm - d_{obs})^t\, C_D^{-1}\, (Gm - d_{obs}) + \left(m - m_{prior}\right)^t\, C_M^{-1}\, (m - m_{prior})\right] \quad (3.7)$$

Where G express the relation between model and data, C_M is priori model covariance matrix, C_D is observed data covariance matrix, m is the unknown model vector, m_{prior} is apriori model vector (RSTT final model) and d_{obs} is the observed travel time matrix.

We assumed this problem as a perfectly linear inverse problem so this misfit function (S) will be a quadratic function with no secondary minima and conjugate directions method converge in a finite number of iteration (disregarding truncation errors) (Tarantola 1987).

3.5.1 Construction of G Matrix

Tomographic inverse problem solves the system for certain model parameters. In this study model parameters consist of mantle slowness at Moho, *s*; square of mantle velocity gradient c^2 and a scalar adjustment to the crustal slowness, *a*. (Myers *et al*. 2010)

We have therefore a system similar to the one we introduced in eq. (2.2) but with several additional components. Referring to eq. (3.2), each row of the G matrix will have 4 components: 1) Mantle slowness term, 2) mantle gradient term, 3) source-side crustal term and 4) receiver-side crustal. Altogether, G matrix can be written as (Myers *et al.* 2010)

$$\begin{bmatrix} x_1^1 & \cdots & x_N^1 & \frac{x_1^1(X_{m,1})^3}{-24V_0\,X_{m,1}} & \cdots & \frac{x_N^1(X_{m,1})^3}{-24V_0\,X_{m,1}} & \sum_{P=1}^{Q}\frac{l_{1p}^1}{v_{1p}} & \cdots & \sum_{P=1}^{Q}\frac{l_{Np}^1}{v_{Np}} \\ \vdots & & \vdots & \vdots & \ddots & \vdots & \vdots & \ddots & \vdots \\ x_1^K & \cdots & x_N^K & \frac{x_1^K(X_{m,k})^3}{-24V_0\,X_{m,k}} & \cdots & \frac{x_n^K(X_{m,k})^3}{-24V_0\,X_{m,k}} & \sum_{P=1}^{Q}\frac{l_{1p}^K}{v_{1p}} & \cdots & \sum_{P=1}^{Q}\frac{l_{Np}^K}{v_{Np}} \end{bmatrix} \quad (3.7)$$

Where x the pn distance or weight for each model node, X_m is the Horizontal distance of Pn ray path along Moho, V_0 is average Pn velocity in mantle, v_p & l is the p wave velocity and length of ray part in a particular crustal layer.

Most important parameter in this G matrix is the weight assigned to nodes for 1st term (mantle slowness term) and 2nd term (mantle gradient term) of G matrix. SLBM (Seismic Location Based Model © Sandia National Laboratories) software is used to extract these weights

3rd and 4th terms of G matrix corresponds to the times for crustal leg of travel time for both source side and receiver side. Crustal model was extracted from SLBM software that consists of number of crustal layers, their thickness and velocities at each node location. By incorporation this crustal model along with source receiver location (longitude, latitude and depth) equation 3.1 is used for calculating travel time for source and receiver side (crustal leg)

3.5.2 Data vector (D) and data covariance (C_D)

Observed data (d_{obs}) in this study consist of a times recorded on various networks in the study area that are reported and relocated by ISC. Various pre-processing have been applied to enhance S/N Ratio of this raw data. Two major processing steps used are

1: Filtering for outliers; to remove the travel times related to wrong picking of phases and recording.

2: Summary rays are used to remove uncertainty on the basis of geographical location of sources for a particular receiver, and to make ray coverage more even. It will certainly reduce the number of rays and enhance number of quality rays which helps to keep the system in the computational limit. In matrix form data vector can be written as

$$\begin{bmatrix} t_1 \\ t_2 \\ \vdots \\ \vdots \\ t_K \end{bmatrix} \qquad (3.8)$$

Where *k* is the total number of rays

In travel time tomography there are various types of errors present in the data that ultimately map into the errors in resulted model parameters. Covariance matrix describes how noise propagates from data to the estimated model. If we assume that errors in the data have Gaussian distribution then data covariance matrix reflects the uncertainty in the travel time recording (Menke 1987)

In tomography we can assume a diagonal covariance matrix with diagonal elements being the variance of the data. We can suppress the influence of any particular noisy ray on the inversion by selecting a large value for its standard deviation. In this study, as the processed data (summary rays) is used for inversion and we hold good a priori information so standard deviation for all the data was considered as constant.

Mathematically covariance matrix for data can be written as

$$C_D = \sigma_d^2 \; I_{K\times K}$$

Where σ_d is the uncertainty attached to the data (standard deviation) and $I_{K\times K}$ is the identity matrix with $K\times K$ order, K being the number of rays used in inversion.

3.5.3 Model vector (M) and model covariance (C_M)

As discussed earlier, we have 3 model parameters i.e. 1) mantle slowness, 2) normalized mantle velocity gradient and 3) crustal modifier. In matrix form, model vector can be written as (Myers *et al.* 2010)

$$\begin{bmatrix} s_1 \\ \vdots \\ s_N \\ c_1^2 \\ \vdots \\ c_N^2 \\ a_1 \\ \vdots \\ a_N \end{bmatrix} \qquad (3.9)$$

Where s is mantle slowness below the Moho (i.e. Pn slowness), c is normalized velocity gradient,$v = v_0\,(1 + cz)$, a is node-specific adjustment to the combined slowness of crustal layers (crust modifier), N being number of nodes used for inversion.

In inversion we try to estimate model parameters that to large extent satisfy the observed data. In this study we followed the conjugate inversion scheme as described by Tarantola (1986). For this scheme we need two sets of model vectors. First belongs to the a-priori model and second to the starting model. We used RSTT final model (for mantle slowness, velocity gradient and crustal correction factor) as a-priori model whereas for starting model we used a null vector for mantle slowness & gradient and for crustal modifier unit matrix is used. We have tried various models as initial model but after inversion we got similar results. This confirms our assumption about linearity of system.

It is noted here that units of these three model parameters are different. Mantle slowness in s/km whereas units of normalized velocity gradient is 1/km and a, crustal modifier is scalar multiplier. So a covariance matrix with constant variance cannot be used. To deal with this problem different values of variance are used for these three model parameters.

Further to keep model smooth, (so there will not be any sudden jump from one node to adjacent nodes) a priori covariance function was used. Considering probability distribution covariance matrix, C_M can be defined as (Montagne *et al.* 1990)

$$C_M = \sigma_0(r_1)\sigma_0\,(r_2)\exp(-\frac{\Delta^2(r_1,r_2)}{2L^2}\,)$$

Δ Is then distance in km between two nodes r_1 &r_2 , σ_0 is priori error on the model in terms of standard deviation that control the amount of perturbation allowed in the different parameters while L is the correlation length that control the smoothing of the models.

3.5.4 Tomographic Formulation

By combining the Green function matrix G, data vector D and Model vector M, tomographic system of equations can be written as (Myers et al., 2010)

$$\begin{bmatrix} x_1^1 & \cdots & x_N^1 & \frac{x_1^1(X_{m,1})^3}{-24V_0\,X_{m,1}} & \cdots & \frac{x_N^1(X_{m,1})^3}{-24V_0\,X_{m,1}} & \sum_{P=1}^{Q}\frac{l_{1p}^1}{v_{1p}} & \cdots & \sum_{P=1}^{Q}\frac{l_{Np}^1}{v_{Np}} \\ \vdots & & \vdots & \vdots & \ddots & \vdots & \vdots & \ddots & \vdots \\ x_1^K & \cdots & x_N^K & \frac{x_1^K(X_{m,k})^3}{-24V_0\,X_{m,k}} & \cdots & \frac{x_n^K(X_{m,k})^3}{-24V_0\,X_{m,k}} & \sum_{P=1}^{Q}\frac{l_{1p}^K}{v_{1p}} & \cdots & \sum_{P=1}^{Q}\frac{l_{Np}^K}{v_{Np}} \end{bmatrix} \times \begin{bmatrix} s_1 \\ \vdots \\ s_N \\ c_1^2 \\ \vdots \\ c_N^2 \\ a_1 \\ \vdots \\ a_N \end{bmatrix} = \begin{bmatrix} t_1 \\ t_2 \\ \vdots \\ \vdots \\ t_K \end{bmatrix}$$

(3.10)

3.4.5 Inversion algorithm

There are several inversion methods that can solve equation 3.10 e.g. Singular value decomposition (SVD) of G, Algebraic (ART), simultaneous iterative reconstruction techniques (SIRT) and conjugate gradient inversion technique. SVD could be a good choice for inversion because it explicitly construct generalized inverse of G and corresponding covariance and resolution matrixes but it is quiet memory intensive. (Song *et al.* 2004)

Due to large tomographic system, fast iterative inversion technique e.g. ART, SIRT or CG is preferred. Among these techniques CG is the most popular technique in solving tomographic problems.

In this study Precondition Conjugate Gradient inversion Algorithm, described by Tarantola 1987, is used to find a best fit model. Flow chart of main algorithm sequence of solution finding is shown in fig. 3.3

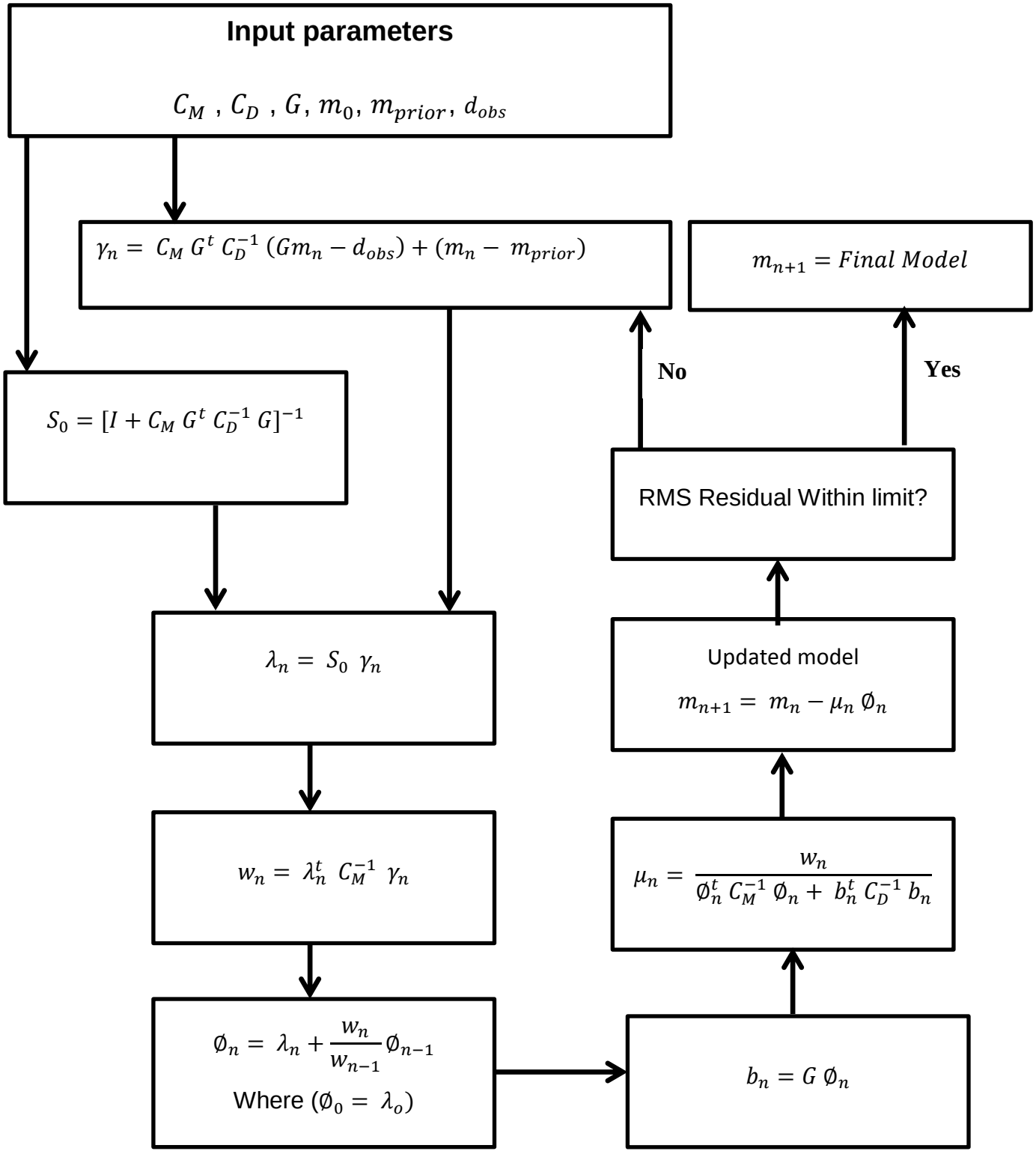

Fig 3.3: Flow chart of main algorithm sequence (After Tarantola 1987)

3.5.6 Analysis of error and resolution

Resolution matrix

Averaging level of model estimate is described by the resolution matrix R. In other words it is a relation between m_{pred} & m_{true} . Resolution matrix is independent of actual model and data; it is only function of data kernel and a priori information added to the problem. (Tarantola 1987).

$$R = (G^t C_D^{-1} G + C_M^{-1})^{-1} G^t C_D^{-1} G \qquad (3.11)$$

If R is an identity matrix than each model parameter is uniquely determined or we can say $m_{pred} = m_{true}$. Size and spread of off-diagonal elements measures the resolution. Farther the matrix from identity, more the model parameters are weighted averages of true model (Tarantola, 1987).

If we consider the natural ordering of the model parameters then the rows of resolution matrix demonstrate the scale features in model that can be actually resolved. Narrow peaks occurring near the main diagonal of the matrix indicate that the model is well resolved. (Menke 1989)

Posterior Covariance matrix

Model covariance quantifies the uncertainties of the estimated parameters associated with data, kernels and errors (Song *et al.* 2004). It depends on the covariance of observed data and how this error is mapped in model parameters. By considering the inverse problem to be linear then the posterior probability density function is Gaussian and covariance operator is given by (Tarantola 1987).

$$C_{\tilde{M}} = (G^t C_D^{-1} G + C_M^{-1})^{-1} \qquad (3.12)$$

Most usual interpretation of posterior covariance matrix is the considering the square root of diagonal elements of this matrix as uncertainties on the posterior model parameters (so called ‘’error bars’’) (Tarantola 1987)

3.5.7 Synthetic test of statistical reliability and resolving power of Pn data

In tomography studies, Checkerboard synthetic test is usually performed to check the quality of inverse solution. It will estimate how well the inversion of the Pn data can resolve the upper mantle velocity anomalies. In checkerboard test we define a true model i.e. a perfect mantle velocity model with some velocity anomalies (checkerboard-10% velocity contrast in our study) of specific size. Synthetic travel times are then calculated by using this synthetic model and locations specified by the source and receiver locations of real data. Mimic random noise is added to these travel times. In last this so called observed data (synthetic travel time) is inverted by the same procedure as used in main inversion. Difference between the retrieved and true model will estimate the quality of inverse solution.

CHAPTER 4: TOMOGRAPHIC INVERSION: APPLICATION TO THE SOUTHERN SCANDINAVIA

The main objective of this study is the mapping of the upper mantle velocity structure in southern Scandinavia. For this purpose we used tomographic inversion of Pn waves, recorded on geographically distributed network of earthquake recording stations.

Tomography starts with identification and picking of phases (travel time for Pn phases). This data is then processed to enhance signal to noise ratio. Procedure continues to the formulation of tomographic equation. Basic parameters for this formulation, along with a priori model, were extracted form SLBM (Seismic location base model ©Sandia National Laboratories) software. This tomographic equation is then inverted for mantle slowness, normalized velocity gradient and scalar adjustment to the crustal slowness at a given number of nodes. This 1D structure is then interpolated between adjacent nodes to get a 2D variation of model parameters. In this study preconditioned conjugate inversion scheme (Tarantola 1987) is used as inversion methodology. Some resolution tests were also performed to analyze the reliability of inversion.

In this chapter we will discuss all these major steps starting form Data selection, pre-processing, a priori model formation, inversion and in last, quality assessment of adopted inversion procedure

4.1 Dataset

Data set used here was retrieved from International seismological network (ISC) bulletin. International Seismological Centre (ISC) was set up in 1964 with the assistance of UNESCO as a successor to the International Seismological Summary (ISS) to follow up the pioneering work of Prof. John Milne and Sir Harold Jeffreys in collecting, archiving and processing seismic station and network bulletins and preparing and distributing the definitive summary of world seismicity. Data available in ISC bulletin is collected from over 130 agencies worldwide and is manually checked by ISC analysts. Data in the Reviewed ISC Bulletin are relocated by ISC, using the ISC location algorithm (ISCloc) (http://www.isc.ac.uk/).

Initially data for this study consist of ~ 9,000 events in total (after sorting of Pn phases) with ~ 95,000 Pn waves (refracted from Moho) recorded on 351 different stations in the area. Data coverage for unprocessed data is shown in Fig 4.1. This dataset contains Information about Station code, Magnitude, Epicenteral distance, Station to event azimuth, Phase, Date of arrival, Time of Arrival, Residuals with respect to reference model, Flag showing whether the phase was time-defining (whether it was used in the computation of an ISC location), Amplitude, Period, Origin date, Origin time, Origin Latitude, Origin Longitude and Origin depth.

This dataset comprises events recorded from 1971 to 2007. All these events are revisited by ISC to confirm hypocenter locations. Two different reference models have been used by ISC for relocation of earthquakes as well as in calculation of residuals. Jeffreys-Bullen (JB) reference model is used for the events recorded earlier than 1st Jan 2006 whereas ak135 model is used afterwards.

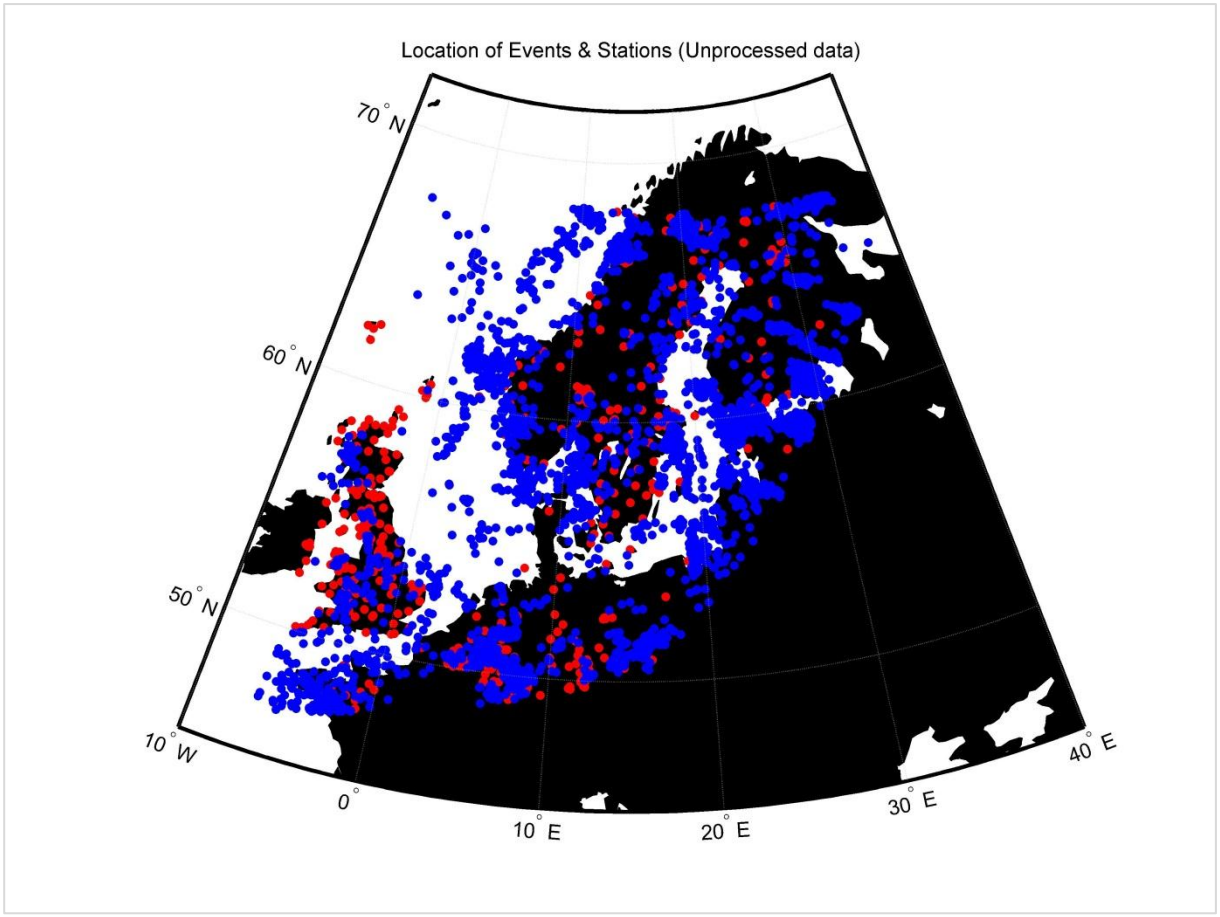

Figure 4.1**:** Data coverage of unprocessed data (Blue are Earthquake locations whereas Red are receivers locations)

Prior to the inversion of the data, various processing techniques have been applied to enhance S/N ratio and to eliminate several discrepancies from the data e.g. uneven distribution of sources.

4.2 Processing of data

Travel time curve of the sorted data (Pn phase) is shown in Fig 4.2. It can be seen that there are a lot of deviations from the straight curve, marked by circles. There could be two reasons for this deviation; either the velocity contrast in the subsurface or the errors in the phase picking/data recording and interpretation. The best fit line (line in fig 4.2, formed by the first order polynomial) suggests that the average velocity in this area is ~ 8km/sec.

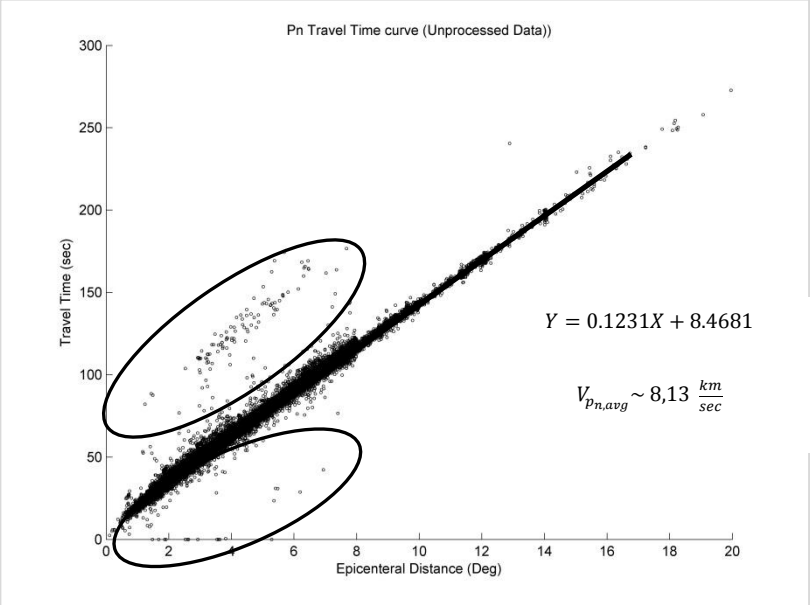

Figure 4.2: Travel time curve for unprocessed data for Pn phase

In this study we applied various filters on this data to increase the S/N ratio. Major processing steps used here are;

- Filtering for minimum magnitude
- Filtering for missing residuals and Origin depth
- Filtering for epicenteral distance
- Filtering for residual limit
- Forming summary rays

- Calculation and analysis of hit count

4.2.1 Filtering for minimum magnitude

Reliability of phase picking depends on magnitude of the source. For events with low magnitude, it is less likely the Pn will have amplitude larger than the background noise level. To avoid this problem we limited our selection to the events having magnitude 3 or greater.

4.2.2 Filtering for missing residuals and origin depths

Dataset retrieved from ISC include travel time residuals with respect to a reference earth model, either from Jeffreys-Bullen (JB) or from ak135 reference earth model. There were some events without pre-defined residuals. These events were excluded from the database. Some other events with missing origin depths were also excluded from the main database.

4.2.3 Filtering for epicenteral distance

Pn wave is a refracted wave from Moho so one cannot expect reception of this wave with epicenteral distance less than the critical distance for refraction. An expected critical distance was calculated by using an average crustal model (ak135 model). All the data having epicenteral distance less than this critical distance (1.799° in this case) was disregarded.

In this study we used SLBM software to extract weights on the nodes (c.f. section 3.5.1) for velocity modeling and this software has restriction on maximum epicenter distance of 15°. An upper bound of 15° was applied on epicenter distance; all the events above this limit were disregarded. Area to be mapped is not very large so this upper bound will not have a major effect on resolution of model.

Travel time curve for unprocessed and semi processed data (after the application of filters for missing residuals, origin depth and epicenteral distance limit) is shown in fig 4.3. Note that some events with very small or zero travel times have been removed.

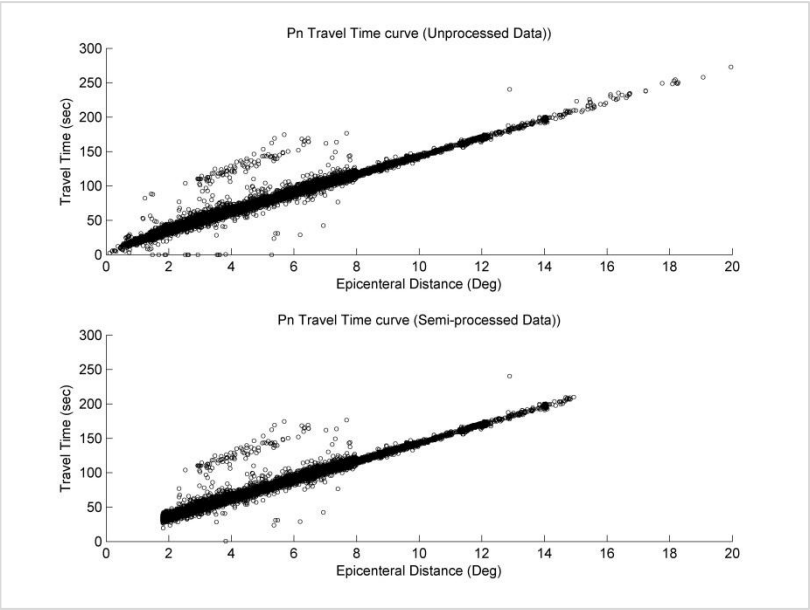

Figure 4.3: Unprocessed and semi processed travel time curve

Effect on residuals with respect to epicenteral distance can be seen in fig 4.4. There is bit reduction in the overall residual range.

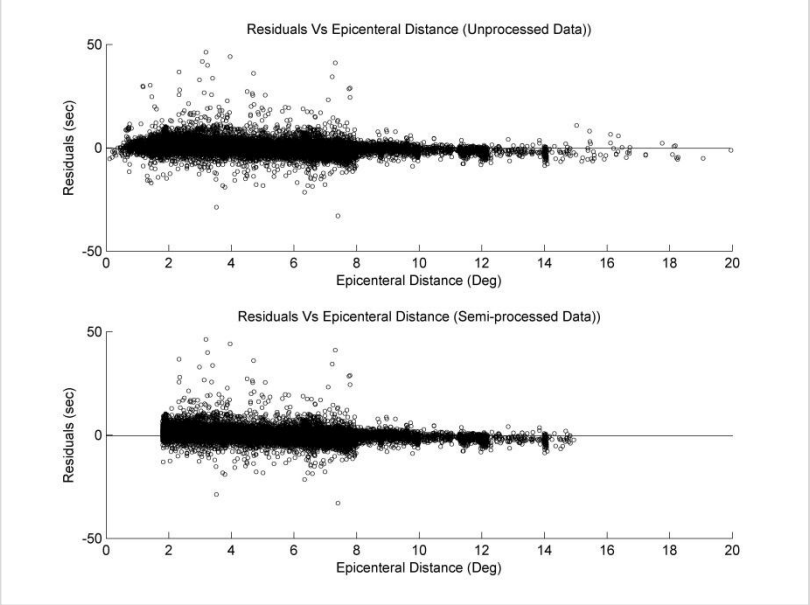

Figure 4.4: Residual vs. Epicenter distance plots of Unprocessed and Semi processed data

4.2.4 Filtering for maximum expected residual limit

Residual distribution of this data is shown in figure 4.5. Most of the residuals are within $\pm$ 10 sec limit. There are only few events with very large residuals, ranging up to $\pm$ 80 sec (shown

in the figure 4.5 (b)). Velocity contrast in the subsurface could not be the reason for such large residuals. These are most probably some other phases picked wrongly as Pn phase.

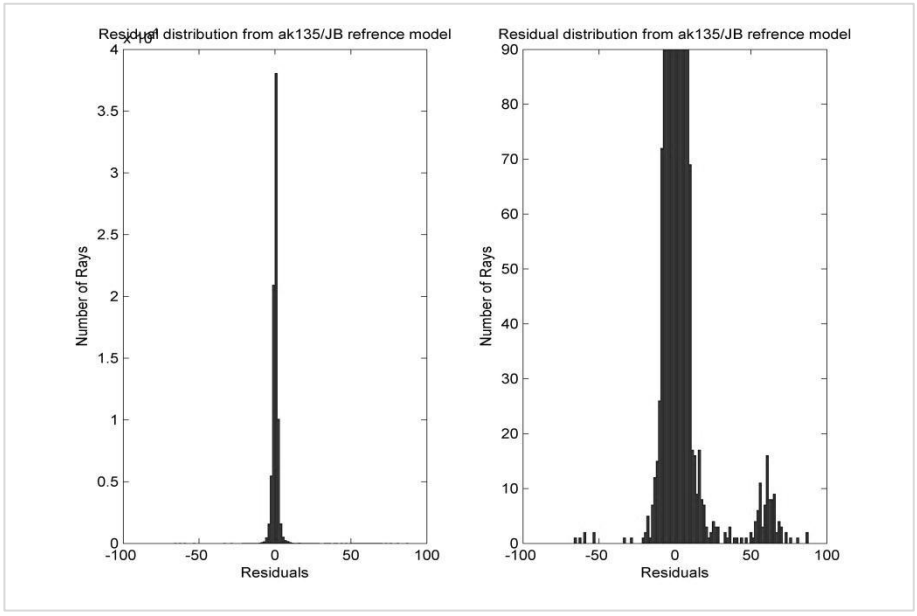

Figure 4.5**:** Residual distribution (a) For whole dataset (b) Enlarged for max 90 rays

On the basis of residual distribution of dataset and probability of having residuals due to expected velocity anomaly, we only owned data having residuals with $\pm$ 4 sec limit. All the remaining data was disregarded.

Travel time curve and residual vs. epicenter distance curve of this processed data is shown in Figure 4.6. Note that data is cleaned now i.e. we have very less deviation from the straight line as well as the residual distribution is now within acceptable limit.

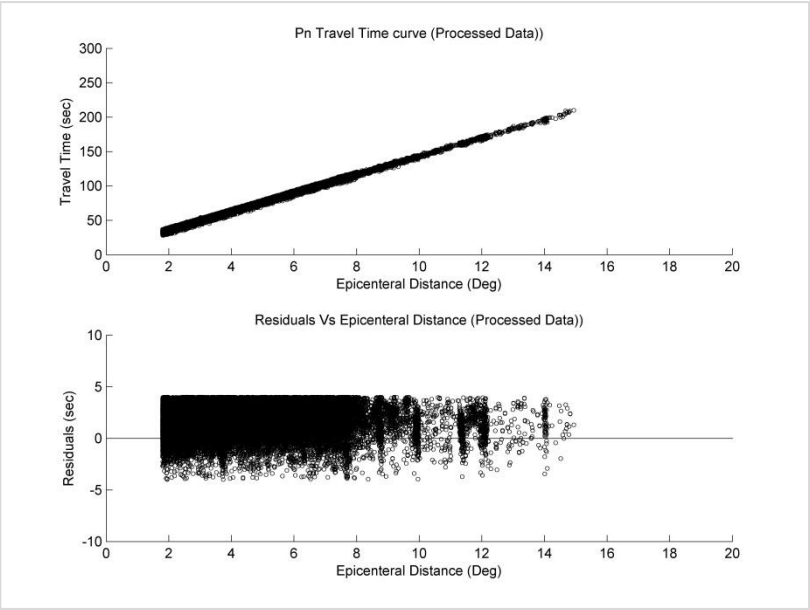

Figure 4.6**:** Travel time curve and Residual vs. Epicenter distance for processed data

4.2.5 Summary Rays

Figure 4.1 shows that the distribution of events is heavily uneven. Especially in north-eastern side of the area where most events are mining explosions. To make this distribution even and to suppress the individual errors, summary rays have been formed. For summary rays, the whole area is divided into rectangular cells with dimension of 0.3°×0.5°. For a particular station, all the events falling in one bin (rectangular box) are gathered and their parameters (e.g. travel time and residual) are averaged out to make one ray. The average location and depth was calculated from the mode of this bin. All the rays for that particular station and events (within in same bin) are replaced by this new ray. Same procedure is repeated for all the stations in the area. Resulted data coverage and their ray paths are shown in Figure 4.7

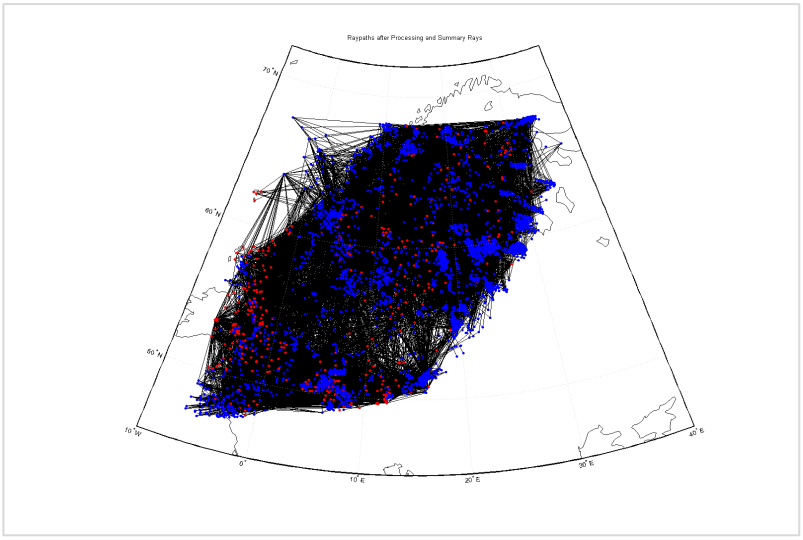

Figure 4.7**:** Ray paths after processing & summary rays

Forming of summary rays did not show any prominent effect on data coverage but now data is more even and also have certainly improved S/N ratio i.e. residuals are less and evenly distributed. It will lead to a reduction in total number of rays so it also helps to reduce computational time for inversion. Pn travel time curve and residual distribution is shown in Figure 4.8

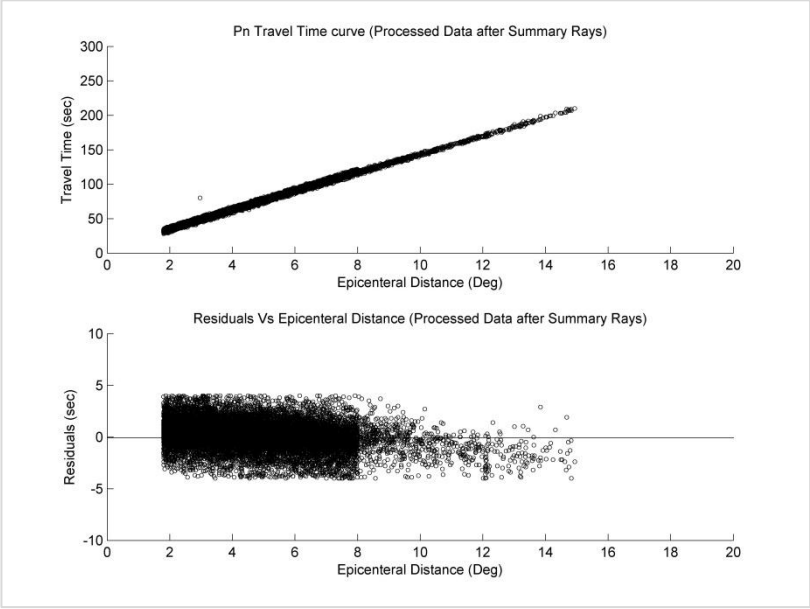

Figure 4.8**:** Travel time curve & Residual vs. Epicenteral distance

4.2.6 Hit count Mapping

Hit count map is generated on the nodes (formed by the bins used for the summary rays) to evaluate the data coverage in the study area. A ray is considered to hit a mode if it passes closest to it than 30% of the distance between adjacent nodes. Resulted node hit count map is shown in figure 4.9. It can be seen that the data coverage is very good in the whole area. Especially in the vicinity of our target area (southern Norway) it is about 150 to 200 rays per node.

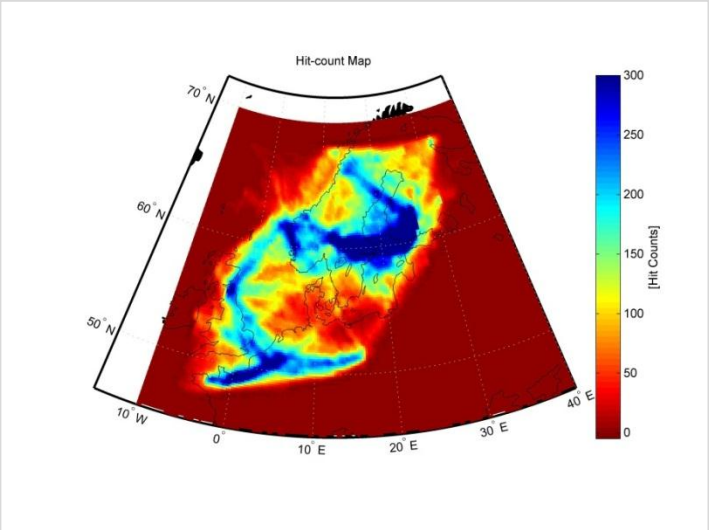

Figure 4.9**:** Hit count map in the area, color scale ranges up to 300 rays per node

4.3 Construction of reference model and synthetic travel times

We start with construction of a reference earth model and further this reference earth model is used to calculate synthetic travel times for the same ray geometry as per the real data. SLBM software is used to calculate these synthetic travel times. Instead of ray tracing, SLBM use great circle path by taking into account of ellipticity of the Earth.

4.3.1 Construction of reference model

Instead of using a heavily averaged and homogeneous reference earth model (e.g. Ak135 or JB model) we considered the final RSTT model (Regional seismic travel time model) by Myers *et al.* (2010) as a reference model in our study. This is a non-homogeneous model with laterally variable upper mantle velocity, velocity gradient and crustal velocities & thickness. This model was formed by a global tomographic formulation that adjusts the

mantle slowness at Moho, mantle velocity gradient and average crustal velocity at geographically distributed nodes. (Myers *et al.* 2010). Reasons for selecting this model are, first the methodology for tomographic formulation of this model is closely align to the methodology used in this study and secondly this model is fairly close to the models presented by various authors, particular to this area. (e.g. Maupin *et al.* 2011, Bannister *et al.* 1991, Husebye *et al.* 1986, Bondo et al. 2009, Weidle & Maupin., 2008).

Construction of reference model for this study was generated by using locations of events and stations from the real data and 1D vertical profile for upper mantle velocity, vertical velocity gradient and crustal information. RSTT final model for all these model parameters was extracted from SLBM software. Main output of this process was

- Geographically distributed Node locations with approximate 1 degree node spacing
- Earth model on these nodes; this includes information about mantle slowness, velocity gradient, crustal velocities and thickness

Geographical locations of nodes are shown in figure 4.10. It can be seen that target area is well covered and density of nodes are quiet sufficient for confident mapping.

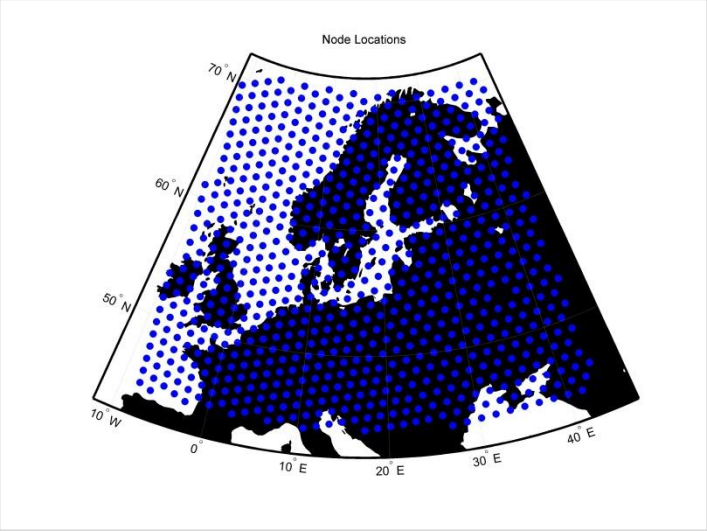

Figure 4.10**:** Geographical locations of nodes

Reference earth model for upper mantle velocity is shown in Figure 4.11. This model shows that in vicinity of Scandinavian mountains (Southern Norway and some part of northern Norway) velocity is relatively low as compared to the eastern part (Sweden area). This model is also used as a priori model as it closely align with the model already published by

various authors (Maupin *et al.* 2011, Bannister *et al.* 1991, Husebye *et al.* 1986, Bondo et al. 2009, Weidle & Maupin., 2008) for this area.

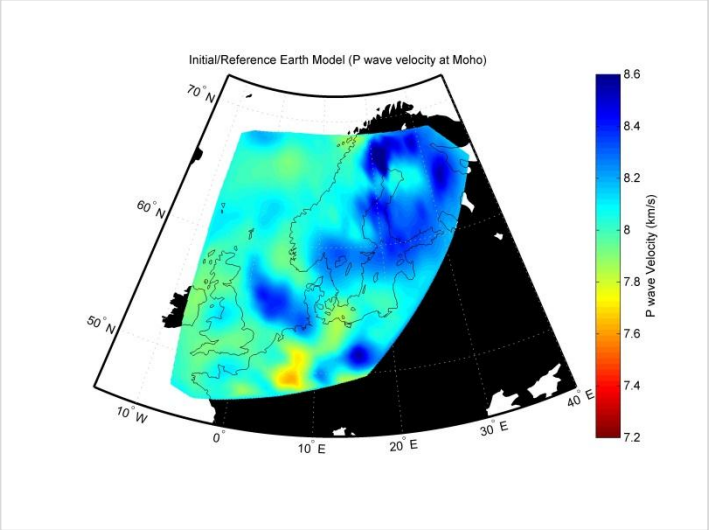

Figure 4.11: Reference model for velocity at Moho

Reference earth model for velocity gradient below Moho is shown in figure 4.12. According to this model, mantle in this area have negative and constant velocity gradient

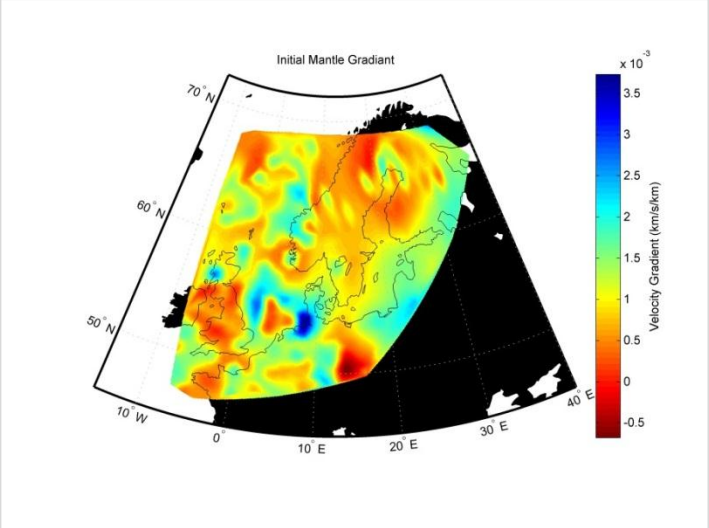

Figure 4.12**:** Reference model for Mantle velocity gradient below Moho

Reference model for Moho depth is shown in figure 4.13. Moho is deeper in the older and thicker part of Baltic shield (Sweden and Eastwards) where as it become shallow in the western part (southern Norway and offshore).

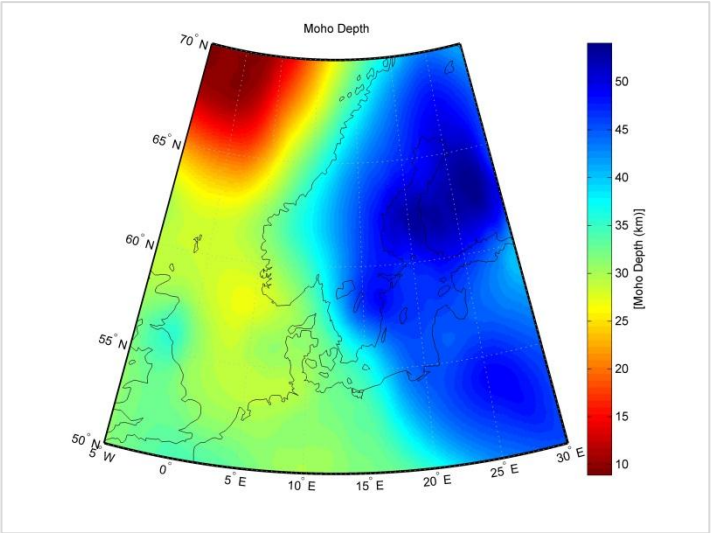

Figure 4.13: Reference model for Moho Depth

4.3.2 Calculation of synthetic travel times

Synthetic travel times are calculated by using equation 3.10 (by incorporating reference model parameters i.e. mantle slowness, velocity gradient and scalar adjustment to the crustal structure). Figure 4.14 shows the Pn travel time curve obtained by calculating synthetic travel times on locations defined by the real dataset (event-station pairs). This synthetic curve is approximately straight with an average velocity of 7.8 km/s.

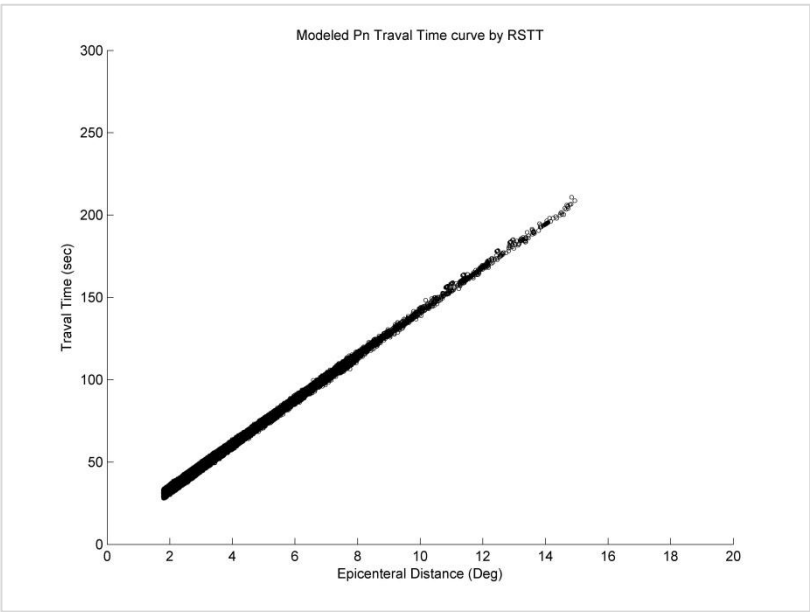

Figure 4.134: Travel time curve abstain by retracing using RSTT model

4.4 Inversion

A preconditioned conjugate inversion algorithm is designed to invert the travel times into 1D structure of the upper mantle (mantle slowness and normalized velocity gradient) and crustal structure at the different nodes. Formulation of tomographic equation is follows by the methodology presented in Myers *et al.* (2010) whereas inversion methodology for this equation follows the methodology presented in Tarantola,(1987). This algorithm is coded in MATLAB along with all preprocessing step explained in Section 4.2 (c.f. Appendix A)

After filtering of data with required parameters inversion procedure starts with the setup of inversion parameters. These parameters include formation of G matrix and model parameters that needs to be inverted.

This algorithm allows to invert travel times for three model parameters i.e. slowness at Moho, velocity gradient below Moho and crustal modifier. Although the objective of this study is to invert and discuss only the upper mantle velocity structure (slowness (S_p) and normalized velocity gradient (C^2)), the crustal structure has a non-negligible influence on the traveltimes and need to be taken into account. The crustal modifier (a) let the crustal traveltimes to vary as a whole in percentage to their initial values. This will help the system to better fit the travel times. (cf. Section 3.4.3)

A priori information for this inversion is defined by a reference earth model (for slowness at Moho, velocity gradient below Moho and crustal information) along its covariance matrix (cf. Section 4.3.1). In this study conjugate gradient least square inversion scheme is used that finds the solution by minimizing the least square error on model. As different model entities have different units so it is not appropriate to use a single value as a priori standard deviation of model vector. For smoothness in the inversion, various combinations for a priori standard deviation were selected and inverted. These combinations of standard deviation along with resulted RMS residuals are shown in table 4.1. Our preferred combination of parameters is used in model M1. Models M2 to M7 show the results when increasing or decreasing by a factor of 10 the standard deviation of one of the other parameters.

Table 4.1

Model	M 1	M 2	M 3	M 4	M 5	M 6	M 7
Sigma 1(for Mantle slowness)	1e-2	1e-1	1e-3	1e-2	1e-2	1e-2	1e-2
Sigma 2 (for Normalize velocity gradient)	2e-4	2e-4	2e-4	2e-2	2e-5	2e-4	2e-4
Sigma 3 (for Crustal correction)	5e-5	5e-5	5e-5	5e-5	5e-5	5e-4	5e-6
RMS Residual	15.13	15.23	15.19	15.12	15.17	15.56	15.45

Table 4.1: Various alternatives of standard deviations tested for a priori model.

Results for these 7 models are shown in Appendix B. RMS residuals for all these models are very similar to each other. To give high weight to mantle slowness as compare to the other model parameters, we selected combination M1 for further analysis.

To keep system smooth we controlled the lateral variation in the first model parameter (velocity at Moho) by introducing coupling among neighboring nodes through a correlation length in the covariance matrix (cf. Section 3.4.3). As we do not expect to have huge variation in vertical velocity gradient and crustal modifier so we used a diagonal covariance matrix for these model parameters. Mathematically by choosing a very small correlation length covariance matrix become close to a diagonal matrix. On the other side, high value of correlation length means that model parameters at adjacent modes are force to stay very close to each other (cf. Section 3.4.3).

Various tests have been performed to analyze the effect of the choice of horizontal correlation length. Absolute residuals for a priori & inverted models and their residual distribution is shown in figure 4.15 and 4.16 respectively. It can be seen that there is no visible difference in misfit reduction in terms of absolute residuals.

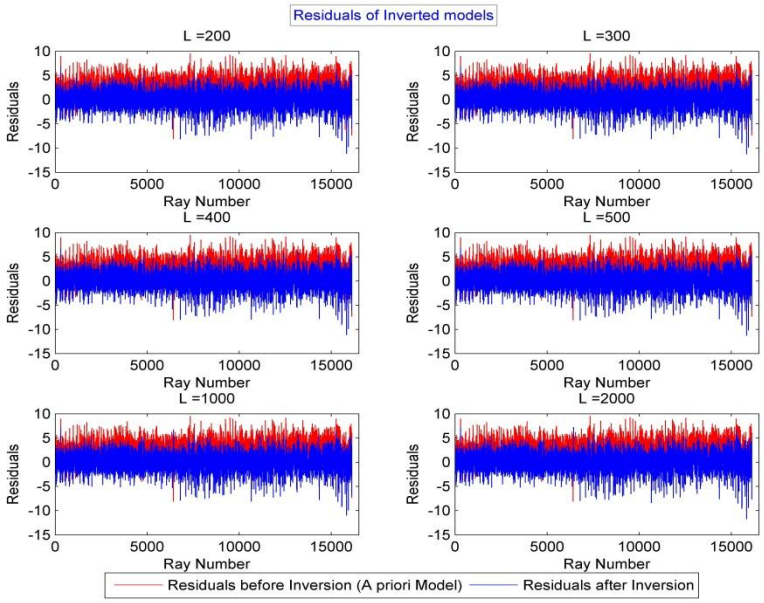

Figure 4.145: Residuals before (a priori model- Red) and after (Blue) inversion for different values of correlation length (L).

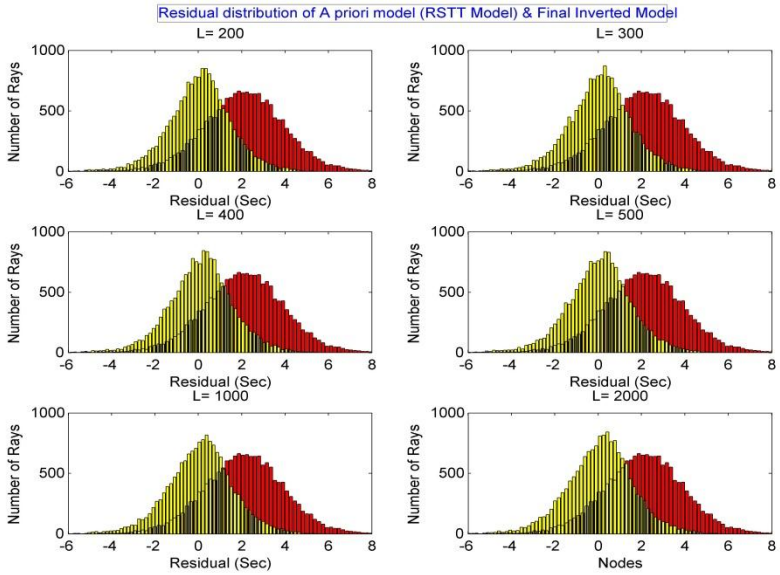

Figure 4.156: Residuals distribution for before (a priori model- Red) and after (Blue) inversion (for different choices of correlation lengths (L)).

For different values of correlation length (L), the percentage change for the inverted velocity (at Moho) with reference to initial /a priori model is shown in figure 4.17. It can be seen that for smaller correlation length, the system varies abruptly with up to 40% change. This huge variation can be explained by very sharp velocity anomalies but required excellent data coverage. For higher values of horizontal correlation length e.g. L= 2000 model is smoothed

making as good choice but it will ultimately reduce the possibility of imaging the small scale anomalies and anomalies with sharp boundaries.

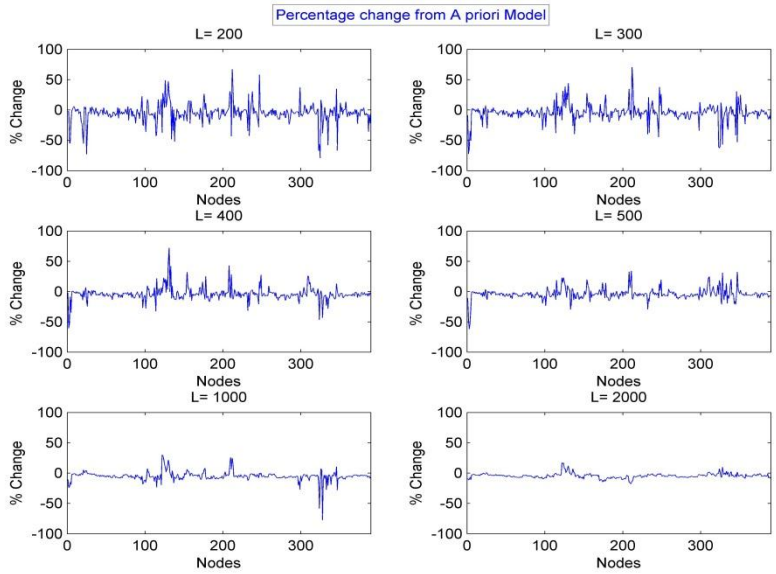

Figure 4.17: Percentage change in mantle slowness for different choices of correlation lengths

Spatial distribution of the percentage change for the inverted velocity (at Moho) with reference to a priori model (for L=300km) is shown in figure 4.18.It can be seen that very large peaks (+- 60%) corresponds to the very narrow zones along the boundaries of mapped area. So choice of a smaller correlation length will not have any negative effect on resolution and reliability of inverse solution.

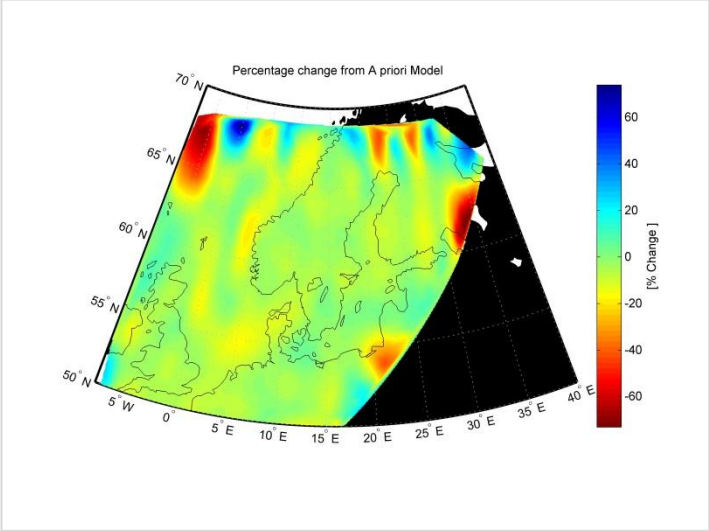

Figure 4.18: special distribution of percentage change in mantle slowness for L=300km.

Over all Data miss fit (RMS residuals) for various correlation lengths (L) is shown in Table 4.2. It can be seen that generally data miss fit reduced by choosing smaller correlation length

Table 4.2

Correlation length	200	300	400	500	1000	2000
RMS Residual (A priori Model)	28.69	28.69	28.69	28.69	28.69	28.69
RMS Residual (After Inversion)	14.99	15.13	15.29	15.23	15.65	15.94

Table 4.2: RMS residuals before and after inversion for different alternatives of horizontal correlation lengths

Inverted models (for mantle velocity) for different choices of correlation lengths are shown in figure 4.19. It can be seen that the overall trend as well as velocity anomalies are the same in all results. The only difference is the smoothness of the model. For smaller correlation lengths, velocity anomalies emerge with sharp boundaries whereas smoothness in the model increases with increasing correlation length.

From all above results it seems the least value of correlation length should be the best choice but a choice of smaller correlation length requires excellent path coverage in all parts of the mapped area. Although we have good path coverage in the area but due to the presence of clusters of events (especially due to events related to mining explosions) the path coverage is not smooth everywhere. By taking in account of all above reasons we have chosen correlation length of 300 km for final inverted model.

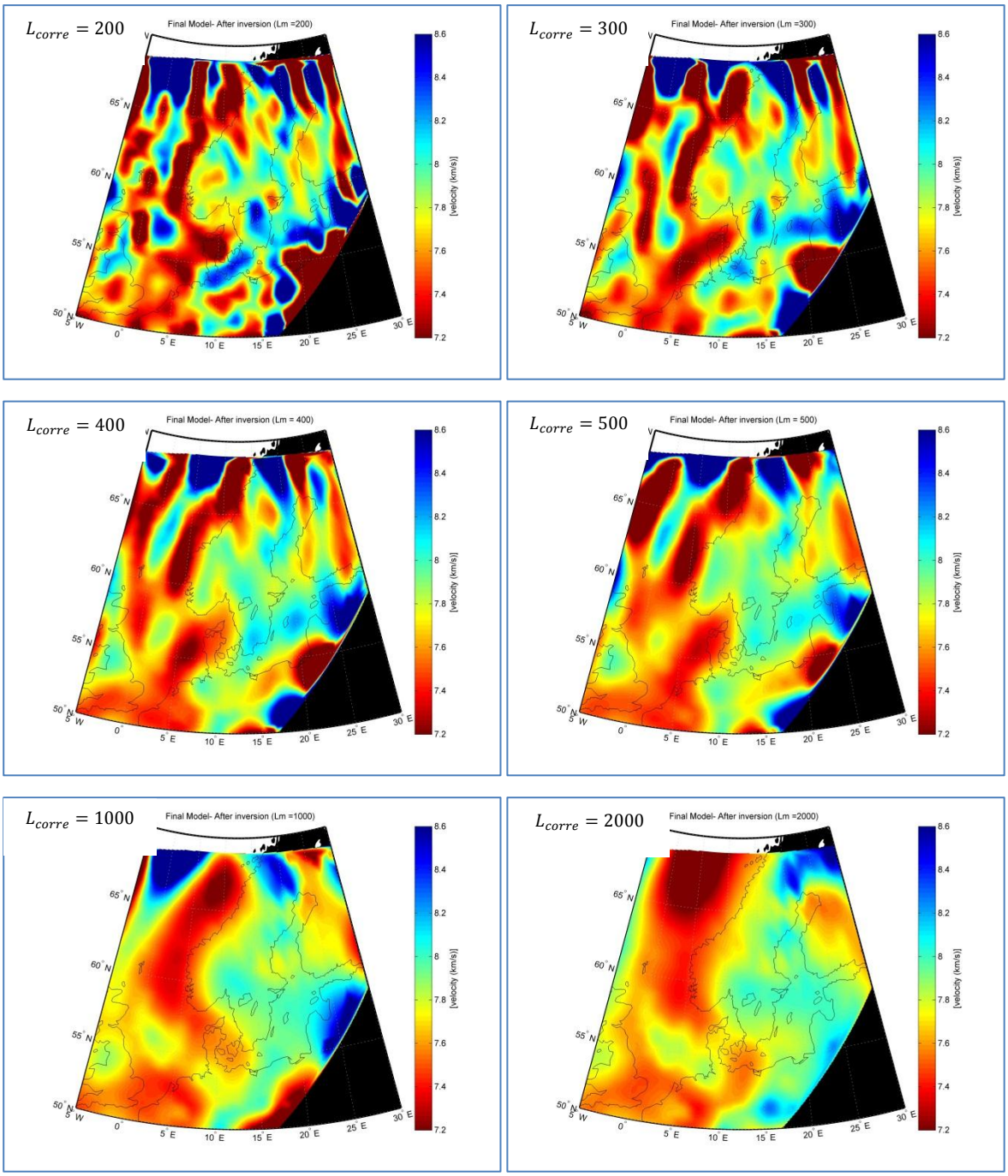

Figure 4.19: Upper mantle velocity models for various choices of horizontal correlation lengths.

Data used in this inversion are travel time observations. One event is recorded on various stations and one station has recorded number of events. So we assumed that there is no coupling between individual data values. A covariance matrix for data is defined as diagonal matrix with fixed standard deviation on its diagonal. There is no definite information about

the uncertainty in the dataset retrieved from ISC bulletin. In this study, a standard value of 0.01 sec is used as standard deviation for observed data.

Initial model in this study consist of null vector for mantle slowness and normalized velocity gradient and unit vector for crustal modifier. RSST (Regional seismic travel time model), presented in Myers *et al.* (2010) is used as a priori model. Inversion algorithm was run in iterative way. After first iteration reduction in the misfit of model with the observed data is very small.

RMS residual for initial and a priori model is 775.7 and 28.49 respectively. After four iterations this residual reduced to 15.13 (98% and 46% reduction with respect to initial and a priori model respectively).

4.5 Model quality assessment

There could be various sources of errors that can be mapped in the reconstruction of subsurface physical properties from travel time data e.g. geometry of sources and receivers, quality of observations and model parameterization. The most important source of errors are the uncertainties in model parameterization, these uncertainties could be due to inappropriateness of starting and a priori model, coarseness of model grid spacing, inaccurate crustal model and correction for topographic effects (Lee *et al.* 2002).

In case of travel time tomography, geometry of source and receiver could be somehow controlled by selecting the source receiver pairs providing good azimuthal coverage. Quality of observations is enhanced by applying various preprocessing of data before inversion. For model parameterization we perform various tests to ensure the quality of resulted model.

Inversion technique ties to find solution by minimizing the misfit between observed and predicted data but there could be many models that satisfy the predicted data without being physically plausible (Asgedom, 2009). Due to all above reasons it is wise to test the inversion for fitness to the observed data and physically plausibility of inverted model. In this tomography study following tests were performed to analyze the quality of solution

1. Data misfit : How well the predicted data (generated by final model) fits with the observed data (travel times)
2. Inversion Reliability: How well the inversion reveal the real subsurface anomalies in the inverted model (Synthetic test)

Misfit between observed and predicated data is defined by RMS residuals, given by

$$RMS = \sqrt{\frac{1}{N}\sum_{i=1}^{N}\frac{\left(d_{obs,i} - d_{prd,i}\right)^2}{\sigma_i^2}}$$

N is the number of data (Number of Pn rays), d_{obs} is the observed data (travel time observations), d_{prd} is the predicted data (Travel times obtained by the forward modeling of inverted model) and σ_i is the travel time uncertainties.

This misfit parameter is a good statistic tool to analyze the quality of inverted model with respect to fit to observed data (Asgedom 2009). As a general rule solution with least RMS could be considered as the best solution. RMS for different models encounter in this study are shown in figure 4.20

We started with the initial model (null vector for mantle slowness & normalized velocity gradient and unit vector for crustal modifier) which gave a RMS residual of 775.2 and a priori model (same as RSTT final model) with RMS residual of 28.5. After inversion, final inverted model with RMS of 15.13 (Iteration 3) was obtained. For the final model there is about 98% reduction from starting model and 47% form a priori model.

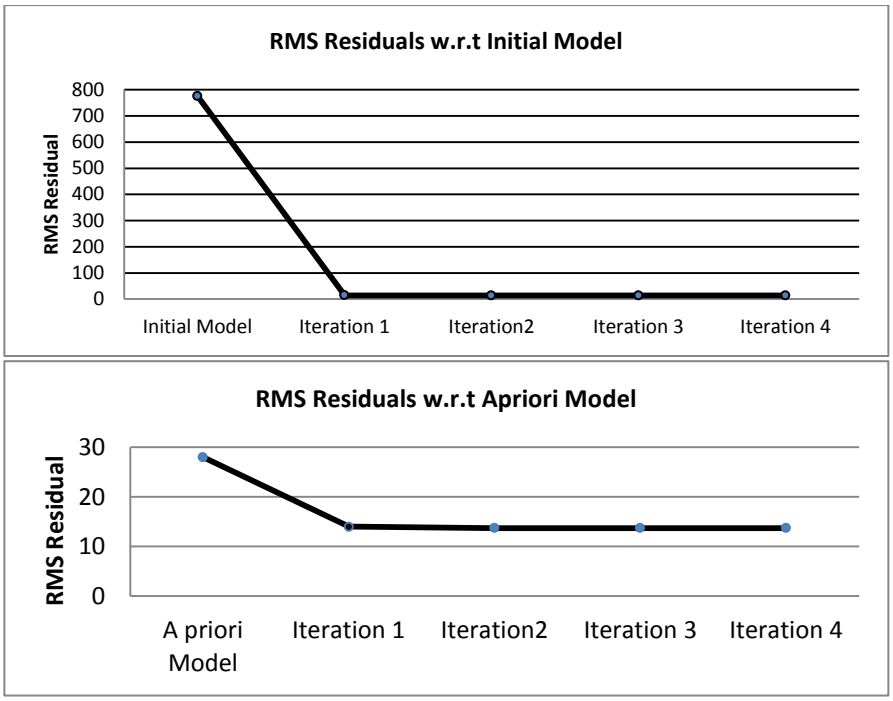

Fig 4.20: RMS residuals of different iteration with respect to Initial model (Upper fig) and A priori Model (lower figure)

Another insight of data misfit is the comparison of absolute residuals of different models. Figure 4.21 (Absolute residuals along ray number) and 4.22 (Histogram of residual distribution) is comparison between residuals of a priori model and final model obtained after inversion. It can be seen that after inversion residual distribution range become narrow and aligned along central line (zero residual).

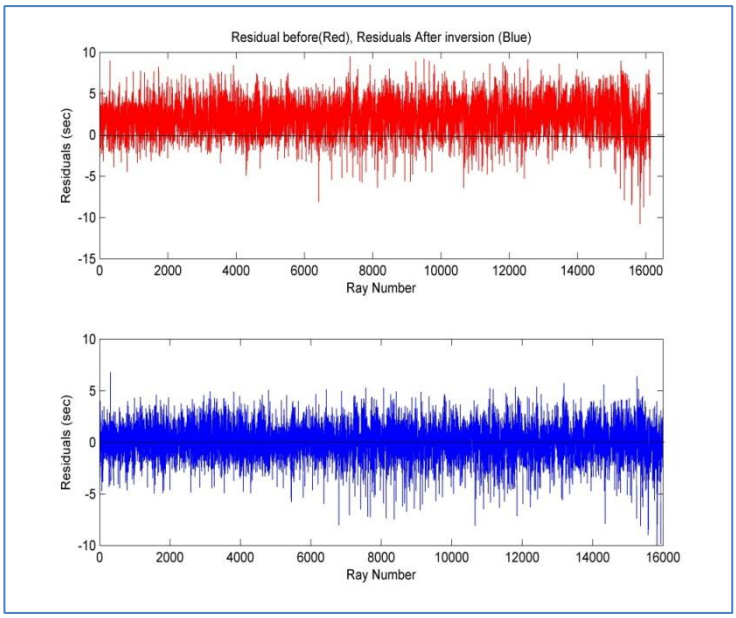

Figure 4.21**:** Residuals before (a priori model-Red) and after inversion (Blue). Black line indicates zero residual level

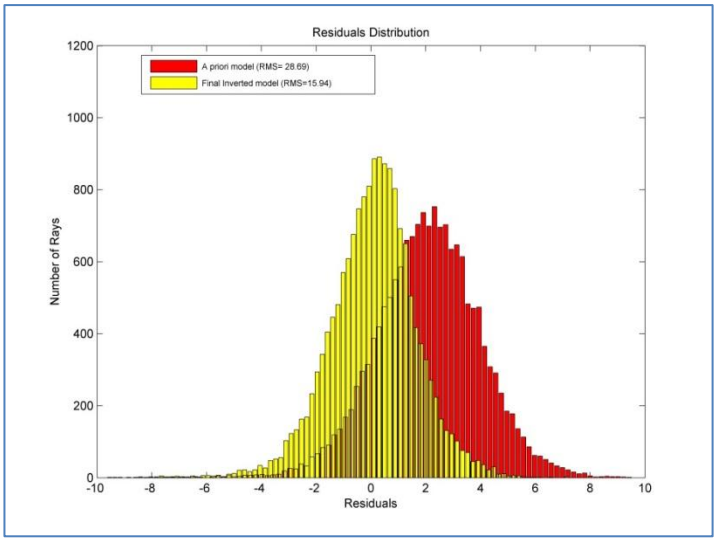

Figure 4.22: Distribution of the travel time residuals before and after inversions

There could be many models with the same residual misfit and many of these models may be not physically plausible. Further it is difficult to estimate parameter uncertainties and resolution of the inverted model due an explicit inverse operator in the computational formulation (Crosson 2007).

Posterior Resolution matrix

Averaging level of model estimate is described by the resolution matrix R. In other words it is a relation between m_{pred} & m_{true} . If R is an identity matrix than each model parameter is uniquely determined or we can say $m_{pred} = m_{true}$. Size and spread of off-diagonal elements measure the resolution. Farther the matrix from identity, more the model parameters are weighted averages of true model. (Tarantola 1987). (C.f. Section 3.5.6)

Plot of randomly selected three rows of Resolution matrix, plotted separately for each of the model parameter (mantle slowness, normalize velocity gradient and crustal modifier) is shown in figure 4.23. It can be seen that although the matrix is not a perfectly diagonal, spread in off diagonal elements is very small. So in conclusion, narrow peaks accruing near the main diagonal (node value for one row) of the matrix indicate that the model is well resolved.

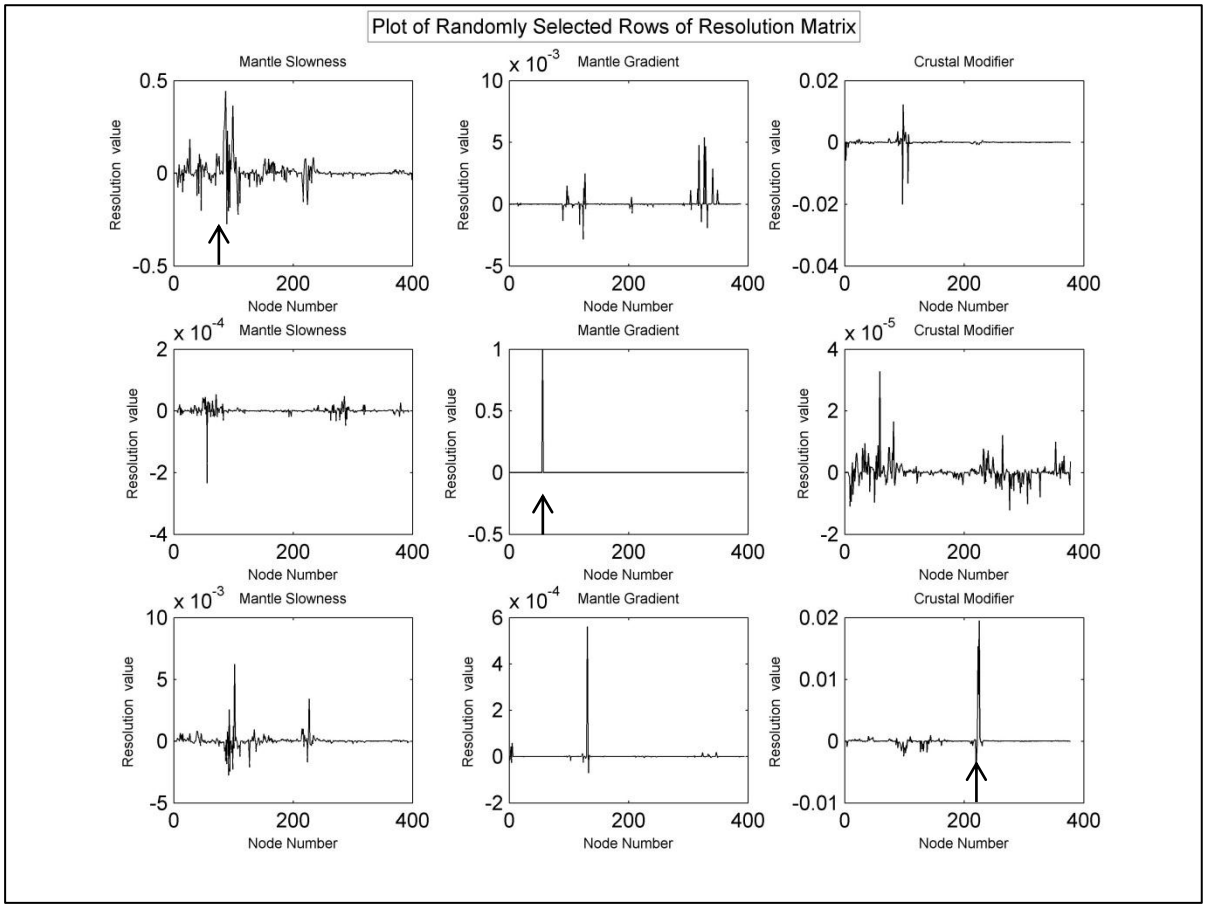

Figure4.23: Plot of Randomly selected 3 rows (Row 1, 450 & 1010) of Resolution matrix. Each row is terminated for number of model parameters i.e. mantle slowness, normalize velocity gradient and crustal modification. Arrow indicates that which model parameter is used for resolution analysis (having highest weightage) in one row of Resolution matrix.

Posterior Covariance matrix

Model covariance quantifies the uncertainties of the estimated parameters associated with data, kernels and errors (Song *et al.* 2004) (c.f. Section 3.5.6)

Plot of square root of diagonal elements of posterior covariance matrix for each model parameter is shown in figure 4.19. These values can be considered as error bars on posterior model vector. It can be seen that the average error bar for mantle slowness is 1×10^{-4} s/km (maximum of 4×10^{-4} s/km), for normalized velocity gradient is 5×10^{-5} (maximum of 2×10^{-4}) and for crustal modifier error bar is 5×10^{-5}. All these values are less than the a priori standard deviation so it shows that the data have contributed to reduce the uncertainty on the model. The spatial distribution of square root of diagonal elements of posterior covariance matrix (for mantle slowness) is shown in figure 4.25. It can be seen that the large errors (peaks in figure 4.24) belongs to the coroners of mapped area.

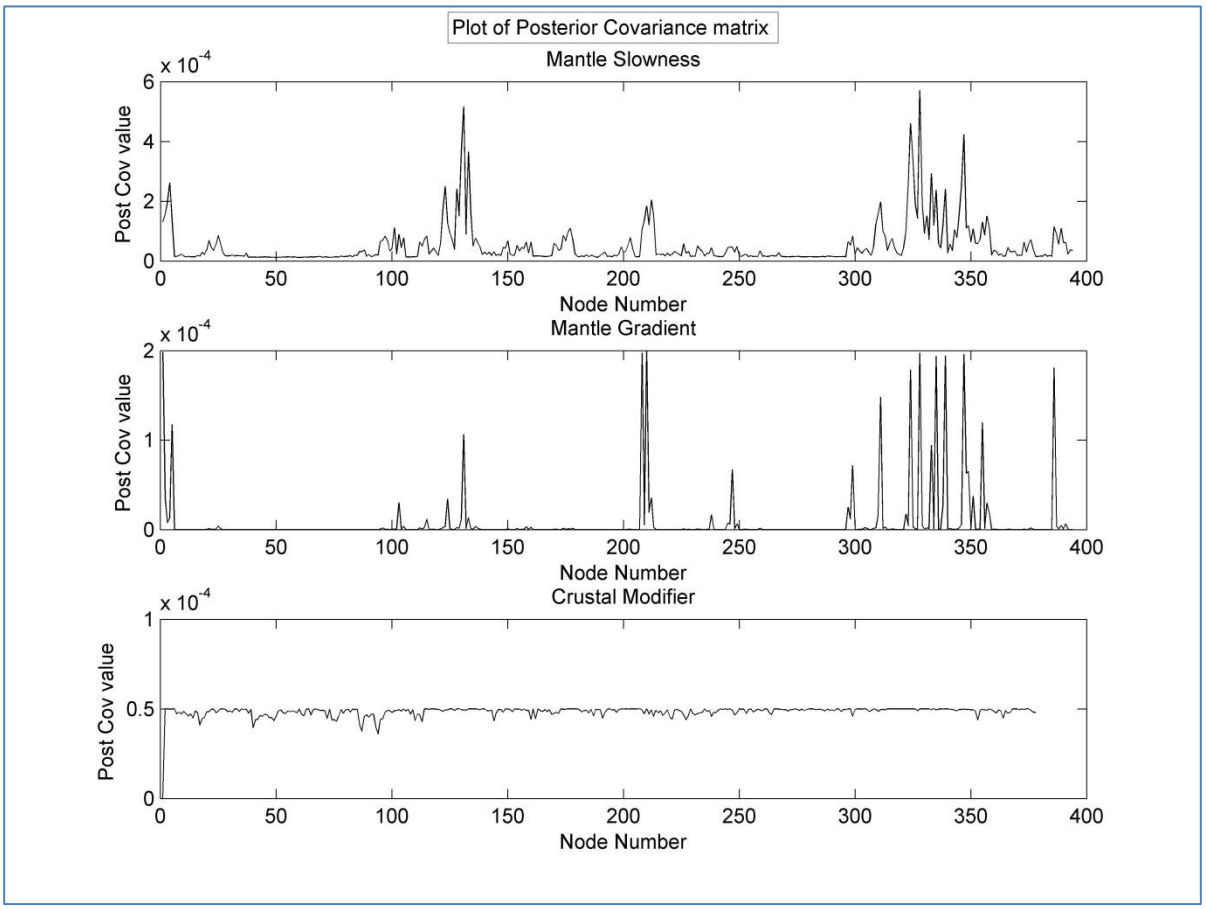

Figure4.24: Plot of square root of diagonal elements of Posterior Covariance matrix for mantle slowness, normalized velocity gradient and crustal modification.

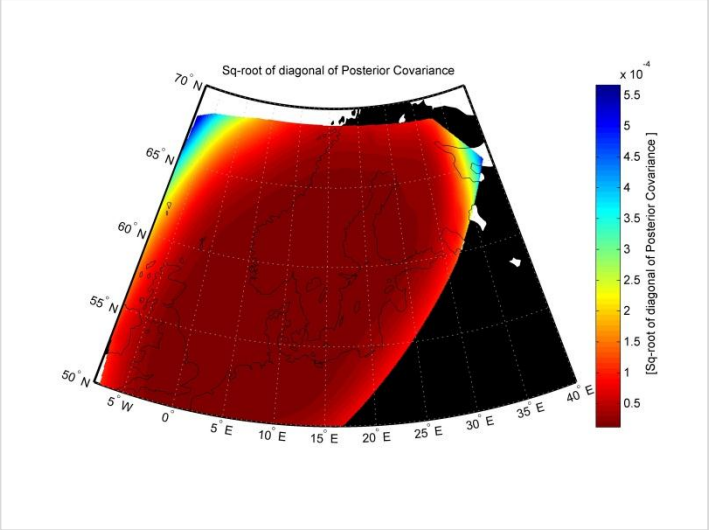

Figure 4.25: Spatial distribution of square root of posterior covariance matrix (for mantle slowness

Checkerboard sensitivity test

Checkerboard sensitivity test is a good tool to analyze the resolving power of tomographic inversion (ability of tomographic inversion to resolve structural details in the earth) (Crosson 2007). In this study, checkerboard test was performed by small perturbation signal (10% velocity contrast from the background model), created in four 3° × 3°, 2D regular checkerboard boxes. Then by forward modeling (Using equation 3.10) synthetic travel times were calculated on all source-station pairs used in original tomography. Random noise with mean value of zero (within limit of $\pm$ 0.05 sec) was added to this data. These synthetic travel times were then inverted in the same manner as the actual data. Comparison of recovered perturbed model with the input model demonstrates the sensitivity of original inversion of real data to recover similar details in real earth (Crosson 2007).

Two main factors that influence the results of checkerboard test could be amplitude & smoothness of the perturbation signal and size of the grid for retrieving model (Crosson 2007). In this study amplitude of velocity anomaly was set 10% lower than the background velocity (we do not expect to have greater velocity contrast in this area). Checkerboard box dimensions was set to 3° × 3°, 2D regular and grid (nodes spacing) was used as same of used in original inversion of real data (1° × 1°). RSTT velocity model of upper mantle was used as a starting model (shown in figure 4.28). To analyze the efficiency of inversion to

reveal anomalous subsurface, a highly averaged model (averaged from RSTT and True with 3:1) is used as a priori model (shown in figure 4.27).

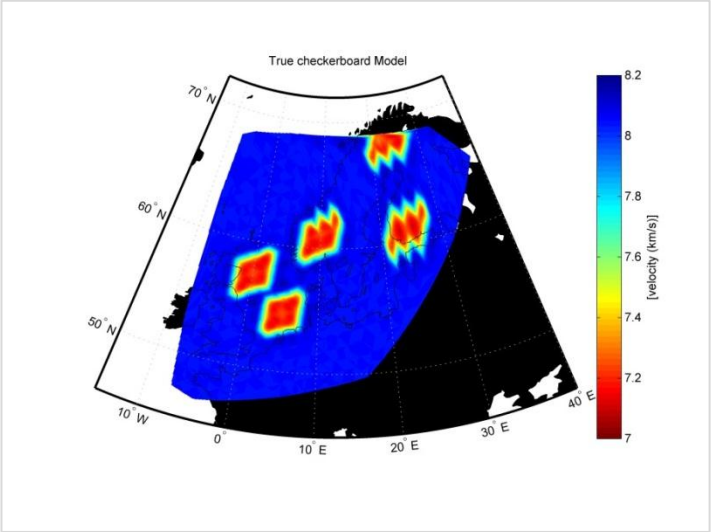

Figure 4.26: True Model (for upper mantle p wave velocity) input for checkerboard test. Background velocity was set as 8 km/s and four checkerboard boxes with velocity of 10% less than the background

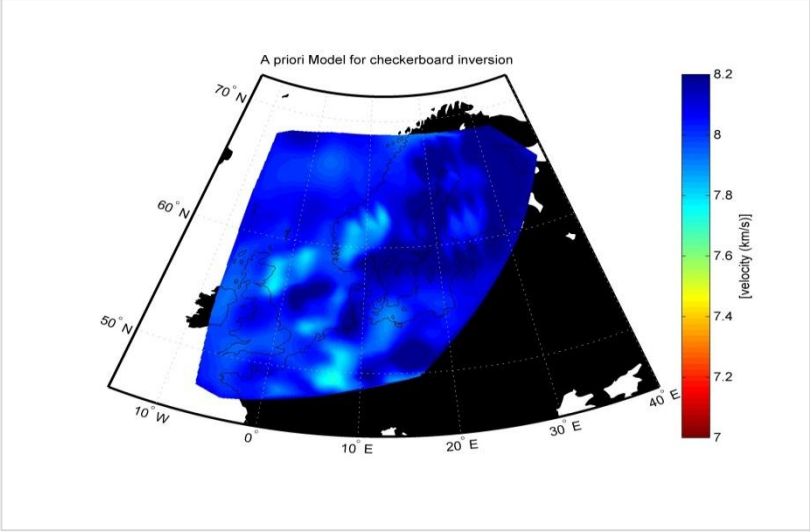

Figure 4.27: A priori model for inversion- a heavily averaged model generated by using RSTT and True model

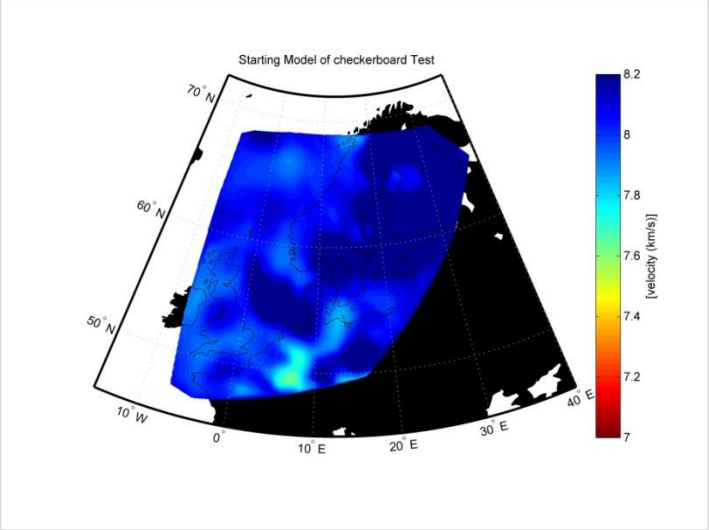

Figure 4.28: Starting model for inversion- Same as RSTT model

Inversion scheme used for this synthetic test is same as used in inversion of real data. Only difference here is that we used a very short correlation length for the formulation of a priori model covariance matrix. Reason for choosing very small correlation length is the fact that in checkerboard model we consider velocity anomalies with a sharp boundary with the background velocity. RMS residual for starting model was 27 that reduced to 0.6 after first iteration.

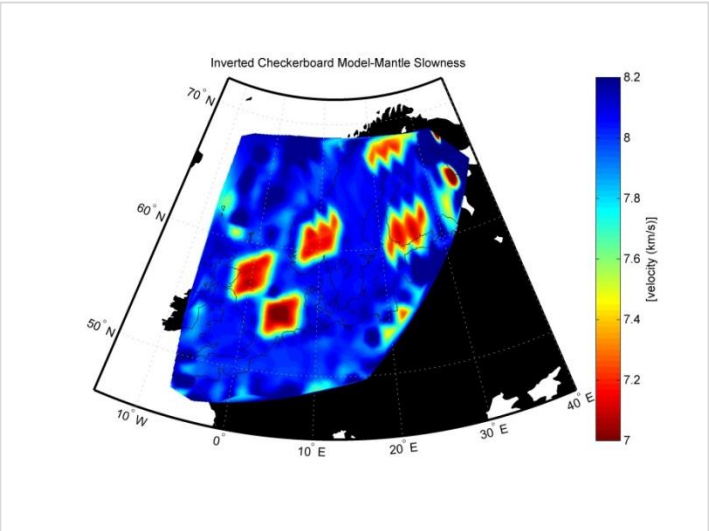

Figure 4.29: Model retrieved after inversion

Model retrieved after inversion is shown in Figure 29. It can be seen that at large extent this inversion was able to extract velocity anomalies, although the selected a priori model was very far from the true model. Further some leakage is observed at the boundaries of mapping

area. As this is the also an approximate boundary of ray coverage and ray density is not smooth so some error in inversion can be expected.

CHAPTER 5: RESULTS AND DISCUSSION

The goal of this study is to see the lateral variation of Pn wave speed for upper mantle beneath southern Scandinavia. Along with Pn velocity, two other parameters that have been analyzed are velocity gradient below Moho and a crustal modifier. These all model parameters were imaged on geographically distributed nodes with node spacing of approximately one deg. In order to extract new information from this tomography as compare the previously similar studies (Bannister *et al.* 1991; Husebye *et al.* 1986) we used a diving wave concept (c.f. section 3.4.2) in tomographic formulation as described by Myers *et al.* (2010). Further, the area to be imaged is extended on the western and southern side of Southern Scandinavia to see extension of velocity structure. Very dense ray path coverage (initially 90,000 rays) is used in this study. All the results presented in this section are generated by using horizontal correlation length of 300 km and a priori standard deviation of 0.001, 0.0002, and 0.00005 for mantle velocity, velocity gradient and crustal modifier respectively. Standard deviation for data was set to 0.01.

5.1 Upper Mantle P wave velocity

Result obtained for upper mantle velocity structure is shown in figure 5.1. A general trend for Baltic shield can be seen that P wave velocity is higher in the thicker and older part (Sweden area and west) and lower velocities in thinner and younger parts (Norway and offshore in west).

Most prominent feature in P wave velocity for Baltic shield area is the low velocity anomaly adjacent to the shore line of northern and central Norway. This low velocity anomaly also seems to extend to central and southern Norway, beneath the apex of Scandinavian mountains. In western side, this low velocity anomaly is possibly being extended to Iceland plume. These North-South trending anomaly from central and southern Norway, across North Sea coincides with Fennoscandian border zone (beneath Denmark). Among negative anomalies (Low velocity) other weak anomalies can be seen in east-central Sweden and another in South-central Finland.

A high velocity anomaly is seen in southern Sweden and central-northeastern Finland (more visible with $L_{Corr} = 2000$ (cf. Figure 5.3 (c))

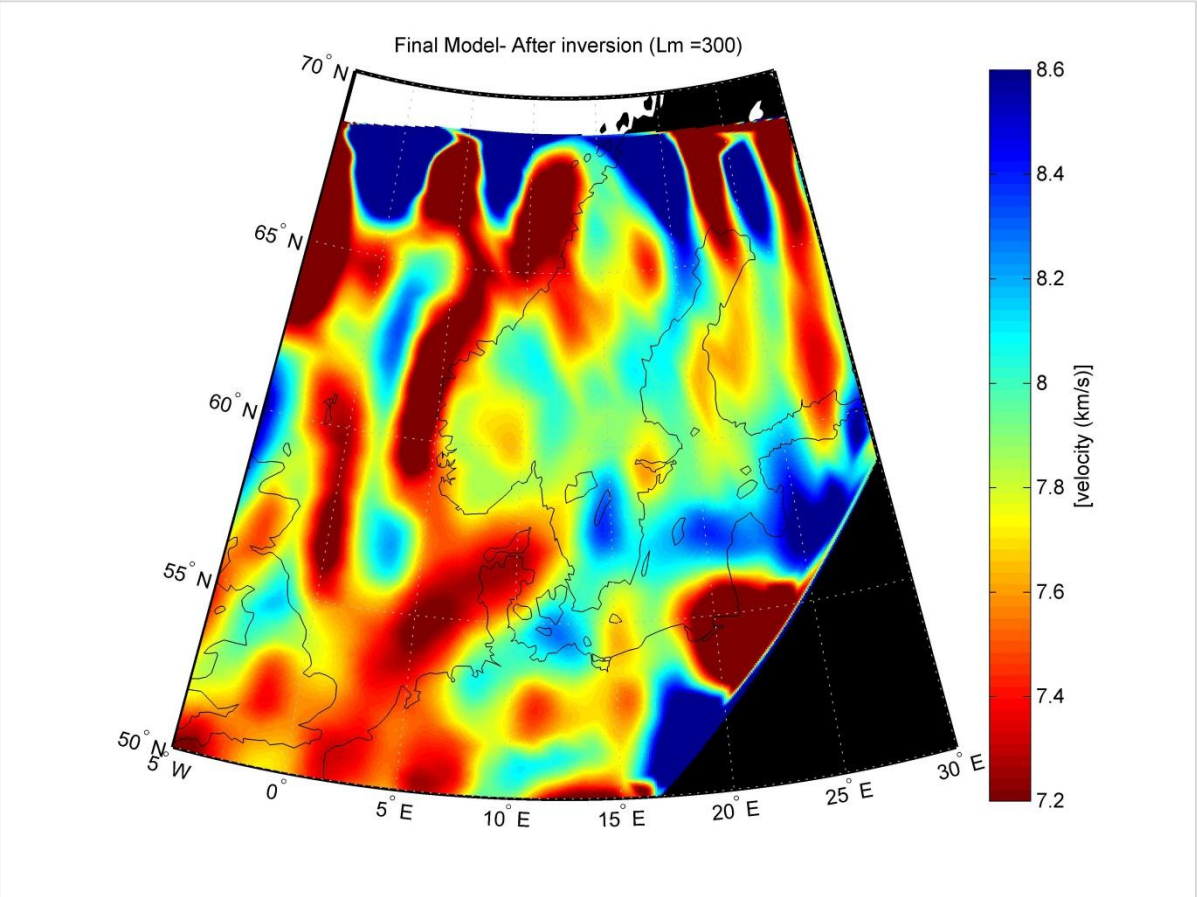

Figure 5.1: Upper mantle p wave velocities estimated from real travel time data. Velocity ranges from 7.2km/s to 8.6 km/s

Result of this inversion study is in good agreement with previous geophysical studies conducted for this area. Most of the previously conducted Pn tomography studies for this area were performed by inverting travel times for only mantle P wave velocities. There is no study in which mantle gradient or crustal modifier is used as unknown in model vector.

Pn tomography study by Bannister *et al.* 1991 (Shown in fig 5.2 (b)) have similar results i.e. low velocity anomalies in central and southern Norway and south- Central Finland. Notable difference between our study and Bannister's study is the continuity of prominent low velocity anomalies (in Central and southern Norway) to the west and further south-east through cost of North Sea to Denmark area.

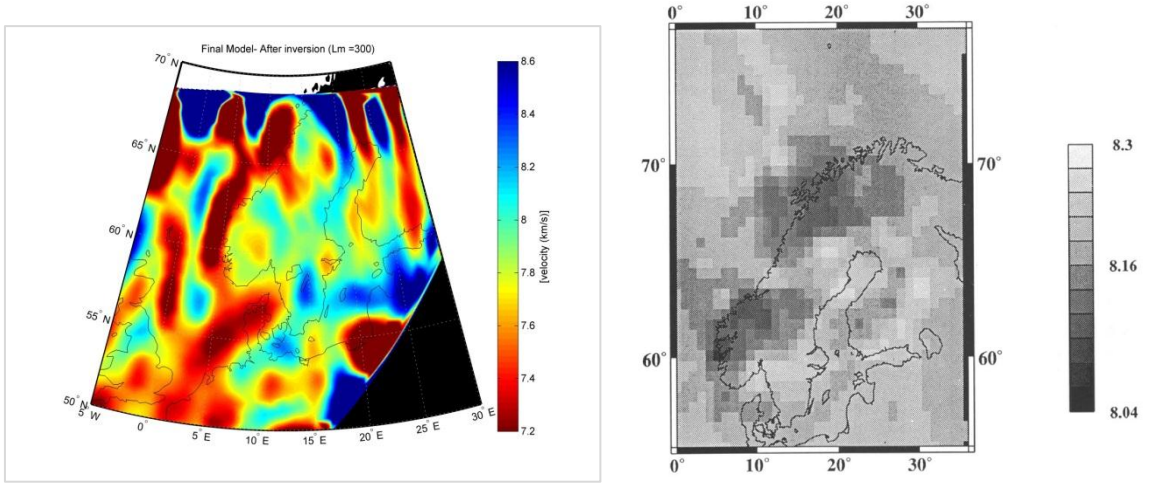

Figure 5.2: (a) Upper mantle p wave velocity map by our study (b) Upper mantle p wave velocity map by Bannister *et al.*1991

Results from p wave travel time residual study by Bondo *et al.* (2009) also support our results i.e. late arrivals in southern Norway and Denmark part (low velocity) and early arrivals for southern Sweden (high velocity). Further the boundary between shield-like structure of Baltic shield and platform-like of southern Norway is also more or less same in both studies .This phenomena is more clear in a smoothed model ($L_{Corr} = 2000$) (figure 5.3 (c))

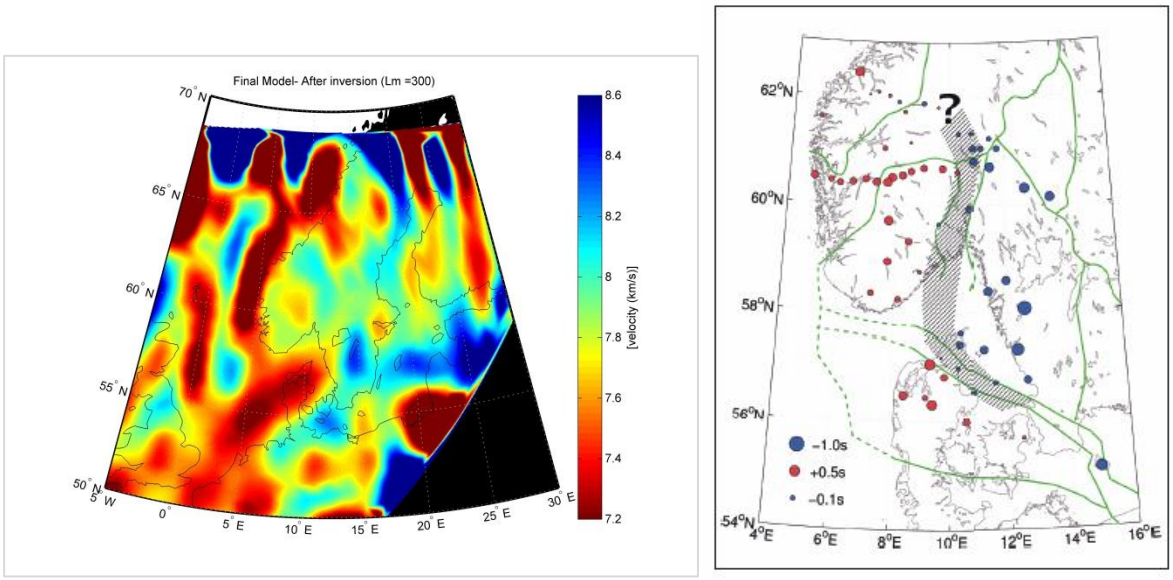

(a) (b)

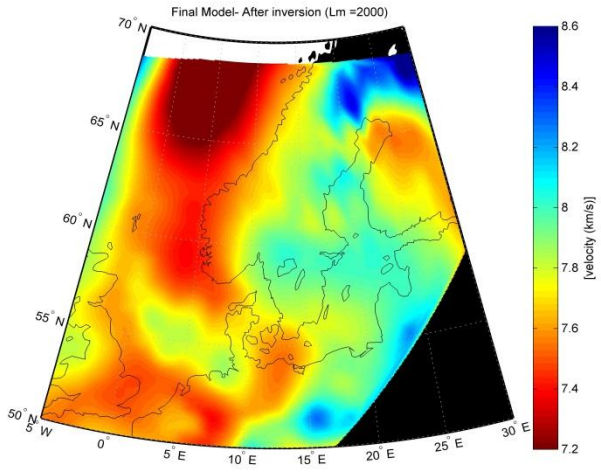

(c)

Figure 5.3: (a) Upper mantle p wave velocity map with horizontal correlation length of 300km (b) Interpreted lithospheric transition zone (hatched) with mean p-residuals after topographic and crustal correction (Bondo *et al.* 2009) (c) Upper mantle p wave velocity map with horizontal correlation length of 2000km (smoothed model)

Results of tomographic mapping of lithosphere-asthenosphere by Husebye et al. (1986) are also very similar to our results. Seismic velocity image for lower lithosphere and/or upper mantle (Husebye *et al.* 1986) is shown in figure 5.4 (b). It can be seen that upper mantle velocity in southern Norway, Oslo Graben and in basin area is low as compared to velocities in the thicker and older part of Baltic shield (southern Sweden). In spite of topographical difference, velocity structure in the southern Norway has good resemblance with the velocities found in Denmark area (low velocity upper mantle)

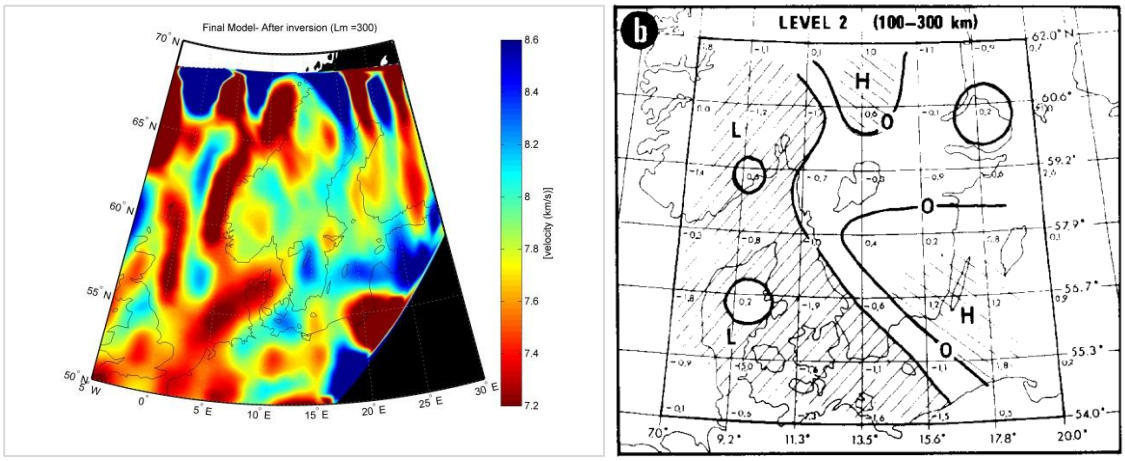

(a) *(b)*

Figure 5.4: (a) Upper mantle p wave velocity map from our study (b) Seismic image of 100-300 km, comprising lower lithosphere and/or upper mantle. L: low velocity region & H: high velocity region by Husebye *et al.*, 1986.

5.2 Upper Mantle p wave velocity gradient

Mantle velocity gradient for this area is shown in the figure 5.5. No high or low velocity anomaly was observed in terms of velocity gradient in this area. Instead, there is a smooth and negative velocity gradient throughout the area.

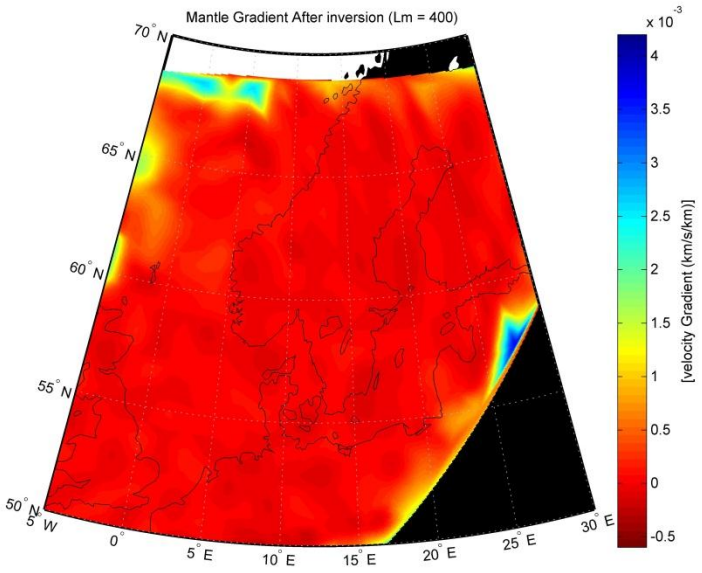

Figure 5.5: Mantle gradient (km/sec/km) of inverted model. Gradient ranges from -0.006 to 0.0042 km/sec/km.

5.3 Crustal modification

As explained earlier, our tomographic formulation gives space to adjust the crustal leg of total travel time. This adjustment is applied to the crustal traveltime and is not interpreted in terms of thickness, velocity and depth of any particular layer. There are various physical parameters for crust (e.g. Thickness/velocity/Depth of any particular layer or a combination of layers) that can be the reason behind the crustal modification. Result after inversion for crustal modifier is shown in figure 5.6.

The most prominent feature in this result is the presence of positive anomaly (greater than one) in the southern Norway. There is already a low velocity anomaly for upper mantle at

the same place (cf. figure 5.1) .This high crustal modifier (greater than one) reflects that the time taken by the wave in the crust is larger than the expected travel time for the given crustal structure. This velocity anomaly can be explained by two alternatives;

1. Crustal velocities are lower in this area as compare to the velocities defined in a priori model.
2. The crust is thicker than defined in the a-priori model and crustal propagation time should therefore be increased
3. There is a possibility that the negative velocity anomaly in the mantle is leaked into to crustal part during inversion. In other words, mantle beneath the southern Norway have lesser velocity than presented in the inverted velocity model

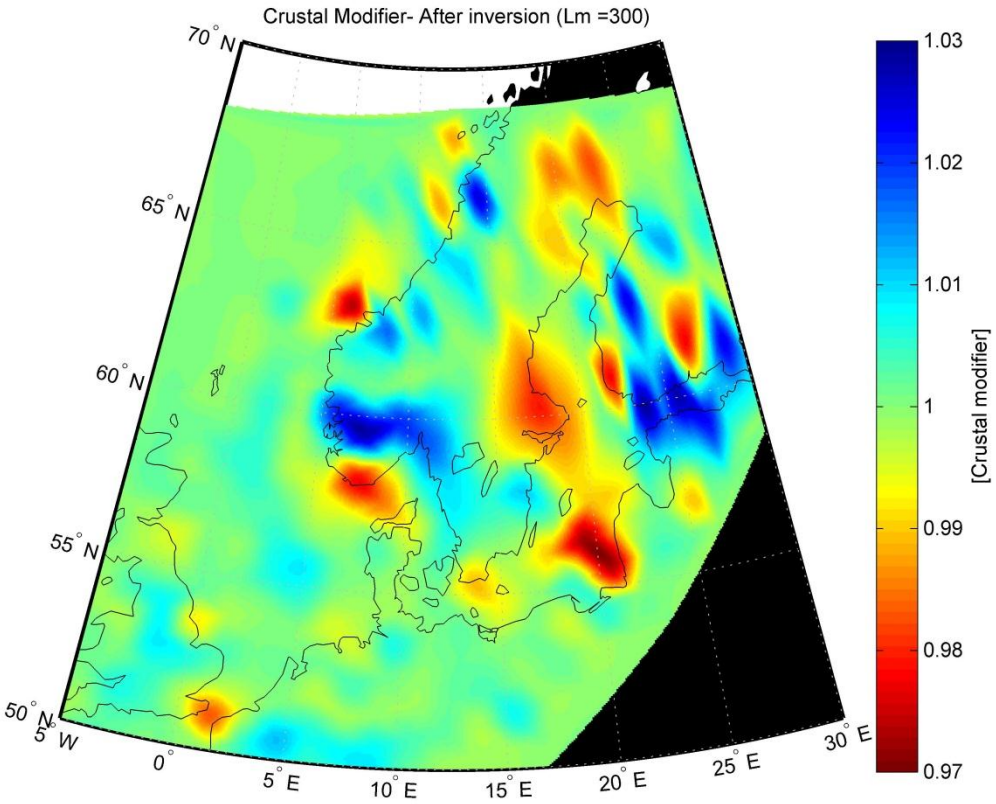

Figure 5.6: Crustal modifier after inversion, value greater than one indicates that time take by wave in crust is higher than expected and values less than unity means the early arrivals. Reasons of these late and early arrivals could be many factors like variation in crustal velocities, Moho depth or it could be the low velocity anomaly in the mantle that is leaked into the crustal part during inversion.

CHAPTER 6: CONCLUSIONS AND FUTURE RECOMMENDATIONS

We have presented results of our Pn tomographic inversion along with comparison of these results with other similar studies. In this chapter we will conclude this study with final remarks and some possible future directions to improve further understanding of subsurface structures and geodynamics of this area.

6.1 Conclusions

Imaging of upper mantle structure is an efficient tool to understand the cause of present day high topography of an area that do not possess any solid evidence of major tectonic activity or any other uplift process. In this thesis we constructed a 2D velocity and velocity gradient model for the upper mantle. Additional information about the velocity structure of crust was also extracted in this inversion (crustal modifier). Results from this study are nicely aligned with the structural features present in this area.

Tomographic formulation of Myers *et al.* (2010) and preconditioned conjugate inversion methodology of Tarantola (1987) is employed to invert travel times for model parameters. In addition to the mantle velocity perturbations this tomographic formulation also allows to image mantle velocity gradient and crustal modification in the subsurface.

Results of mantle velocity imaging indicates a general trend of low velocity in the thinner and younger part of Baltic shield (Norway and offshore) whereas high velocity in the thicker and older parts (Sweden and Baltic).

Further, as expected, low velocities are observed in the younger part of central Europe. North Sea is observed to have high velocity surrounded by low velocities of southern Scandinavia and central Europe.

Velocity structure beneath southern and central Norway is anomalous (having low velocity) with respect to the rest of Baltic shield. These low velocities are probably being connected to Iceland plume in west by a narrow channel where low velocities are related to hot and

shallow mantle beneath the plume. These results are in good agreement with previous studies (Bannister *et al.* 1991; Bondo *et al.* 2009; Husebye *et al.* 1986)

Another important observation is the crustal modifier after inversion. In southern Norway crustal modifier greater than one suggests that either the crust in this area is of low velocity as compared to the rest or it could be a low velocity anomaly in the mantle that is leaked into the crustal part during inversion. Both these possible scenarios lead to the idea that upper mantle and/or lower crust are anomalous in this area (having low velocity).That can be the cause of formation and sustainability of high topography of Scandinavian mountains.

6.2 Future work

Future work that could further help to understand the subsurface structure beneath the southern Scandinavia could be directed to the following directions

- It would be advantages to perform a P wave tomography first to estimate the true velocity structure of the crust. Then by keeping the crustal structure fixed, a Pn tomography could be performed with better efficiency.
- Add anisotropic parameters as unknown in model parameters to see if any anisotropy is present in this area.
- Perform inversion with both Sn and Pn waves simultaneously on same data set and methodology. Anomalies form Sn study can be then compared to the results of Pn to increase confidence.
- Include data from further west (Mid-Atlantic ridge area) to properly resolve connection of low velocity anomaly in southern Scandinavia to the Iceland plume
- Transform Pn velocity into other physical parameters e.g. temperature and density and correlate these anomalies to geodynamic process involved in uplifting.

References

1. Bannister, S.C., Ruud, B.O. & Husebye, E.S., 1991. Tomographic estimates of sub-Moho seismic velocities in Fennoscandia and structural implications, *Tectonophysics,* **189,** 37–53.
2. Bondo Medhus, A., Balling, N., Jacobsen, B.H., Kind, R. & England, R.W., 2009. Deep structural differences in southwestern Scandinavia revealed by P-wave travel time residuals, *Norwegian J. Geol.,* **89,** 203–214.
3. Crosson, S., 2007. Checkerboard Test for 3-D Tomography Model of Washington Cascadia Margin., *Earth and Space Sciences, University of Washington, Seattle, Washington*
4. Ebbing, J. & Olsen, O., 2005. The Northern and Southern Scandes— structural differences revealed by an analysis of gravity anomalies, the geoid and regional isostasy, *Tectonophysics,* **411,** 73–87.
5. Frederiksen, S., Nielsen, S.B. & Balling, N., 2001. A numerical dynamic model for the Norwegian-Danish Basin, *Tectonophysics,* **343,** 165–183. Gorbatschev, R. & Bogdanova, S., 1993. Frontiers in the Baltic Shield, *Precambrian Res.,* **64,** 3–21.
6. Fjldskaar, W., 1997. Flexural rigidity of Fennoscandia inferred from the postglacial uplift, *Tectonics.,* **16-4,** 596-608
7. Fjeldskaar, W., Lindholm, C., Dehls, J.F., Fjeldskaar, I., 2000, Postglacial uplift, neotectonics and seismicity in Fennoscandia, *Quaternary Science Review*., **19**, 1413-1422
8. Gadallah, M.R., 1994. Reservoir Seismology: Geophysics in Nontechnical Language. Tulsa, klahoma: *PennWell Books.*
9. Husebye, E.S., Hovland, J., Christofferson, A., A° strøm, K., Slunga, R. & Lund, C.E., 1986. Tomographic mapping of the lithosphere and asthenosphere beneath Southern Scandinavia and adjacent areas, *Tectonophysics,* **128,** 229–250.
10. Lay, T., Wakkace, T. C., 1995. Modern Global Semiology, *Academic press, ISBN 13:978-0-12-732870-6*
11. Lee, H.K.W., Kanamori, H., Jennings, P.C., Kisslinger, C., 2002, An international handbook of earthquake and engineering seismology, *International association of seismology and physics of earth interior (IASPEI).,* ISBN 0-12-440652-1

12. Maupin, V., 2011. Upper-mantle structure in southern Norway from beamforming of Rayleigh wave data presenting multipathing, *Geophys. J. Int.,* **185,** 985–1002.
13. Menke, V., 1987. Geophysical data analysis: Discrete inverse theory. *International geophysics series*, **45.** ISBN: 0-12-490921-3
14. Montagner, J.P., & Tanimoto, T., 1990. Global Anisotropy in the upper mantle inferred from the regionalization of phase velocities. *Journal of Geophysical Research*. **95**, 4797-4819
15. Myers, S., Begnaud, M., Ballard, S., Payanos, M., Phillips, W.S., Ramirez, A., Antolik, M., Hutchenson, K., Dwyer, J., Rowe, C., and Wangner, G., 2010. A crustal and upper-mantle model of Eurasia and North Africa for Pn Travel-time Calculation, *Bulletin of the seismological society of America*, **100**, 640-656
16. Nielsen, S.B. *et al.,* 2009. The evolution of western Scandinavian topography: a review of Neogene uplift versus ICE (isostasy-climate-erosion) hypothesis, *J. Geodyn.,* **47,** 72–95.
17. Padina, S., Churchill, D., Bording. R.P., 2006. Travel time inversion in seismic tomography. Retrieved from: *http://www.cs.mun.ca/~davidc/publications/HPCSPaper.pdf*
18. Pasyanos, M. E., Walter, W. R., Flanagan, M. P., Goldstein, P., and Bhattacharyya, J., 2004. Building and testing an a priori geophysical model for western Eurasia and North Africa, *Pure & Applied Geophysics*. **161**, 235–281.
19. Pérez-Gussinyé, M., A.R. Lowry, A.B. Watts & I. Velicogna, 2004. On the recovery of the effective elastic thickness using spectral methods: examples from synthetic data and from the Fennoscandian Shield. *Journal of Geophysical Research*, doi:10.1029/2003JB002788
20. Poudjom Djomani Y.H., Fairhead J.D. & Griffin W.L., 1999, The flexural rigidity of Fennoscandia: reflection of the tectonothermal age of the lithospheric mantle, *Earth and Planetary Science Letters*, **174**, 139-154.
21. Rohrman, M., and P. van der Beek., 1996. Cenozoic postrift domal uplift of North Atlantic margins: An asthenospheric diapirism model. *Geology*, 24, 901-904
22. Smelror, M., J. Dehls, J. Ebbing, E.R.Lundin, O. Nordgulen, P.T. Osmundsen, O. Olesen, D. Ottesen, C. Pascal, T. F. Redfield, and L. Rise., 2007. Towards a 4D

topographic view of the Norwegian Sea margin. *Global and Planetary Changes*, **58**, 382-410.

23. Stratford, W., Thybo, H., Faleide, J.I., Olesen, O. & Tryggvason, A., 2009. New Moho map for onshore southern Norway, *Geophys. J. Int.,* **178,** 1755–1765.
24. Song, L.-P., Koch, M., and Schlittenhardt, J., 2004. 2-D Pn-velocity tomography underneath Germany using regional travel times. *Geophysics. Journal International.* **157,** 645–663.
25. Svenningsen, L., Balling, N., Jacobsen, B, Kind, R, Wylegalla, K. & Schweitzer, J., 2007. Crustal root beneath the highlands of southern Norway resolved by teleseismic receiver functions, *Geophys. J. Int.,* **170,** 1129–1138.
26. Tarantola, A., 1987. Inverse Problem Theory: Methods for data fitting and model parameter estimation. *Elsevier science B.V.* ISBN 0-444-42765-1 (U.S)
27. Weidle, C. & Maupin, V., 2008. An upper-mantle S-wave velocity model for northern Europe from Love and Rayleigh group velocities, *Geophys. J. Int.,* **175,** 1154–1168.
28. Zhao, L.-S., 1993. Lateral variations and azimuthal isotropy of Pn velocities beneath Basin and Range province, *Journal of Geophysical Research*. **98**, 22109– 22122.
29. Zhao, L.-S., and J. Xie., 1993. Lateral variations in compressional velocities beneath the Tibetan Plateau from Pn travel time tomography, *Geophys. J. Int.*, **115**, 1070–1084.

Appendix A

1) Pre-Processing of Raw data

```
clc; clear all; close all;clf
%% ------------------Preprocessing of Data ----------------------------------------%%
%Author:
% Adnan Latif
% University of Oslo-Oslo, Norway
% adn_latif@hotmail.com
% Version: Oct/12

%% ------------------------------------ Data Import-----------------------------%%
dist1 =pndata1(:,7);baz1=pndata1(:,8); res1=pndata1(:,13); tdef1=pndata1(:,14);
amp1=pndata1(:,15); per1=pndata1(:,16); orid1 =pndata1(:,1);
stalat1=pndata1(:,4); stalong1=pndata1(:,5); staele1=pndata1(:,6); orlat1 =pndata1(:,20);
orlong1 =pndata1(:,21); ordepth1 =pndata1(:,22);
ormag1=pndata1(:,25); tt1 =pndata1(:,27);

%%  Replacing NaN in residual & origion depth
% Replacing NaN in residual & origion depth to 10000
k = find(isnan(res1))'; res1(k) = 10000; l=find(isnan(ordepth1))'; ordepth1(l)=10000;
a3=find(tt1==0);tt1(a3)=10000;
a1=find(res1==0);res1(a1)=0.0001;a2=find(ordepth1==0);ordepth1(a2)=0.0001;%
Replacing 0 into 0.0001
pndata2=[stalat1,stalong1,dist1,staele1,orid1,orlat1,orlong1,ordepth1,ormag1,tt1,res1,baz1];
% New Data Set
clearvars('k','a3','l','a1','a2','stalat1','stalong1','dist1','staele1','orid1','orlat1','orlong1','ordepth1',
'ormag1','tt1','res1','tdef1','baz1','per1','amp1')

%% Replacing the data which do not have residuals or origion depth (now having
valuse 10000)
s0=size(pndata2); sz0=s0(1,1);
pndata3=zeros(sz0,12);
for i=1:1:sz0
   if pndata2(i,11)==10000 || pndata2(i,8)==10000 || pndata2(i,10)==10000;
      pndata3(i,:)=0; else  pndata3(i,:)=pndata2(i,:); end

end
clearvars('s0','sz0','i','pndata2')

%% ----------------------------------------Filtering of data----------------------------------%%
dist11=1.799;dist22=15; % Epicentral distance for filter
s3= size(pndata3); sz3=s3(1,1); pndata4=zeros(sz3,12);
for ai=1:1:sz3;
      if pndata3(ai,3)<=dist11||pndata3(ai,3)>=dist22; pndata4(ai,:)=0; else
pndata4(ai,:)=pndata3(ai,:); end
```

```
end
pndata4(all(pndata4==0,2),:)=[]; % Removing zeros rows from the filtered data
clearvars('dist11','dist22','s3','sz3','pndata3','ai')
%% Calculation of arrival times from RSTT model, Using SLBM
str1=size(pndata4(:,1));
str2=str1(1,1);
pndata_r=zeros(str2,8);
for rst=1:1:str2
cm1='bin/slbmtestcc models/na1010pn Pn';
orlatrst= num2str(pndata4(rst,6)); orlongrst= num2str(pndata4(rst,7)); ordepthrst=
num2str(pndata4(rst,8));
stalatrst= num2str(pndata4(rst,1)); stalongrst= num2str(pndata4(rst,2)); staelerst=
num2str((pndata4(rst,4))/1000);
cm2=[cm1,' ',orlatrst,' ',orlongrst,' ',ordepthrst,' ',stalatrst,' ',stalongrst,' ',staelerst];
[sb,sd]=system (cm2);

pndata_r(rst,1)=str2num (sd(1,326:333));pndata_r(rst,2)=str2num
(sd(1,356:364));pndata_r(rst,3)=str2num (sd(1,388:395));pndata_r(rst,4)=str2num
(sd(1,418:426));
pndata_r(rst,5)=str2num (sd(1,454:461));pndata_r(rst,6)=str2num
(sd(1,489:496));pndata_r(rst,7)=str2num (sd(1,523:531));
pndata_r(rst,8)=str2num (sd(1,559:566));
end
clearvars('str1','str2','s3','sz3','pndata3','rst','cm1','orlatrst','orlongrst','ordepthrst','stalatrst','stal
ongrst','staelerst','cm2','sb','sd')

% New data set
%pndata_r=[distance,Traval Time, TT uncertainty, Slowness, SH Unvertainty, dtt/dlat,
dtt/dlon, dtt/depth]
res_rst=pndata4(:,10)-pndata_r(:,2);
pndata4_2=[pndata4(:,1:10),res_rst,pndata4(:,12)]; %For residuals from RSTT model
pndata4_1=pndata4;
clearvars('res_rst','pndata4')% 'pndata_r' have to be deleted in the last

%% ----------------------------------Filtring for Residuals ----------------------------%%
reslim=4; % Residual Limit for filter on aki 35
s4= size(pndata4_1); sz4=s4(1,1); pndata5=zeros(sz4,12);
for ai=1:1:sz4;
      if pndata4_1(ai,11)> reslim || pndata4_1(ai,11)<-(reslim); pndata5(ai,:)=0; else
pndata5(ai,:)=pndata4_1(ai,:); end
end
pndata5(all(pndata5==0,2),:)=[]; % Removing zeros rows from the filtered data
clearvars('s4','sz4','ai')

% For Residualts for RSTT
s4= size(pndata4_2); sz4=s4(1,1); pndata5_2=zeros(sz4,12);
for ai=1:1:sz4;
```

```
    if pndata4_2(ai,11)> reslim || pndata4_2(ai,11)<-(reslim); pndata5_2(ai,:)=0; else
pndata5_2(ai,:)=pndata4_2(ai,:); end
end
pndata5_2(all(pndata5_2==0,2),:)=[]; % Removing zeros rows from the filtered data %
Change from pndata5_1 to pndata5_2
clearvars('reslim','s4','sz4','ai')

%% Total Number of Events used
ori=pndata5(1,5);
num=1;
for i=1:size(pndata5)
   if pndata5(i,5)== ori;
      num=num + 0; else num=num + 1; end ;
   ori=pndata5(i,5);
end
Total_Number_of_Events = num;
clearvars('ori','num','i','ori')

%% Assigning Bin Number
dl=0.3; dln=0.5; % size of bins
ll=[40:dl:70]';lln=[-10:dln:40]'; bin=[ll,lln];
sz5=size(pndata5); s5=sz5(1,1);
bin_lat=zeros(s5,1);
for z=1:s5;
 for z1=1:size(bin);
      if  pndata5(z,6)>=bin(z1,1)&& pndata5(z,6)< bin(z1+1,1);
          bin_lat(z)=z1;
      end
 end
end

bin_long=zeros(s5,1);
for zz=1:s5;
 for zz1=1:size(bin);
      if  pndata5(zz,7)>=bin(zz1,2)&& pndata5(zz,7)< bin(zz1+1,2);
          bin_long(zz)=zz1;
      end

 end
end
binno=(bin_lat-1)*100 +bin_long;

pndata5_1=[pndata5,binno];% New Data Matrix

clearvars('bin','sz5','s5','bin_lat','z','bin_long','zz','binno','z1','zz1')

%% ----------------------Assigning station IDs to stations ----------------------------%%
[~, index3] = sort(pndata5_1(:,1));
```

```
pndata6= pndata5_1(index3,:);
stalatT1=0;stalongG1=0;stid=0;
sz5=size(pndata5); s5=sz5(1,1);
for a=1:s5;
    if pndata6(a,1)==stalatT1 && pndata6(a,2)==stalongG1;
      staiD(a)=stid;
    else
       staiD (a)=stid+1;
      stid=stid+1;
     end
       stalatT1=pndata6(a,1); stalongG1=pndata6(a,2);
end
Station_id=staiD';

pndata7=[Station_id,pndata6];% New Data Matrix

clearvars('pndata6','stalatT1','stalongG1','sz5','s5','stid','a','staiD','Station_id','pndata6','index3'
,'pndata5')

%% ----------Making saperate columns for events falling on each station----------%%
ad=1;
ae=1;
data_out=zeros(10000,6708);
stid1=pndata7(1,1);
for ab=1:size(pndata7);
   if pndata7(ab,1)==stid1;
       data_out(ae,ad)= pndata7(ab,1); data_out(ae,ad+1)=pndata7(ab,2);
data_out(ae,ad+2)=pndata7(ab,3);  data_out(ae,ad+3)=pndata7(ab,4);
       data_out(ae,ad+4)=pndata7(ab,5);   data_out(ae,ad+5)=pndata7(ab,6);
data_out(ae,ad+6)=pndata7(ab,7);   data_out(ae,ad+7)=pndata7(ab,8);
       data_out(ae,ad+8)=pndata7(ab,9);   data_out(ae,ad+9)=pndata7(ab,10);
data_out(ae,ad+10)=pndata7(ab,11);   data_out(ae,ad+11)=pndata7(ab,12);
       data_out(ae,ad+12)=pndata7(ab,13); data_out(ae,ad+13)=pndata7(ab,14);
       ae=ae+1;
   else
       ad=ad+14;
       ae=1;
       data_out(ae,ad)= pndata7(ab,1); data_out(ae,ad+1)=pndata7(ab,2);
data_out(ae,ad+2)=pndata7(ab,3);  data_out(ae,ad+3)=pndata7(ab,4);
       data_out(ae,ad+4)=pndata7(ab,5);   data_out(ae,ad+5)=pndata7(ab,6);
data_out(ae,ad+6)=pndata7(ab,7);   data_out(ae,ad+7)=pndata7(ab,8);
       data_out(ae,ad+8)=pndata7(ab,9);   data_out(ae,ad+9)=pndata7(ab,10);
data_out(ae,ad+10)=pndata7(ab,11);   data_out(ae,ad+11)=pndata7(ab,12);
       data_out(ae,ad+12)=pndata7(ab,13); data_out(ae,ad+13)=pndata7(ab,14);
       stid1=pndata7(ab,1);

   end
```

```
end
data_out(all(data_out==0,2),:)=[];
clearvars('ad','ae','stid1','ab','pndata7')

%% ------------------ Formaing Summary rays----------------------------%%
sdata=[];
al=1;
sz6=size(data_out); s6=sz6(1,2);
for af=1:14:s6
   be(:,1:14) = data_out(:,af:af+13);
   ff=size(be);gg=ff(1,1);
   be(all(be==0,2),:)=[];
   [~, index4] = sort(be(:,14));
   Asort4= be(index4,:);

%-------------------------------------------------------------------%
   binidd=0;
   staidd1=0;stalatt1=0;stalongg1=0;staelee1=0;distt1=0;bazz1=0;
   ress1=0;orlatt1=0;orlongg1=0;ordepthh1=0;ormagg1=0;ttt1=0;binnoo1=0;
   ai=1;
   ak=1;
   for ag=1:size(Asort4,1)
      if Asort4(ag,14)==binidd;

         sdata(ai,1)=(Asort4(ag,1)+staidd1)/(ak+1);staidd1=sdata(ai,1)*(ak+1);
sdata(ai,2)=(Asort4(ag,2)+stalatt1)/(ak+1);stalatt1=sdata(ai,2)*(ak+1);
         sdata(ai,3)=(Asort4(ag,3)+stalongg1)/(ak+1);stalongg1=sdata(ai,3)*(ak+1);
sdata(ai,4)=(Asort4(ag,4)+staelee1)/(ak+1);staelee1=sdata(ai,4)*(ak+1);
         sdata(ai,5)=(Asort4(ag,5)+distt1)/(ak+1);distt1=sdata(ai,5)*(ak+1);
sdata(ai,6)=(Asort4(ag,6)+bazz1)/(ak+1);bazz1=sdata(ai,6)*(ak+1);
         sdata(ai,7)=(Asort4(ag,7)+ress1)/(ak+1);ress1=sdata(ai,7)*(ak+1);
sdata(ai,8)=(Asort4(ag,8)+orlatt1)/(ak+1);orlatt1=sdata(ai,8)*(ak+1);
         sdata(ai,9)=(Asort4(ag,9)+orlongg1)/(ak+1);orlongg1=sdata(ai,9)*(ak+1);
sdata(ai,10)=(Asort4(ag,10)+ordepthh1)/(ak+1);ordepthh1=sdata(ai,10)*(ak+1);

sdata(ai,11)=(Asort4(ag,11)+ormagg1)/(ak+1);ormagg1=sdata(ai,11)*(ak+1);sdata(ai,12)=(
Asort4(ag,12)+ttt1)/(ak+1);ttt1=sdata(ai,12)*(ak+1);
         sdata(ai,13)=(Asort4(ag,13)+binnoo1)/(ak+1);binnoo1=sdata(ai,13)*(ak+1);
sdata(ai,14)=(Asort4(ag,14)+binnoo1)/(ak+1);binnoo1=sdata(ai,14)*(ak+1);
         ak=ak+1;

       else
         sdata(ai+1,1)=Asort4(ag,1);sdata(ai+1,2)=Asort4(ag,2);
sdata(ai+1,3)=Asort4(ag,3);sdata(ai+1,4)=Asort4(ag,4);
         sdata(ai+1,5)=Asort4(ag,5);sdata(ai+1,6)=Asort4(ag,6);sdata(ai+1,7)=Asort4(ag,7);
sdata(ai+1,8)=Asort4(ag,8);
         sdata(ai+1,9)=Asort4(ag,9);
sdata(ai+1,10)=Asort4(ag,10);sdata(ai+1,11)=Asort4(ag,11); sdata(ai+1,12)=Asort4(ag,12);
```

```
        sdata(ai+1,13)=Asort4(ag,13);  sdata(ai+1,14)=Asort4(ag,14);

        staidd1=Asort4(ag,1);stalatt1=Asort4(ag,2); stalongg1=Asort4(ag,3);
        staelee1=Asort4(ag,4);distt1=Asort4(ag,5);bazz1=Asort4(ag,6);
        ress1=Asort4(ag,7);orlatt1=Asort4(ag,8);orlongg1=Asort4(ag,9);
        ordepthh1=Asort4(ag,10);ormagg1=Asort4(ag,11);ttt1=Asort4(ag,12);

        binnoo1=Asort4(ag,14);
         ai=ai+1;
         ak=1;
         binidd=Asort4(ag,14);
      end
   end
   sdata(all(sdata==0,2),:)=[];
   sd=size(sdata);sd1=sd(1,1);

   sumdata(al:(al-1)+sd1,1:14)=sdata(:,1:14);
    al=al+sd1;

clearvars('Asort4','index4','ag','ai','ak','bazz1','be','binidd','binnoo1','distt1','ff','gg','index2','ord
epthh1','orlatt1','orlongg1','ormagg1','ress1','sdata','staelee1','staidd1','stalatt1','stalongg1','ttt1'
,'sd','sd1');

end

clearvars('sdata','al','sz6','s6','af','data_out')
% sumdata=[stationID,
stalat,stalong,dist,staele,orid,orlat,orlong,ordepth,ormag,tt,res,baz,oribinno];

%% ----------------------------------------Calculating hitcount----------------------------%%
% Making cordinates of nodepoints
h1=size(lln); h3=size(ll);
nodp=zeros (h1(1,1)*h3(1,1),2);
h4=1; h5=1;
for h7=1:1:h3(1,1)
h6=1;
for h2=h5:1:h5+(h1(1,1)-1)
   nodp(h2,1)=ll(h4,1); nodp(h2,2)=lln(h6,1);
   h6=h6+1;
end
h4=h4+1; h5=h5+h1(1,1);
end
clearvars('h1','lln','ll','h1','h2','h3','h4','h5','h6','h7')

%% -------------------------------Claculating hit count for each node-------------------%%
h8=size(nodp); h10=size(sumdata);
ep=80; xe=dl*(ep/100);ye=dln*(ep/100);e=((xe)^2 +(ye)^2)^(0.5); % ep%tolerateable limit
from main node
```

```
nodp1_1=zeros (h10(1,1),h8(1,1));

for h11=1:1:h10(1,1);
x1=sumdata(h11,3);x2=sumdata(h11,8);
y1=sumdata(h11,2); y2=sumdata(h11,7);
alpha=(y2-y1)/(x2-x1);
  for h9=1:1:h8(1,1);
    nodx=nodp(h9,2); nody=nodp(h9,1);
    if x2 >= x1
       if y2 >= y1
          if nodx >=x1 && nodx<= x2 && nody >=y1 && nody<= y2 && alpha*(nodx-
x1)+y1-nody>=-e && alpha*(nodx-x1)+y1-nody<=e; nodp1_1(h11,h9)=1;
          else nodp1_1(h11,h9)=0;end
       elseif y2 <= y1;
          if nodx >=x1 && nodx<= x2 && nody >=y2 && nody<= y1 && alpha*(nodx-
x1)+y1-nody>=-e && alpha*(nodx-x1)+y1-nody<=e; nodp1_1(h11,h9)=1;
          else nodp1_1(h11,h9)=0;end
       end

    elseif x2 <= x1
       if y2 >= y1
          if nodx <=x1 && nodx >= x2 && nody >=y1 && nody<= y2 && alpha*(nodx-
x1)+y1-nody>=-e && alpha*(nodx-x1)+y1-nody<=e; nodp1_1(h11,h9)=1;
          else nodp1_1(h11,h9)=0;end
       elseif y2 <= y1
          if nodx <=x1 && nodx>= x2 && nody >=y2 && nody<= y1 && alpha*(nodx-
x1)+y1-nody>=-e && alpha*(nodx-x1)+y1-nody<=e;  nodp1_1(h11,h9)=1;
          else nodp1_1(h11,h9)=0;end
       end
    end
  end
end

sumnod=sum(nodp1_1); nodp2=sumnod';
nodp3=[nodp(:,1:2),nodp2(:,1)];

clearvars('h8','h10','ep','xe','ye','e','nodp_1','nodp','sumnod','h11','h10','x1','y1','x2','y2','alpha','
h9','h8','nodx','nody','dl','dln','nodp1_1','nodp2')

%% Data Out for SLBM input
sz=size(sumdata);s=sz(1,1);
uncert=ones(s,1)*(-999.000);
dataslbm=[sumdata(:,7),sumdata(:,8),sumdata(:,9),sumdata(:,2),sumdata(:,3),-
1*(sumdata(:,5)),sumdata(:,4),sumdata(:,11),uncert,uncert];
xlswrite('data.xls',dataslbm)
clearvars('sz','s','uncert')
```

Final Output: Summary ray data:
Information consist of
Station ID, Station Latitude, Station Longitude, Station Elevation, Epicenteral distance, Event ID, Event Latitude, Event Longitude, Event depth, Event Magnitude, Residual, Back azimuth and Event Bin Number

sumdata=[stationID,stalat,stalong,dist,staele,orid,orlat,orlong,ordepth,ormag,tt,res,baz,oribinno];

2) Inversion

```
%% ----------------------------------Inversion ---------------------------------------%%
%Author:
% Adnan Latif
% University of Oslo-Oslo, Norway
% adn_latif@hotmail.com
% Version: Oct/12
%%----------------------------------------------------------------------------------------%%

% sumdata=[stationID, stalat,stalong,dist,staele,orid,orlat,orlong,ordepth,ormag,
tt,res,baz,oribinno];

%% Weights import from the file from SLBM output
% For Ray j=1,2,3..., i=1, i+9,i+18..,Source Lat= weights_data(1,i), Source Long=
weights_data(2,i),Source Depth= weights_data(3,i)
% Receiver Lat= weights_data(4,i),Receiver Long= weights_data(5,i),Receiver
Elevation = weights_data(6,i)
% Distance = weights_data(1,i+1), Mangle Distance = % weights_data(2,i+1),Travel
Time = weights_data(3,i+1),
% Travel Time Uncertainity = weights_data(4,i+1), Slowness = weights_data(5,i+1), Vm
= weights_data(1,i+2),
% Gm = weights_data(2,i+2),H = weights_data(3,i+2),C= weights_data(4,i+2), Cm =
weights_data(5,i+2),
% Node Ids & Weigts for % Mantle = weights_data(:,i+3:i+4)
% Node Ids & Weigts for Crust-Source = weights_data(:,i+5:i+6)
% Node Ids & Weigts for Crust-Source = weights_data(:,i+7:i+8)

%% Generation of weights file from SLBM ---------Must Run from Linux Machine
system('bin/slbmweights ipdata/sn.dat test1/weights2.dat')
%% Transforming to matlab database
d=1;
ima=1;
d3=26146;% Total number of pn rays
weights_data=zeros(200,d3*9);
for i=1:d3
importdata('test1/weights2.dat',' ',d);
str='ans.data';
eval(['locinfo=',str,';']);
clearvars('ans','str');
imp1=size(locinfo);imp2=imp1(1,2);

importdata('test1/weights2.dat',' ',d+2);
str='ans.data';
eval(['dmtts=',str,';']);
clearvars('ans','str');
imp3=size(dmtts);imp4=imp3(1,2);

importdata('test1/weights2.dat',' ',d+4);
```

```
str='ans.data';
eval(['zaho=',str,';']);
clearvars('ans','str');
imp5=size(zaho);imp6=imp5(1,2);

importdata('test1/weights2.dat',' ',d+6);
str='ans.data';
eval(['mnode=',str,';']);
clearvars('ans','str');
imp7=size(mnode); imp8=imp7(1,1);
e=d+7;

importdata('test1/weights2.dat',' ',e+imp8);
str='ans.data';
eval(['snode=',str,';']);
clearvars('ans','str');
imp9=size(snode); imp10=imp9(1,1);

importdata('test1/weights2.dat',' ',e+imp8+imp10+1);
str='ans.data';
eval(['rnode=',str,';']);
clearvars('ans','str');
imp11=size(rnode); imp12=imp11(1,1);

weights_data(1:imp2,ima)=locinfo'; weights_data(1:imp4,ima+1)=dmtts';
weights_data(1:imp6,ima+2)=zaho';
weights_data(1:imp8,ima+3:ima+4)=mnode;
weights_data(1:imp10,ima+5:ima+6)=snode;
weights_data(1:imp12,ima+7:ima+8)=rnode;

ima=ima+9;
d=e+imp8+imp10+imp12+2;
clearvars('locinfo','dmtts','zaho','mnode','snode','rnode','imp1','imp2','imp3','imp4','imp5','i
mp6','imp7','imp8','imp9','imp10','imp11','imp12','e')
end
clearvars('d','ima','i','d3')
weights_data(all(weights_data==0,2),:)=[];
weights_data=weights_data(:,any(weights_data));

%% Executing and importaing crustal strucutre information from SLBM -Must
Run from Linux Machine
d2=748; % Total Number of nodes in given area (area defined in file test1/areatoinvert)
d1=0;imh=1;imi=10;
for i=1:d2
   imd='fortran90/slbmcrustalstructure';
   ime=num2str(i);
   imf='test1/structureAT3.dat';
   img=[imd,' ',ime,' ',imf];
```

```
    system(img);
importdata('test1/structureAT3.dat',' ',d1);
str='ans';
eval(['crststr=',str,';']);
clearvars('ans','str');
crust_strc(imh:imi,1:7)=crststr;

imh=imh+10; imi=imi+10;
clearvars('crststr');
end
clearvars('imi','imh','d1','i','imd','ime','imf','img','d2');

%% Replacing 0 with 0.001 to avoid NaN while calculating time
a1=find(crust_strc==0);crust_strc(a1)=0.0001;
clearvars('a1')

%% Caclulation of Radius of Earth ar each node
imj=size(crust_strc); imk=imj(1,1);iml=imk/10;
a=6378.135; % Equatorial Radius
b=6356.750;% Polar Radius
h=1;
g=1;
for i=1:iml
c=(a^2.*cos(crust_strc(h,3)))^2;d=(a^2.*sin(crust_strc(h,3)))^2;e=(a.*cos(crust_strc(h,3)
))^2;f=(a.*sin(crust_strc(h,3)))^2;
crust_strc(g,5)=((c+d)/(e+f))^(0.5);
h=h+10;
g=g+10;
clearvars('c','d','e','f');
end
clearvars('h','g','imj','imk','iml','i','a','b');

%% Node Ids generation.....iml .....nodes
imj=size(crust_strc); imk=imj(1,1);iml=imk/10;
x=1;
nodid=zeros(iml,1);
for i=1:iml
    nodid(i,1)=x;
    x=x+1;
end
clearvars('x','i','imj','imk','iml');

%% Formation of 'G' matrix (First Term)
imj=size(nodid); imk=imj(1,1);
 a=5;b=4;
ima=size(weights_data);imb=ima(1,2);
imc=imb/9;
G1=zeros(imc,3*imk);
```

```
for k=1:imc

   for i=1:imk; % total number of ifs will depend on rwos in matrix
weights_data.....After removing rows with all zeros
      if nodid (i,1)== weights_data(1,b); G1(k,i)= weights_data(1,a);      elseif nodid
(i,1)== weights_data(2,b); G1(k,i)= weights_data(2,a);
      elseif nodid (i,1)== weights_data(3,b); G1(k,i)= weights_data(3,a);   elseif nodid
(i,1)== weights_data(4,b); G1(k,i)= weights_data(4,a);
      elseif nodid (i,1)== weights_data(5,b); G1(k,i)= weights_data(5,a);   elseif nodid
(i,1)== weights_data(6,b); G1(k,i)= weights_data(6,a);
      elseif nodid (i,1)== weights_data(7,b); G1(k,i)= weights_data(7,a);   elseif nodid
(i,1)== weights_data(8,b); G1(k,i)= weights_data(8,a);
      elseif nodid (i,1)== weights_data(9,b); G1(k,i)= weights_data(9,a);   elseif nodid
(i,1)== weights_data(10,b); G1(k,i)= weights_data(10,a);
      elseif nodid (i,1)== weights_data(11,b); G1(k,i)= weights_data(11,a); elseif nodid
(i,1)== weights_data(12,b); G1(k,i)= weights_data(12,a);
      elseif nodid (i,1)== weights_data(13,b); G1(k,i)= weights_data(13,a); elseif nodid
(i,1)== weights_data(14,b); G1(k,i)= weights_data(14,a);
      elseif nodid (i,1)== weights_data(15,b); G1(k,i)= weights_data(15,a); elseif nodid
(i,1)== weights_data(16,b); G1(k,i)= weights_data(16,a);
      elseif nodid (i,1)== weights_data(17,b); G1(k,i)= weights_data(17,a); elseif nodid
(i,1)== weights_data(18,b); G1(k,i)= weights_data(18,a);
      elseif nodid (i,1)== weights_data(19,b); G1(k,i)= weights_data(19,a); elseif nodid
(i,1)== weights_data(20,b); G1(k,i)= weights_data(20,a);
      elseif nodid (i,1)== weights_data(21,b); G1(k,i)= weights_data(21,a); elseif nodid
(i,1)== weights_data(22,b); G1(k,i)= weights_data(22,a);
      elseif nodid (i,1)== weights_data(23,b); G1(k,i)= weights_data(23,a); elseif nodid
(i,1)== weights_data(24,b); G1(k,i)= weights_data(24,a);
      elseif nodid (i,1)== weights_data(25,b); G1(k,i)= weights_data(25,a); elseif nodid
(i,1)== weights_data(26,b); G1(k,i)= weights_data(26,a);
      elseif nodid (i,1)== weights_data(27,b); G1(k,i)= weights_data(27,a); elseif nodid
(i,1)== weights_data(28,b); G1(k,i)= weights_data(28,a);
      elseif nodid (i,1)== weights_data(29,b); G1(k,i)= weights_data(29,a); elseif nodid
(i,1)== weights_data(30,b); G1(k,i)= weights_data(30,a);
      elseif nodid (i,1)== weights_data(31,b); G1(k,i)= weights_data(31,a); elseif nodid
(i,1)== weights_data(32,b); G1(k,i)= weights_data(32,a);
      elseif nodid (i,1)== weights_data(33,b); G1(k,i)= weights_data(33,a); elseif nodid
(i,1)== weights_data(34,b); G1(k,i)= weights_data(34,a);
      elseif nodid (i,1)== weights_data(35,b); G1(k,i)= weights_data(35,a);

      else G1(k,i)= 0;

      end

   end
a=a+9;
b=b+9;
end
```

```
clearvars('imj','imk','k','a','i','b','ima','imb','imc');

%% Formation of 'G' matrix (2nd Term)
imj=size(nodid); imk=imj(1,1);
ima=size(weights_data);imb=ima(1,2);
imc=imb/9;
a=2;b=3;
for k=1:imc
for j=imk+1:2*imk;
   G1(k,j)=(G1(k,j-imk).*(weights_data(2,a))^2)/(-24*weights_data(1,b));
end
a=a+9;
b=b+9;
end
clearvars('a','b','k','j','imk','imj','ima','imb','imc');

%% Caculating times (multiplied by weights) for crustal phases
imj=size(nodid); imk=imj(1,1);
ima=size(weights_data);imb=ima(1,2);
imc=imb/9;
crstnod=zeros(6,2*imc);
d=6;ab=1;n=1;
for l=1:imc;
   t6=zeros(8,1);
   for k=1:3;
   e=1;
   a=2;b=2;c=1;t1=0;
      for j=1:imk;
         if weights_data(k,d)==crust_strc (e,1);
         p=(weights_data(5,d-4)).*(180/3.1416);
               for i=1:8;
               % sumdata=[stationID,
stalat,stalong,dist,staele,orid,orlat,orlong,ordepth,ormag,tt,res,baz,oribinno];    if
crust_strc(a,1) > weights_data(3,n)
                  r1=crust_strc(c,5)- crust_strc(a,1); r2=crust_strc(c,5)-
crust_strc(a+1,1);v1=crust_strc(b,2);
                  t2=(((r1^2)/(v1^2))-(p^2))^(0.5); t3=(((r2^2)/(v1^2))-(p^2))^(0.5);
                  r3=crust_strc(c,5)- weights_data(3,n); r4=r1;v2=crust_strc(b-1,2);
                  t4=(((r3^2)/(v2^2))-(p^2))^(0.5); t5=(((r4^2)/(v2^2))-(p^2))^(0.5);
t6(i,1)=t4-t5;
                  else t2=0;t3=0;t6(i,1)=0; end
               t=t2-t3; t1=t1+t; a=a+1; b=b+1;
               end
            a1=find(t6==0);t6(a1)=[];
            a3=size(t6);a4=a3(1,1);
            if a4==0
              r5=crust_strc(c,5)- weights_data(3,n); r6=crust_strc(c,5)-
crust_strc(a,1);v3=crust_strc(b-1,2);
```

```
            t7=(((r5^2)/(v3^2))-(p^2))^(0.5); t8=(((r6^2)/(v3^2))-(p^2))^(0.5); t9=t7-t8;

crstnod(k,ab)=weights_data(k,d);crstnod(k,ab+1)=(abs(t1)+abs(t9))*(weights_data(k,d+1
));
          else

crstnod(k,ab)=weights_data(k,d);crstnod(k,ab+1)=(abs(t1)+abs(t6(1,1)))*(weights_data(
k,d+1));

clearvars('r1','r2','r3','r4','r5','r6','v1','v2','v3','t1','t2','t3','t4','t5','t6','t','a1','a3','a4','t7','t8','t9')
  end
      a=a-8;b=b-8;
      end
      e=e+10;a=a+10;b=b+10;c=c+10;
      end

   end
clearvars('a','b','c','e','i','j','k')

d=d+2;
t1=0;
   for k=1:3;
   e=1;
   a=2;b=2;c=1;t1=0;
      for j=1:imk;
      if weights_data(k,d)==crust_strc (e,1)
         p=(weights_data(5,d-6)).*(180/3.1416);
         for i=1:8;
               if crust_strc(a,1) > weights_data(6,n)8.0400
               r1=crust_strc(c,5)- crust_strc(a,1); r2=crust_strc(c,5)-crust_strc(a+1,1);
               v1=crust_strc(b,2);
               t2=(((r1^2)/(v1^2))-(p^2))^(0.5); t3=(((r2^2)/(v1^2))-(p^2))^(0.5);
               r3=crust_strc(c,5)- weights_data(6,n); r4=r1;
               v2=crust_strc(b-1,2);
               t4=(((r3^2)/(v2^2))-(p^2))^(0.5); t5=(((r4^2)/(v2^2))-(p^2))^(0.5);
               t6(i,1)=t4-t5;
            else t2=0;t3=0;
               end
         t=t2-t3; t1=t1+t; a=a+1; b=b+1;
          end
      a1=find(t6==0);t6(a1)=[];
      a3=size(t6);a4=a3(1,1);
        if a4==0

crstnod(k+3,ab)=weights_data(k,d);crstnod(k+3,ab+1)=abs(t1)*(weights_data(k,d+1));
        else
```

```
crstnod(k+3,ab)=weights_data(k,d);crstnod(k+3,ab+1)=(abs(t1)+abs(t6(1,1)))*(weights_
data(k,d+1));
      clearvars('r1','r2','r3','r4','r5','r6','v1','v2','t1','t2','t3','t4','t5','t6','t','a1','a3','a4')
        end
    a=a-8;b=b-8;
     end
     e=e+10;a=a+10;b=b+10;c=c+10;
     end
  end
clearvars('a','b','c','e','i','j','k','p','r1','r2','t','t1','v1')
ab=ab+2;8.0400
d=d+7;
n=n+9;

end

clearvars('ab','d','ima','imb','imc','imj','imk','l','t2','t3','n')

%% Formation of 'G' matrix (3nd Term)
imj=size(nodid); imk=imj(1,1);
ima=size(weights_data);imb=ima(1,2);
imc=imb/9;c=1;
G2=zeros(imc,imk);
for k=1:imc
   for m=1:imk
     if nodid(m,1)== crstnod(1,c);  G2(k,m)=crstnod(1,c+1);
     elseif nodid(m,1)== crstnod(2,c);G2(k,m)=crstnod(2,c+1);
     elseif nodid(m,1)== crstnod(3,c);G2(k,m)=crstnod(3,c+1);
     elseif nodid(m,1)== crstnod(4,c);G2(k,m)=crstnod(4,c+1);
     elseif nodid(m,1)== crstnod(5,c);G2(k,m)=crstnod(5,c+1);
     elseif nodid(m,1)== crstnod(6,c);G2(k,m)=crstnod(6,c+1);
     else G2(k,m)=0;
     end
  end
 c=c+2;
end

G(:,1:imk)=G1(:,1:imk);G(:,imk+1:2*imk)=G1(:,imk+1:2*imk);G(:,2*imk+1:3*imk)=G
2;
clearvars('k','m','c','ima','imb','imc','imj','imk','m','G2','G1')

%% Moho depth
adn=size(crust_strc); adp=adn(1,1)/10;
aba=10;ami=1;
for i=1:adp
  moho_depth(i,1)=crust_strc(ami,1);
  moho_depth(i,2)=crust_strc(ami,3);
```

```
    moho_depth(i,3)=crust_strc(ami,4);
    aba=aba+10;
    ami=ami+10;
end
clearvars('adn','adp','aba','i','ami')
```

%% Removing data with zero values in

```
% Divideing main G into its 3 Compnents
imj=size(crust_strc); imk=imj(1,1);iml=imk/10;
G2=G(:,1:iml);G3=G(:,iml+1:2*iml);G4=G(:,2*iml+1:3*iml);

% Removing zero columns and finding node IDs of useable nodes
a2=any(G2,1)';a3=any(G3,1)';a4=any(G4,1)';
for i=1:size(a2)
    if a2(i,1)==0; mnode1(i,1)=0;
    else mnode1(i,1)=i; end
end
a1=find(mnode1==0);mnode1(a1)=[];clearvars ('i','a1');
for i=1:size(a3)
    if a3(i,1)==0; mnode2(i,1)=0;
    else mnode2(i,1)=i; end
end
a1=find(mnode2==0);mnode2(a1)=[];clearvars ('i','a1');
for i=1:size(a4)
    if a4(i,1)==0; mnode3(i,1)=0;
    else mnode3(i,1)=i; end
end
a1=find(mnode3==0);mnode3(a1)=[];clearvars ('i','a1');

% Removing zero columns from main G
G=G(:,any(G));
clearvars('G2','G3','G4','imj','imk','iml','a2','a3','a4')

%% Initial Model
% Extracting Mantel velocities from Crust_strc data ..... vel_nod
imj=size(crust_strc); imk=imj(1,1);iml=imk/10;
vel_nod=zeros(iml,2);
a=1;b=10;
for i=1:iml

vel_nod(i,1)=crust_strc(a,1);vel_nod(i,2)=crust_strc(b,2);vel_nod(i,3)=crust_strc(a,6);vel
_nod(i,4)=crust_strc(a,3);vel_nod(i,5)=crust_strc(a,4);
a=a+10;b=b+10;
end
clearvars('a','b','i','imj','imk','iml')

% velocities for the useable nodes..... vel_mantle
```

```
imj=size(mnode1); imk=imj(1,1);
iml=size(vel_nod);imm=iml(1,1);
b=1;
for i=1:imm
   for j=1:imk
      if vel_nod(i,1)== mnode1(j,1);
         vel_mantle(b,1)= vel_nod(i,1); vel_mantle(b,2)=
vel_nod(i,2);vel_mantle(b,3)=vel_nod(i,3);
         vel_mantle(b,4)=vel_nod(i,4);vel_mantle(b,5)=vel_nod(i,5);
      end
   end
   b=b+1;
end
vel_mantle(all(vel_mantle==0,2),:)=[];
clearvars('b','i','j','imj','imk','iml','imm')

% velocities for the useable nodes.....for crustal nodes..... vel_crust
imj=size(mnode3); imk=imj(1,1);
iml=size(vel_nod);imm=iml(1,1);
b=1;
for i=1:imm
   for j=1:imk
      if vel_nod(i,1)== mnode3(j,1);
         vel_crust(b,1)= vel_nod(i,1);
vel_crust(b,2)=vel_nod(i,4);vel_crust(b,3)=vel_nod(i,5);
      end
   end
   b=b+1;
end
vel_crust(all(vel_crust==0,2),:)=[];
clearvars('b','i','j','imj','imk','iml','imm')

%% Assigning values to the initial model
imj=size(mnode1); imk=imj(1,1);
for i=1:imk
   intmod1(i,1)=1/vel_mantle(i,2);
end
clearvars('i','imk','imj')
imj=size(mnode2); imk=imj(1,1);
for i=1:imk
   intmod2(i,1)=(vel_mantle(i,3)./vel_mantle(i,2))^2;
end
clearvars('i','imk','imj')
imj=size(mnode3); imk=imj(1,1);
for i=1:imk
   intmod3(i,1)=0.1;
end
clearvars('i','imk','imj')
```

```
imj=size(intmod1); imk=imj(1,1);iml=size(intmod2); imm=iml(1,1);imn=size(intmod3);
imo=imn(1,1);
initial_model(1:imk,1)=intmod1;initial_model(imk+1:imk+imm,1)=intmod2;initial_mod
el(imk+imm+1:imk+imm+imo,1)=intmod3;
clearvars('mnode1','mnode2','mnode3')
G1(:,1:imk)=G(:,1:imk);
G1(:,imk+1:imk+imm)=G(:,imk+1:imk+imm);G1(:,imk+imm+1:imk+imm+imo)=G(:,i
mk+imm+1:imk+imm+imo).*10;

%% Peramitrization for Inversion
dprd=G1*initial_model;% Forward Modeling
k1=size(G1);
M=k1(1,2);% Total Number of Rays
N=k1(1,1); % Total Number of Nodes (will be set after knowing the number of noeds
produced from RSTT output)
d_obs= sumdata(:,11); % Actual Travel times
clearvars('k1')

%Model covariance
sigma_d=1e-1;
covD=eye(N,N)*sigma_d^2;
sig_m1=1e-2;
sig_m2=2e-4;
sig_m3=5e-5;

covM=zeros(M,M);
aa=size(intmod1);
bb=size(intmod2);
cc=size(intmod3);
for i=1:aa
   covM(i,i)=sig_m1^2;
end
for j=aa+1:aa+bb
   covM(j,j)=sig_m2^2;
end
for k=aa+bb+1:aa+bb+cc
   covM(k,k)=sig_m3^2;
end
clearvars('sig_m1','sig_m2','sig_m3','i','j','k')

% With guasin distribution on mantel slowness
maininput=vel_mantle;
ab=size(maininput); ac=ab(1,1);
cm=zeros(ac,ac);
Lm=300;
sigm_m=1e-2;
for j=1:ac;
```

```
for i=1:ac
   aal=(maininput(j,4)); aaln=(maininput(j,5));
   bbl=(maininput(i,4)); bbln=(maininput(i,5));
   del=111*((bbl-aal)^2 +(bbln-aaln)^2)^(0.5);
   cm(j,i)=sigm_m^2*exp(-del^2/(2*(Lm)^2));
end
end
clearvars ('maininput','ab','ac','Lm','del','i','j','aal','aaln','bbl','bbln')

covm=zeros(M,M);
covm(1:aa,1:aa)=cm(:,:);
covm(aa+1:aa+bb+cc,aa+1:aa+bb+cc)=covM(aa+1:aa+bb+cc,aa+1:aa+bb+cc);
clearvars('aa','bb','cc','cm')

%% Preconditined conjugate Gradient Inversion
clearvars('mpr','s','rms','a','b','c','mf','so','phi_old','gama','lamda','w_new','w_old','itreation'
)
m=zeros(M,1);
mpr=initial_model;
a=covm*G1'*(inv(covD));%NOt changed in iteration % Elapsed time is 409.146092
seconds
I=eye(M,M);%NOt changed in iteration
so=inv(I+a*G1);%NOt changed in iteration
s=(1/sigma_d)*(d_obs-G1*m);
rms=sqrt(s'*s/N)
iteration=0;
for i=1
   gama=a*(G1*m-d_obs)+(m-mpr);
   lamda=so*gama;
   w_new=lamda'*inv(covm)*gama;
 if iteration==0;w_old=w_new; else w_old=w_old; end
 if iteration==0; phi_old=zeros(M,1); else phi_old=phi_old; end
   phi_new= lamda + (w_new/w_old)*phi_old;
   bn=G1*phi_new;
   mu=w_new/(phi_new'*inv(covm)*phi_new +bn'*inv(covD)*bn);
   m=m-mu*phi_new;
   phi_old= phi_new;
   w_old= w_new;
   s=(1/sigma_d)*(d_obs-G1*m);
   rms=sqrt(s'*s/N)
   RMS(i+1,1)=rms;
   iteration=iteration+1
end
mf300=m; % Final Model

%% Resolution Analysis
R1=G1'*inv(covD)*G1;
R2=inv(R1 + inv(covm));
```

```
R=R2*R1;
CovmP=R2;
post_error_bar=(diag(CovmP)).^(0.5);

%% Exterction of Final model for plotting
velocity_mantle=1./mf300(1:imk,1);% Mantel velocity of final model
gradient_c_sqr=mf300(imk+1:imk+imm,1); % Velocity gradient 'c' of final model
gradiant=(((abs(gradient_c_sqr)).^(0.5))./8.04)-(1.58e-4);
crustal_correction= (mf300(imk+imm+1:imk+imm+imo,1))*10;% Node specific
adjustment to the slowness of each crustal layer (Crustal modifier)
nodloc=[vel_mantle(:,1),vel_mantle(:,4),vel_mantle(:,5)];% Nodes locations for mantle
velocities
```

Final Output:

Mantle velocity, velocity gradient and crustal modifier at specified nodes

final_data=[velocity_mantle, gradiant, crustal_correction]

Resolution and Covariance Matrix

R, CovmP

3) Checkerboard test

```
%% ------------------------------------ Checkerboard Test ---------------------------------
    %Author:
    % Adnan Latif
    % University of Oslo-Oslo, Norway
    % adn_latif@hotmail.com
    % Version: Oct/12
%%-------------------------------------------------------------------------------------------%%
%     Note: Need mff_2100 from inversion of Real data
%% ------------------------------------------------------------------------------------------------
imj=size(intmod1); imk=imj(1,1);
iml=size(intmod2); imm=iml(1,1);
imn=size(intmod3); imo=imn(1,1);
cboard_box=[270,255,256,248,247,254,209,271,252,541,549,221,550,542,538,543,539,540,
383,346,341,344,471,472,384,381,470,413,431,430,238,237,223,222,224,240,631,232,231,2
30,551,554,718,717,555]';

initial_model_c1=zeros(imk,1);

for i=1:imk
   for j=1:size(cboard_box)
       if vel_mantle(i,1)==cboard_box(j,1);
        initial_model_c1(i,1)=7.245;

       end
   end
end
for i=1:imk
    if initial_model_c1(i,1)==7.245;
    initial_model_c(i,1)=initial_model_c1(i,1);
    else
      initial_model_c(i,1)=8.05;
    end
end


% Model for check board test Note: mff_2100 is the final model from Inversion
initial_model_cb(1:imk,1)=1./initial_model_c;  % initial model for check board test -Matntel
slowness
initial_model_cb(imk+1:imk+imm+imo,1)=mff_2100(imk+1:imk+imm+imo,1);% initial
model for check board test -Matntel gradiant and crutal correction

test=(initial_model_cb +initial_model+initial_model+ initial_model)./4; % ,Mixing of
models for a priori model formation

% model for ploting check board test model
velocity_mantle_syn=1./initial_model_cb(1:imk,1);% mantle velocitys
```

```
nodelat_mantel= vel_mantle(:,4); nodelong_mantel= vel_mantle(:,5); % Nodes locations for mantle velocities
nodloc=[vel_mantle(:,1),nodelat_mantel(:,:),nodelong_mantel(:,:)];

% Coveriance of Model and Data
k1=size(G1);
M=k1(1,2);% Total Number of Rays
N=k1(1,1); % Total Number of Nodes (will be set after knowing the number of noeds produced from RSTT output)
d_obs=G1*initial_model_cb;% Forward Modeling
clearvars('k1')

sigma_d=1e-1;
covD=eye(N,N)*sigma_d^2;
sig_m1=1e-2;
sig_m2=2e-4;
sig_m3=5e-4;

covM=zeros(M,M);
aa=size(intmod1);
bb=size(intmod2);
cc=size(intmod3);
for i=1:aa
   covM(i,i)=sig_m1^2;
end
for j=aa+1:aa+bb
   covM(j,j)=sig_m2^2;
end
for k=aa+bb+1:aa+bb+cc
   covM(k,k)=sig_m3^2;
end
clearvars('sig_m1','sig_m2','sig_m3','i','j','k')

% With guasin distribution on mantel slowness
maininput=vel_mantle;
ab=size(maininput); ac=ab(1,1);
cm=zeros(ac,ac);
Lm=100;
sigm_m=1e-2;
for j=1:ac;
for i=1:ac
   aal=(maininput(j,4)); aaln=(maininput(j,5));
   bbl=(maininput(i,4)); bbln=(maininput(i,5));
   del=111*((bbl-aal)^2 +(bbln-aaln)^2)^(0.5);
   cm(j,i)=sigm_m^2*exp(-del^2/(2*(Lm)^2));
end
end
clearvars ('maininput','ab','ac','Lm','del','i','j','aal','aaln','bbl','bbln')
```

```
covm=zeros(M,M);
covm(1:aa,1:aa)=cm(:,:);
covm(aa+1:aa+bb+cc,aa+1:aa+bb+cc)=covM(aa+1:aa+bb+cc,aa+1:aa+bb+cc);
clearvars('aa','bb','cc','cm','covM')

% Starting Model
for i=1:imk
   im_man(i,1)=8.05;
end
mo(1:imk,1)=1./im_man(:,1);
mo(imk+1:imk+imm+imo,1)=mff_2100(imk+1:imk+imm+imo,1);

%% Preconditined Conjugate Gradient Inversion
clearvars('mpr','s','rms','a','b','c','mff_2100','so','phi_old','gama','lamda','w_new','w_old','itreati
on')
m=initial_model;%initial_model;% Starting Model
mpr=test;
a=covm*G1'*(inv(covD));%NOt changed in iteration % Elapsed time is 409.146092 seconds
I=eye(M,M);%NOt changed in iteration
so=inv(I+a*G1);%NOt changed in iteration
s=(1/sigma_d)*(d_obs-G1*m);
rms=sqrt(s'*s/N)
RMS(1,1)=rms;
iteration=0;
for i=1:1
   gama=a*(G1*m-d_obs)+(m-mpr);
   lamda=so*gama;
   w_new=lamda'*inv(covm)*gama;
 if iteration==0;w_old=w_new; else w_old=w_old; end
 if iteration==0; phi_old=zeros(M,1); else phi_old=phi_old; end
   phi_new= lamda + (w_new/w_old)*phi_old;
   bn=G1*phi_new;
   mu=w_new/(phi_new'*inv(covm)*phi_new +bn'*inv(covD)*bn);
   m=m-mu*phi_new;
   phi_old= phi_new;
   w_old= w_new;
   s=(1/sigma_d)*(d_obs-G1*m);
   rms=sqrt(s'*s/N)
   RMS(i+1,1)=rms;
   iteration=iteration+1;
end
%%
mff_2100_syn=m % Final Model
velocity_mantle_sy_output=1./mff_2100_syn(1:imk,1); % Mantle velocities output for
Checkboared test
gradient_sy_output=mff_2100_syn(imk+1:imk+imm,1); % Velocity gradient output for
Checkboard test
```

```
crustal_correction_sy_output= (mff_2100_syn(imk+imm+1:imk+imm+imo,1))*10;% Node specific adjustment to the slowness of each crustal layer (Crustal modifier)
nodloc=[vel_mantle(:,1),vel_mantle(:,4),vel_mantle(:,5)];% Nodes locations for mantle velocities
```

4) Plotting

```
%%-------------------------------------------------------------------------------------------------%%
    %Author:
    % Adnan Latif
    % University of Oslo-Oslo, Norway
    % adn_latif@hotmail.com
    % Version: Oct/12
%%-------------------------------------------------------------------------------------------------%%
%% ----------------------------------------Pre-Processing Results-------------------------%%

%Figure 4.1 Location of stations & events
figure(1)
latlim=[45 72]; longlim=[-10 40]; worldmap(latlim, longlim);
land=shaperead('landareas','UseGeocoords',true); setm(gca,'ffacecolor');
geoshow(land,'facecolor','k')
hold on; scatterm(pndata1(:,4), pndata1(:,5),17,'r','filled'); hold all; scatterm(pndata1(:,20),
pndata1(:,21),17,'b','filled');
title('Location of Events & Stations (Unprocessed data)')
print('-djpeg','-r500','4_1-Location of stations & events')

% Figure 4.2 Travel Time curve (Unprocessed Data)
figure (2)
scatter(pndata1(:,7),pndata1(:,27),5,[0 0 0]); axis([0 20 0 300]); ylabel('Travel Time
(sec)');xlabel('Epicenteral Distance (Deg)')
title('Pn Travel Time curve (Unprocessed Data))')
print('-djpeg','-r500','4_2-Pn Travel Time curve (Unprocessed Data)')

% Figure 4.3 Pn Travel Time curve (Semi-processed Data)
figure (3)
subplot(2,1,2),scatter(pndata4(:,3),pndata4(:,10),10,[0 0 0]); axis([0 20 0 300]);
ylabel('Travel Time (sec)');xlabel('Epicenteral Distance (Deg)')
title('Pn Travel Time curve (Semi-processed Data))')
subplot(2,1,1),scatter(pndata1(:,7),pndata1(:,27),10,[0 0 0]); axis([0 20 0 300]);
ylabel('Travel Time (sec)');xlabel('Epicenteral Distance (Deg)');
title('Pn Travel Time curve (Unprocessed Data))')
print('-djpeg','-r500','4_3-Pn Travel Time curve (Semi-processed Data)')

% Figure 4.4 Residuals Vs Epicenteral Distance(Sami-processed Data)
figure (4)
subplot(2,1,2),scatter(pndata4(:,3),pndata4(:,11),10,[0 0 0]);axis([0 20 -50 50]);
ylabel('Residuals (sec)');xlabel('Epicenteral Distance (Deg)')
title('Residuals Vs Epicenteral Distance (Semi-processed Data))')
subplot(2,1,1),scatter(pndata1(:,7),pndata1(:,13),10,[0 0 0]); axis([0 20 -50 50]);
ylabel('Residuals (sec)');xlabel('Epicenteral Distance (Deg)')
annotation('line',[0.130625 0.9025],[0.753690036900369 0.753690036900369]);
annotation('line',[0.130625 0.905625],[0.279442804428044 0.279442804428044]);
```

```
title('Residuals Vs Epicenteral Distance (Unprocessed Data))')
print('-djpeg','-r500','4_4-Residuals Vs Epicenteral Distance(Sami-processed Data)');

% Figure 4.5 (a & b)Residuals Vs Epicenteral Distance(Sami-processed Data)
figure(5)
subplot(1,2,1), hist(pndata4_1(:,11),100);axis([-100 100 0 40000]); ylabel('Number of
Rays');xlabel('Residuals')
title('Residual distribution from ak135/JB reference model')
subplot(1,2,2),hist(pndata4_1(:,11),100);axis([-100 100 0 90]); ylabel('Number of
Rays');xlabel('Residuals')
title('Residual distribution from ak135/JB reference model')
print('-djpeg','-r500','4_5-Residuals Vs Epicenteral Distance(Sami-processed Data)')

% Figure 4.6 Residuals Vs Epicenteral+Travel time curve(Processed Data)
figure (6)
subplot(2,1,1),scatter(pndata5_2(:,3),pndata5_2(:,10),10, [0 0 0]); axis([0 20 0
300]);ylabel('Travel Time (sec)');xlabel('Epicenteral Distance (Deg)')
title('Pn Travel Time curve (Processed Data))')
subplot(2,1,2),scatter(pndata5_2(:,3),pndata5_2(:,11),10, [0 0 0]);axis([0 20 -10 10])
ylabel('Residuals (sec)');xlabel('Epicenteral Distance (Deg)'); annotation('line',[0.130625
0.905625],[0.280365313653136 0.280365313653136]);
title('Residuals Vs Epicenteral Distance (Processed Data))')
print('-djpeg','-r500','4_6-Residuals Vs Epicenteral+Travel time curve(Processed Data)')

% Figure 4.7 Ray Paths-Summary Rays
figure(7)
latlim=[45 72]; longlim=[-10 40]; worldmap (latlim,
longlim);land=shaperead('landareas','UseGeocoords',true); setm(gca,'ffacecolor');
geoshow(land,'facecolor','w'); hold on
for i=1:1:size(sumdata)
   linem([sumdata(i,2); sumdata(i,7)],[sumdata(i,3); sumdata(i,8)],'k-'); hold all
end
scatterm(pndata1(:,4), pndata1(:,5),17,'r','filled'); hold all; scatterm(pndata1(:,20),
pndata1(:,21),17,'b','filled');
title('Ray paths after Processing and Summary Rays')
print('-djpeg','-r500','4_7-Ray Paths-Summary Rays')

% Figure 4.8 Residuals Vs Epicenteral + Travel time curve(Processed + Summary
Rays Data)
figure (8)
subplot(2,1,1),scatter(sumdata(:,4),sumdata(:,11),10,[0 0 0]); axis([0 20 0 300]);
ylabel('Travel Time (sec)');xlabel('Epicenteral Distance (Deg)')
title('Pn Travel Time curve (Processed Data after Summary Rays)')
subplot(2,1,2),scatter(sumdata(:,4),sumdata(:,12),10,[0 0 0]);axis([0 20 -10 10])
ylabel('Residuals (sec)');xlabel('Epicenteral Distance (Deg)'); title('Residuals Vs Epicenteral
Distance (Processed Data after Summary Rays)')
annotation('line',[0.130625 0.905625],[0.279442804428044 0.279442804428044]);
```

```
print('-djpeg','-r500','4_8-Residuals Vs Epicenteral + Travel time curve(Processed + Summary Rays Data)')

% Figure 4.9 Hit count map
figure(9)
latlim=[45 72]; longlim=[-15 40]; worldmap (latlim, longlim);
land=shaperead('landareas','UseGeocoords',true); setm(gca,'ffacecolor');
geoshow(land,'facecolor','w');hold on
x_h=nodp3(:,2); y_h=nodp3(:,1); z_h=nodp3(:,3);  x_hres = 175; y_hres = 175; cm_h = 'default';
x_hmin = min(x_h); y_hmin = min(y_h); x_hmax = max(x_h); y_hmax = max(y_h); x_hi = linspace(x_hmin, x_hmax, x_hres); y_hi = linspace(y_hmin, y_hmax, y_hres);
rotate3d off; [XI_h, YI_h] = meshgrid(x_hi, y_hi); ZI_h = griddata(x_h, y_h, z_h, XI_h, YI_h, 'cubic');
surfacem(YI_h,XI_h,ZI_h); cmap=flipud(colormap('jet')); colormap(cmap); h = colorbar;
ylabel(h,'[Hit Counts]'); set(gca, 'CLim', [-5, 300]);
title('Hit-count Map ')
print('-djpeg','-r500','4_9-Hit count map)')

% Figure 4.10 Location of Nodes
figure(10)
latlim=[42 72]; longlim=[-12 47]; worldmap (latlim,
longlim);land=shaperead('landareas','UseGeocoords',true);
setm(gca,'ffacecolor'); geoshow(land,'facecolor','w');hold on
nodloc=[vel_nod(:,1),vel_nod(:,4),vel_nod(:,5)]; p = nodloc(:,:); scatterm(p(:,2), p(:,3), 'filled')
% labels = num2str(p(:,1),'%d'); textm(p(:,2), p(:,3), labels, 'horizontal','left', 'vertical','bottom')
title('Node Locations '); clearvars('latlim','longlim','land','setm')
print('-djpeg','-r500','4_10-Node locations')

% Figure 4.11 Refrence Model(Mantle velocity)
figure(11)
nodloc=[vel_mantle(:,1),vel_mantle(:,4),vel_mantle(:,5)];
latlim=[45 72]; longlim=[-15 40]; worldmap (latlim, longlim);
land=shaperead('landareas','UseGeocoords',true); setm(gca,'ffacecolor');
geoshow(land,'facecolor','w');hold on
y_h=nodloc(1:imk,2); x_h=nodloc(1:imk,3); z_h=1./initial_model(1:size(y_h));x_hres = 500; y_hres = 500;cm_h = 'default';
x_hmin = min(x_h); y_hmin = min(y_h);x_hmax = max(x_h); y_hmax = max(y_h); x_hi = linspace(x_hmin, x_hmax, x_hres); y_hi = linspace(y_hmin, y_hmax, y_hres);
rotate3d off; [XI_h, YI_h] = meshgrid(x_hi, y_hi); ZI_h = griddata(x_h, y_h, z_h, XI_h, YI_h, 'cubic');
surfacem(YI_h,XI_h,ZI_h); cmap=flipud(colormap('jet')); colormap(cmap);h = colorbar;
set(gca, 'CLim', [7.0, 8.2]); ylabel(h,'P wave Velocity (km/s)');
title('Initial/Reference Earth Model (P wave velocity at Moho)'); print('-djpeg','-r500','4_11-Refrence Model (P wave)')
```

```
% Figure 4.12 Refrence Model (Mantle gradiant)
figure(12)
nodloc=[vel_mantle(:,1),vel_mantle(:,4),vel_mantle(:,5)];
latlim=[45 72]; longlim=[-15 40]; worldmap (latlim, longlim);
land=shaperead('landareas','UseGeocoords',true); setm(gca,'ffacecolor');
geoshow(land,'facecolor','w');hold on
y_h=nodloc(1:imk,2); x_h=nodloc(1:imk,3); z_h=Initial_gradient; x_hres = 500; y_hres =
500; cm_h = 'default';
x_hmin = min(x_h); y_hmin = min(y_h); x_hmax = max(x_h); y_hmax = max(y_h); x_hi =
linspace(x_hmin, x_hmax, x_hres); y_hi = linspace(y_hmin, y_hmax, y_hres);
rotate3d off; [XI_h, YI_h] = meshgrid(x_hi, y_hi); ZI_h = griddata(x_h, y_h, z_h, XI_h,
YI_h, 'cubic');
surfacem(YI_h,XI_h,ZI_h); title('Initial Mantle Gradiant') ;cmap=flipud(colormap('jet'));
colormap(cmap); h = colorbar; ylabel(h,'Velocity Gradient (km/s/km)');
print('-djpeg','-r500','4_12-Refrence Model (Mantle gradient)')

% Figure 4.13 Moho depth map
figure(13)
latlim=[50 70]; longlim=[-5 30]; worldmap (latlim, longlim);
land=shaperead('landareas','UseGeocoords',true); setm(gca,'ffacecolor');
geoshow(land,'facecolor','w');hold on
y_h=moho_depth(:,2); x_h=moho_depth(:,3); z_h=moho_depth(:,1);
x_hres = 500; y_hres = 500;cm_h = 'default'; x_hmin = min(x_h); y_hmin = min(y_h);
x_hmax = max(x_h); y_hmax = max(y_h); x_hi = linspace(x_hmin, x_hmax, x_hres); y_hi =
linspace(y_hmin, y_hmax, y_hres);
rotate3d off; [XI_h, YI_h] = meshgrid(x_hi, y_hi); ZI_h = griddata(x_h, y_h, z_h, XI_h,
YI_h, 'cubic');
surfacem(YI_h,XI_h,ZI_h); cmap=flipud(colormap('jet')); colormap(cmap); h = colorbar;
ylabel(h,'[Moho Depth (km)]');
title('Moho Depth'); print('-djpeg','-r500',' 4_13-Moho Depth ')
clearvars('latlim','longlim','land','setm','y_h','x_h','z_h','x_hres','y_hres','cm_h','x_hmin','y_hm
in','x_hmax','y_hmax','x_hi','y_hi','XI_h','YI_h')

%  Figure 4.14 Travel time curve for RSTT model
figure(14)
scatter(pndata_r(:,1),pndata_r(:,2),10,[0 0 0]); axis([0 20 0 300])
ylabel('Traval Time (sec)');xlabel('Epicenteral Distance (Deg)'); title('Modeled Pn Traval
Time curve by RSTT')
print('-djpeg','-r500','4_14-Refrence Model (Travel Time Curve)')

%Figure 4.15  Residuals-before & After Inversion
figure(15)
subplot(3,2,1),resi=d_obs-G1*initial_model; plot(resi,'r'); axis([0 16500 -15 10]);xlabel('Ray
Number'); ylabel('Residuals'); hold on;resf1=d_obs-G1*mf200; plot(resf1,'b');title('L =200')
subplot(3,2,2),resi=d_obs-G1*initial_model; plot(resi,'r'); axis([0 16500 -15 10]);xlabel('Ray
Number'); ylabel('Residuals'); hold on;resf2=d_obs-G1*mf300; plot(resf2,'b'); title('L =300')
subplot(3,2,3),resi=d_obs-G1*initial_model; plot(resi,'r'); axis([0 16500 -15 10]);xlabel('Ray
Number'); ylabel('Residuals'); hold on;resf3=d_obs-G1*mf400; plot(resf3,'b'); title('L =400')
```

```
subplot(3,2,4),resi=d_obs-G1*initial_model; plot(resi,'r'); axis([0 16500 -15 10]);xlabel('Ray Number'); ylabel('Residuals'); hold on;resf4=d_obs-G1*mf500; plot(resf4,'b'); title('L =500')
subplot(3,2,5),resi=d_obs-G1*initial_model; plot(resi,'r'); axis([0 16500 -15 10]);xlabel('Ray Number'); ylabel('Residuals'); hold on;resf5=d_obs-G1*mf1000; plot(resf5,'b'); title('L =1000')
subplot(3,2,6),resi=d_obs-G1*initial_model; plot(resi,'r'); axis([0 16500 -15 10]);xlabel('Ray Number'); ylabel('Residuals'); hold on;resf6=d_obs-G1*mf2000; plot(resf6,'b'); title('L =2000')
legend1 = legend ('Residuals before Inversion (A priori Model)' ,'Residuals after Inversion')
set(legend1,'Orientation','horizontal','Position',[0.0630430735930715 0.00567465956989533 0.897447619047619 0.0571428571428572]);
p=mtit('Residuals of Inverted models','fontsize',10,'color',[0 0 1],'xoff',-.01,'yoff',.025);
set(p.th,'edgecolor',.5*[1 1 1]);
print('-djpeg','-r500','4_15-Residuals_Before_&_After__Inversion_L_Test')
```

%Figure 14.16 Histogram of residuals before and after inversion

```
figure(16)
subplot(3,2,1), resi1=d_obs-G1*initial_model;[nb,xb]= hist(resi1,110);axis([-6 8 0 1000]);bh=bar(xb,nb);set(bh,'facecolor',[1 0 0]);
hold on; resi2=d_obs-G1*mf200; [nc,xc]=hist(resi2,110);axis([-6 8 0 1000]);bh=bar(xc,nc);set(bh,'facecolor',[1 1 0]);
xlabel('Residual (Sec)'); ylabel('Number of Rays '); title('L= 200')
subplot(3,2,2), resi1=d_obs-G1*initial_model;[nb,xb]= hist(resi1,110);axis([-6 8 0 1000]);bh=bar(xb,nb);set(bh,'facecolor',[1 0 0]);
hold on; resi2=d_obs-G1*mf300; [nc,xc]=hist(resi2,110);axis([-6 8 0 1000]);bh=bar(xc,nc);set(bh,'facecolor',[1 1 0]);
xlabel('Residual (Sec)'); ylabel('Number of Rays '); title('L= 300')
subplot(3,2,3), resi1=d_obs-G1*initial_model;[nb,xb]= hist(resi1,110);axis([-6 8 0 1000]);bh=bar(xb,nb);set(bh,'facecolor',[1 0 0]);
hold on; resi2=d_obs-G1*mf400; [nc,xc]=hist(resi2,110);axis([-6 8 0 1000]);bh=bar(xc,nc);set(bh,'facecolor',[1 1 0]);
xlabel('Residual (Sec)'); ylabel('Number of Rays '); title('L= 400')
subplot(3,2,4), resi1=d_obs-G1*initial_model;[nb,xb]= hist(resi1,110);axis([-6 8 0 1000]);bh=bar(xb,nb);set(bh,'facecolor',[1 0 0]);
hold on; resi2=d_obs-G1*mf500; [nc,xc]=hist(resi2,110);axis([-6 8 0 1000]);bh=bar(xc,nc);set(bh,'facecolor',[1 1 0]);
xlabel('Residual (Sec)'); ylabel('Number of Rays '); title('L= 500')
subplot(3,2,5), resi1=d_obs-G1*initial_model;[nb,xb]= hist(resi1,110);axis([-6 8 0 1000]);bh=bar(xb,nb);set(bh,'facecolor',[1 0 0]);
hold on; resi2=d_obs-G1*mf1000; [nc,xc]=hist(resi2,110);axis([-6 8 0 1000]);bh=bar(xc,nc);set(bh,'facecolor',[1 1 0]);
xlabel('Residual (Sec)'); ylabel('Number of Rays '); title('L= 1000')
subplot(3,2,6), resi1=d_obs-G1*initial_model;[nb,xb]= hist(resi1,110);axis([-6 8 0 1000]);bh=bar(xb,nb);set(bh,'facecolor',[1 0 0]);
hold on; resi2=d_obs-G1*mf2000; [nc,xc]=hist(resi2,110);axis([-6 8 0 1000]);bh=bar(xc,nc);set(bh,'facecolor',[1 1 0]);
xlabel('Nodes'); ylabel('Number of Rays '); title('L= 2000')
```

```
p=mtit('Residual distribution of A priori model (RSTT Model) & Final Inverted
Model','fontsize',10,'color',[0 0 1],'xoff',-.01,'yoff',.029);
set(p.th,'edgecolor',.5*[1 1 1]);
print('-djpeg','-r500',' 4_16-Residuals before and after inversion')
```

% Figure 4.17 %Change Between Initial & Final model

```
figure(17)
subplot(3,2,1), diff1=((initial_model(:,1)-mf200(:,1))./initial_model(:,1)).*100;
plot(diff1);xlabel('Nodes'); ylabel('% Change '); axis([0 390 -100 100]); title('L= 200')
subplot(3,2,2), diff1=((initial_model(:,1)-mf300(:,1))./initial_model(:,1)).*100;
plot(diff1);xlabel('Nodes'); ylabel('% Change '); axis([0 390 -100 100]); title('L= 300')
subplot(3,2,3), diff1=((initial_model(:,1)-mf400(:,1))./initial_model(:,1)).*100;
plot(diff1);xlabel('Nodes'); ylabel('% Change '); axis([0 390 -100 100]); title('L= 400')
subplot(3,2,4), diff1=((initial_model(:,1)-mf500(:,1))./initial_model(:,1)).*100;
plot(diff1);xlabel('Nodes'); ylabel('% Change ');axis([0 390 -100 100]); title('L= 500')
subplot(3,2,5), diff1=((initial_model(:,1)-mf1000(:,1))./initial_model(:,1)).*100;
plot(diff1);xlabel('Nodes'); ylabel('% Change');axis([0 390 -100 100]); title('L= 1000')
subplot(3,2,6), diff1=((initial_model(:,1)-mf2000(:,1))./initial_model(:,1)).*100;
plot(diff1);xlabel('Nodes'); ylabel('% Change');axis([0 390 -100 100]); title('L= 2000')
p=mtit('Percentage change from A priori Model','fontsize',10,'color',[0 0 1],'xoff',-
.01,'yoff',.025);
set(p.th,'edgecolor',.5*[1 1 1]);
print('-djpeg','-r500',' 4_17-Change Between Initial & Final model_Mantle slowness_L_test')
```

% Figure 4.18 % Spatial distribution for Change Between Initial & Final model

```
figure(18)
diff1=((initial_model(:,1)-mf300(:,1))./initial_model(:,1)).*100
nodloc=[vel_mantle(:,1),vel_mantle(:,4),vel_mantle(:,5)];
latlim=[50 70]; longlim=[-8 40]; worldmap (latlim, longlim);
land=shaperead('landareas','UseGeocoords',true); setm(gca,'ffacecolor');
geoshow(land,'facecolor','w');hold on
y_h=nodloc(:,2); x_h=nodloc(:,3); z_h=diff1(1:394,:); x_hres = 500; y_hres = 500;cm_h =
'default';x_hmin = min(x_h); y_hmin = min(y_h);
x_hmax = max(x_h); y_hmax = max(y_h); x_hi = linspace(x_hmin, x_hmax, x_hres); y_hi =
linspace(y_hmin, y_hmax, y_hres);
rotate3d off; [XI_h, YI_h] = meshgrid(x_hi, y_hi); ZI_h = griddata(x_h, y_h, z_h, XI_h,
YI_h, 'cubic');surfacem(YI_h,XI_h,ZI_h);
cmap=flipud(colormap('jet'));colormap(cmap); h = colorbar; ylabel(h,'[% Change ]');
title('Percentage change from A priori Model')
print('-djpeg','-r500',' 4_18-Percentage change from A priori Modell')
```

% 4.21 Residual before and after inversion

```
figure(19)
resi=d_obs-G1*initial_model; plot(resi,'r')
axis([0 16500 -15 10]);xlabel('Ray Number'); ylabel('Residuals (sec)');hold on
resf=d_obs-G1*mf300; plot(resf,'b'); title('Residual before(Red), Residuals After inversion
(Blue)')
```

```
legend1 = legend('Resudals for A priori model (RMS= 28.69)', 'Residuals for Final Inverted
model (RMS=15.13)')
set(legend1,'Position',[0.429389880952376 0.163743923153517 0.208125
0.0387453874538745]);
print('-djpeg','-r500',' 4_21- Residuals after M2')
```

% 4.22 Histogram before and after inversion

```
figure(20)
resi1=d_obs-G1*initial_model;[nb,xb]= hist(resi1,100);axis([-10 10 0
1300]);bh=bar(xb,nb);set(bh,'facecolor',[1 0 0]);hold on;
resi2=d_obs-G1*mf300; [nc,xc]=hist(resi2,100);axis([-10 10 0
1200]);bh=bar(xc,nc);set(bh,'facecolor',[1 1 0]);
ylabel('Number of Rays');xlabel('Residuals'); title('Residuals Distribution')
legend1 = legend('A priori model (RMS= 28.69)', 'Final Inverted model (RMS=15.13)')
set(legend1,'Position',[0.131324041811841 0.820481630452313 0.453571428571428
0.1],'FontSize',7);
print('-djpeg','-r500',' 4_22-Residuals before and after inversion (M2)')
```

% Plot of Resolution Matix

```
figure(21)
subplot(3,3,1),plot(R(1,1:400),'Color',[0 0 0]);xlabel('Node Number','FontSize',
7);ylabel('Resolution  value ','FontSize', 7);   title('Mantle Slowness','FontSize', 7)
subplot(3,3,2),plot(R(1,401:788),'Color',[0 0 0]); xlabel('Node Number','FontSize',
7);ylabel('Resolution  value ','FontSize', 7); title('Mantle Gradient','FontSize', 7)
subplot(3,3,3),plot(R(395,788:1165),'Color',[0 0 0]);xlabel('Node Number','FontSize',
7);ylabel('Resolution  value ','FontSize', 7); title('Crustal Modifier','FontSize', 7)
subplot(3,3,4),plot(R(450,1:394),'Color',[0 0 0]);;xlabel('Node Number','FontSize',
7);ylabel('Resolution  value ','FontSize', 7);   title('Mantle Slowness','FontSize', 7)
subplot(3,3,5),plot(R(450,395:788),'Color',[0 0 0]);xlabel('Node Number','FontSize',
7);ylabel('Resolution  value ','FontSize', 7); title('Mantle Gradient','FontSize', 7)
subplot(3,3,6),plot(R(450,788:1165),'Color',[0 0 0]);xlabel('Node Number','FontSize',
7);ylabel('Resolution  value ','FontSize', 7); title('Crustal Modifier','FontSize', 7)
subplot(3,3,7),plot(R(1010,1:394),'Color',[0 0 0]);xlabel('Node Number','FontSize',
7);ylabel('Resolution  value ','FontSize', 7);   title('Mantle Slowness','FontSize', 7)
subplot(3,3,8),plot(R(1010,395:788),'Color',[0 0 0]);xlabel('Node Number','FontSize',
7);ylabel('Resolution  value ','FontSize', 7); title('Mantle Gradient','FontSize', 7)
subplot(3,3,9),plot(R(1010,788:1165),'Color',[0 0 0]);xlabel('Node Number','FontSize',
7);ylabel('Resolution  value ','FontSize', 7); title('Crustal Modifier','FontSize', 7)
p=mtit('Plot of Randomly Selected Rows of Resolution Matrix','fontsize',10,'color',[0 0
0],'xoff',-.01,'yoff',.029);
set(p.th,'edgecolor',.5*[1 1 1]);
print('-djpeg','-r500',' 4_23-Plot of Resolution Matix')
```

% Plot of posteriori covariance matrix

```
figure(22)
subplot(3,1,1),plot(post_error_bar(1:394,1),'Color',[0 0 0]);xlabel('Node Number');
ylabel('Post Cov value ');  title('Mantle Slowness')
```

```
subplot(3,1,2),plot(post_error_bar(395:788,1),'Color',[0 0 0]);xlabel('Node Number');
ylabel('Post Cov value ');  title('Mantle Gradient')
subplot(3,1,3),plot(post_error_bar(788:1165,1),'Color',[0 0 0]);xlabel('Node Number');
ylabel('Post Cov value ');  title('Crustal Modifier');axis([0 400 0 0.0001])
p=mtit('Plot of Posterior Covariance matrix ','fontsize',10,'color',[0 0 0],'xoff',-
.01,'yoff',.029);
set(p.th,'edgecolor',.5*[1 1 1]);
 print('-djpeg','-r500',' 4_24-Plot of Posterior Covariance matrixx')

% Spatial distribution for posteriori covariance matrix
figure(23)
nodloc=[vel_mantle(:,1),vel_mantle(:,4),vel_mantle(:,5)];
latlim=[50 70]; longlim=[-8 40]; worldmap (latlim, longlim);
land=shaperead('landareas','UseGeocoords',true); setm(gca,'ffacecolor');
geoshow(land,'facecolor','w');hold on
y_h=nodloc(:,2); x_h=nodloc(:,3); z_h=post_error_bar(1:394,:); x_hres = 500; y_hres =
500;cm_h = 'default';x_hmin = min(x_h); y_hmin = min(y_h);
x_hmax = max(x_h); y_hmax = max(y_h); x_hi = linspace(x_hmin, x_hmax, x_hres); y_hi =
linspace(y_hmin, y_hmax, y_hres);
rotate3d off; [XI_h, YI_h] = meshgrid(x_hi, y_hi); ZI_h = griddata(x_h, y_h, z_h, XI_h,
YI_h, 'cubic');surfacem(YI_h,XI_h,ZI_h);
cmap=flipud(colormap('jet'));colormap(cmap); h = colorbar; ylabel(h,'[Sq-root of diagonal of
Posterior Covariance ]');
title('Sq-root of diagonal of Posterior Covariance')
print('-djpeg','-r500',' 4_25-Spatial distribution of Sq-root of diagonal of Posterior
Covariance')

%% ---------------------------------CheckerBoard Test------------------------------------ %%
%Figure 4.26 CheckBoard Test-  True model
figure(24)
nodloc=[vel_mantle(:,1),vel_mantle(:,4),vel_mantle(:,5)];
latlim=[45 72]; longlim=[-15 40]; worldmap (latlim, longlim);
land=shaperead('landareas','UseGeocoords',true); setm(gca,'ffacecolor');
geoshow(land,'facecolor','w');hold on
y_h=nodloc(:,2); x_h=nodloc(:,3); z_h=1./initial_model_cb (1:394,:); x_hres = 500; y_hres =
500;cm_h = 'default';x_hmin = min(x_h); y_hmin = min(y_h);
x_hmax = max(x_h); y_hmax = max(y_h); x_hi = linspace(x_hmin, x_hmax, x_hres); y_hi =
linspace(y_hmin, y_hmax, y_hres);
rotate3d off; [XI_h, YI_h] = meshgrid(x_hi, y_hi); ZI_h = griddata(x_h, y_h, z_h, XI_h,
YI_h, 'cubic');surfacem(YI_h,XI_h,ZI_h);
cmap=flipud(colormap('jet'));colormap(cmap); h = colorbar; ylabel(h,'[velocity (km/s)]');
set(gca, 'CLim', [7.0, 8.2]);
title('True checkerboard Model')
print('-djpeg','-r500',' 4_26-CheckBoard Test-  True model')

% Figure 4.27 CheckBoard Test-  a priori model
figure(25)
```

```
latlim=[45 72]; longlim=[-15 40]; worldmap (latlim, longlim);
land=shaperead('landareas','UseGeocoords',true); setm(gca,'ffacecolor');
geoshow(land,'facecolor','w');hold on
y_h=nodloc(:,2); x_h=nodloc(:,3); z_h=(1./test(1:imk,1)); x_hres = 500; y_hres = 500;cm_h
= 'default'; x_hmin = min(x_h); y_hmin = min(y_h);
x_hmax = max(x_h); y_hmax = max(y_h); x_hi = linspace(x_hmin, x_hmax, x_hres); y_hi =
linspace(y_hmin, y_hmax, y_hres);
rotate3d off; [XI_h, YI_h] = meshgrid(x_hi, y_hi); ZI_h = griddata(x_h, y_h, z_h, XI_h,
YI_h, 'cubic'); surfacem(YI_h,XI_h,ZI_h);
cmap=flipud(colormap('jet')); colormap(cmap); h = colorbar; ylabel(h,'[velocity (km/s)]');
set(gca, 'CLim', [7.0, 8.2]);
title('A priori Model for checkerboard inversion')
print('-djpeg','-r500',' 4_27-CheckerBoard Test-a priori model')

% Figure 4.28 CheckBoard Test-  starting model
figure(26)
latlim=[45 72]; longlim=[-15 40]; worldmap (latlim, longlim);
land=shaperead('landareas','UseGeocoords',true); setm(gca,'ffacecolor');
geoshow(land,'facecolor','w');hold on
y_h=nodloc(:,2); x_h=nodloc(:,3); z_h=1./initial_model(1:394,:); x_hres = 500; y_hres =
500;cm_h = 'default'; x_hmin = min(x_h); y_hmin = min(y_h); % Axes Limits
x_hmax = max(x_h); y_hmax = max(y_h); x_hi = linspace(x_hmin, x_hmax, x_hres); y_hi =
linspace(y_hmin, y_hmax, y_hres);
rotate3d off; [XI_h, YI_h] = meshgrid(x_hi, y_hi); ZI_h = griddata(x_h, y_h, z_h, XI_h,
YI_h, 'cubic');surfacem(YI_h,XI_h,ZI_h);
cmap=flipud(colormap('jet')); colormap(cmap); h = colorbar; ylabel(h,'[velocity (km/s)]');
set(gca, 'CLim', [7.0, 8.2]);
title('Starting Model of checkerboard Test')
print('-djpeg','-r500',' 4_28-CheckBoard Test-Starting model')

% Figure 4.29 CheckBoard Test-Final Inverted Model
figure(27)
latlim=[45 72]; longlim=[-15 40]; worldmap (latlim, longlim);
land=shaperead('landareas','UseGeocoords',true); setm(gca,'ffacecolor');
geoshow(land,'facecolor','w');hold on
y_h=nodloc(:,2); x_h=nodloc(:,3); z_h=1./final_model_checkerboard(1:size(y_h));
x_hres = 500; y_hres = 500;cm_h = 'default'; x_hmin = min(x_h); y_hmin = min(y_h);
x_hmax = max(x_h); y_hmax = max(y_h); x_hi = linspace(x_hmin, x_hmax, x_hres); y_hi =
linspace(y_hmin, y_hmax, y_hres);
rotate3d off; [XI_h, YI_h] = meshgrid(x_hi, y_hi); ZI_h = griddata(x_h, y_h, z_h, XI_h,
YI_h, 'cubic'); surfacem(YI_h,XI_h,ZI_h);
cmap=flipud(colormap('jet')); colormap(cmap); h = colorbar; ylabel(h,'[velocity (km/s)]');
set(gca, 'CLim', [7.0, 8.2]);
title('Inverted Checkerboard Model-Mantle Slowness')
print('-djpeg','-r500',' 4_29-CheckBoard Test-Final model')

%% ----------------------------------Inversion Results---------------------------------- %%
% Figure 5.1 Inversion Resutls - Final model-mantle slowness
```

```
figure(28)
nodloc=[vel_mantle(:,1),vel_mantle(:,4),vel_mantle(:,5)];% Node Locations
velocity_mantle=(1./mf300(1:imk,1));% mantle velocity
latlim=[50 70]; longlim=[-5 30]; worldmap (latlim, longlim);
land=shaperead('landareas','UseGeocoords',true); setm(gca,'ffacecolor');
geoshow(land,'facecolor','w');hold on
y_h=nodloc(1:imk,2); x_h=nodloc(1:imk,3); z_h=velocity_mantle; x_hres = 500; y_hres =
500;cm_h = 'default';
x_hmin = min(x_h); y_hmin = min(y_h); x_hmax = max(x_h); y_hmax = max(y_h); x_hi =
linspace(x_hmin, x_hmax, x_hres); y_hi = linspace(y_hmin, y_hmax, y_hres);
rotate3d off; [XI_h, YI_h] = meshgrid(x_hi, y_hi); ZI_h = griddata(x_h, y_h, z_h, XI_h,
YI_h, 'cubic');
surfacem(YI_h,XI_h,ZI_h); cmap=flipud(colormap('jet')); colormap(cmap);h = colorbar;
ylabel(h,'[velocity (km/s)]');set(gca, 'CLim', [7.2, 8.6]);
title('Final Model- After inversion L=300 km')
print('-djpeg','-r500',' 5_1-Inversion Resutls - Final model-mantle slowness L=300km')
```

% Figure 5.3(c) Inversion Resutls - Final model-mantle slowness (L=2000 km)

```
figure(29)
nodloc=[vel_mantle(:,1),vel_mantle(:,4),vel_mantle(:,5)];% Node Locations
velocity_mantle=(1./mf2000(1:imk,1));% mantle velocity
latlim=[50 70]; longlim=[-5 30]; worldmap (latlim, longlim);
land=shaperead('landareas','UseGeocoords',true); setm(gca,'ffacecolor');
geoshow(land,'facecolor','w');hold on
y_h=nodloc(1:imk,2); x_h=nodloc(1:imk,3); z_h=velocity_mantle; x_hres = 500; y_hres =
500;cm_h = 'default';
x_hmin = min(x_h); y_hmin = min(y_h); x_hmax = max(x_h); y_hmax = max(y_h); x_hi =
linspace(x_hmin, x_hmax, x_hres); y_hi = linspace(y_hmin, y_hmax, y_hres);
rotate3d off; [XI_h, YI_h] = meshgrid(x_hi, y_hi); ZI_h = griddata(x_h, y_h, z_h, XI_h,
YI_h, 'cubic');
surfacem(YI_h,XI_h,ZI_h); cmap=flipud(colormap('jet')); colormap(cmap);h = colorbar;
ylabel(h,'[velocity (km/s)]');set(gca, 'CLim', [7.2, 8.6]);
title('Final Model- After inversion L =2000')
print('-djpeg','-r500',' 5_3(c)-Inversion Resutls - Final model-mantle slowness L0 2000')
```

% Figure 5.5 Inversion Resutls - Final model- velcity gradient

```
figure(30)
gradient_c_sqr=mf300(imk+1:imk+imm,1); % Velocity gradient 'c' of final model
gradiant=(((abs(gradient_c_sqr)).^(0.5))./8.04)-(1.58e-4);% Real Gradient
latlim=[50 70]; longlim=[-5 30] ; worldmap (latlim, longlim);
land=shaperead('landareas','UseGeocoords',true); setm(gca,'ffacecolor');
geoshow(land,'facecolor','w');hold on
y_h=nodloc(1:imk,2); x_h=nodloc(1:imk,3); z_h=gradiant; x_hres = 500; y_hres =
500;cm_h = 'default'; x_hmin = min(x_h); y_hmin = min(y_h);
x_hmax = max(x_h); y_hmax = max(y_h); x_hi = linspace(x_hmin, x_hmax, x_hres); y_hi =
linspace(y_hmin, y_hmax, y_hres);
rotate3d off; [XI_h, YI_h] = meshgrid(x_hi, y_hi); ZI_h = griddata(x_h, y_h, z_h, XI_h,
YI_h, 'cubic');
```

```
surfacem(YI_h,XI_h,ZI_h);cmap=flipud(colormap('jet')); colormap(cmap); h = colorbar;
ylabel(h,'[velocity Gradient (km/s/km)]');%set(gca, 'CLim', [-0.0006, 0.0042]);
title('Mantle Gradient After inversion L=300 km')
print('-djpeg','-r500',' 5_5-Inversion Resutls - Final model- velcity gradient L=300 km')

% Figure 5.6 Inversion Resutls - Final model- Crustal correction
figure(31)
crustal_correction= (mf300(imk+imm+1:imk+imm+imo,1))*10;% Real crustal modifier
latlim=[50 70]; longlim=[-5 30]; worldmap (latlim, longlim);
land=shaperead('landareas','UseGeocoords',true); setm(gca,'ffacecolor');
geoshow(land,'facecolor','w');hold on
y_h=vel_crust(:,2); x_h=vel_crust(:,3); z_h=crustal_correction;
x_hres = 500; y_hres = 500;cm_h = 'default'; x_hmin = min(x_h); y_hmin = min(y_h);
x_hmax = max(x_h); y_hmax = max(y_h); x_hi = linspace(x_hmin, x_hmax, x_hres); y_hi =
linspace(y_hmin, y_hmax, y_hres);
rotate3d off;[XI_h, YI_h] = meshgrid(x_hi, y_hi); ZI_h = griddata(x_h, y_h, z_h, XI_h,
YI_h, 'cubic');
surfacem(YI_h,XI_h,ZI_h); cmap=flipud(colormap('jet')); colormap(cmap);h = colorbar;
ylabel(h,'[Crustal modifier]');
title('Crustal Modifier- After inversion L=300 km')
print('-djpeg','-r500',' 5_6-Inversion Resutls - Final model- Crustal correction L=300')
```

Appendix B

Results of tests for a priori model standard deviation

Model	M 1	M 2	M 3	M 4	M 5	M 6	M 7
Sigma 1(for Mantle slowness)	1e-2	1e-1	1e-3	1e-2	1e-2	1e-2	1e-2
Sigma 2 (for Normalize velocity gradient)	2e-4	2e-4	2e-4	2e-2	2e-5	2e-4	2e-4
Sigma 3 (for Crustal correction)	5e-5	5e-5	5e-5	5e-5	5e-5	5e-4	5e-6
RMS Residual	15.13	15.23	1.3e+3	15.12	15.17	15.56	15.45

- **Mantle velocity at moho**

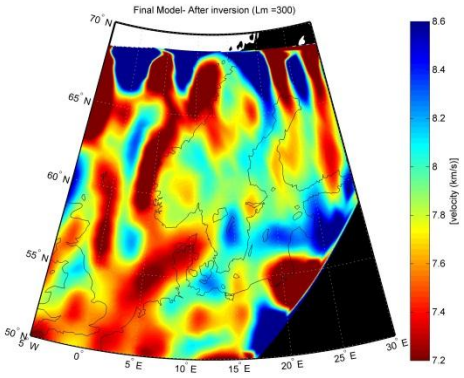

M1

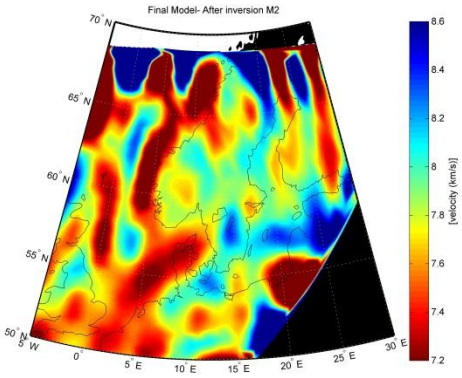

M2

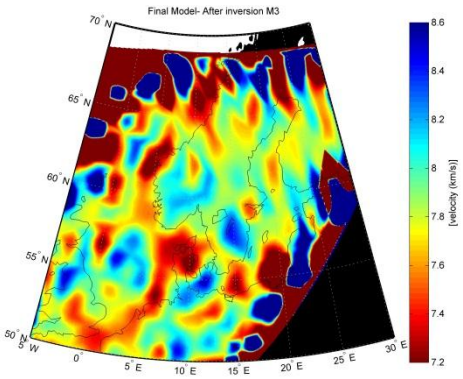

M3

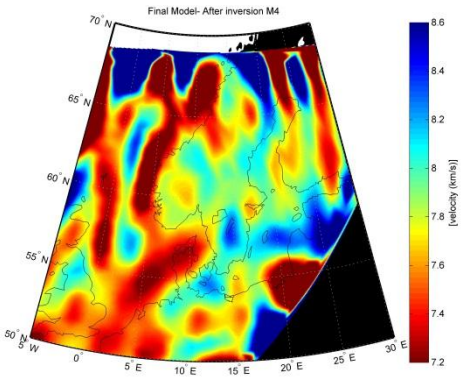

M4

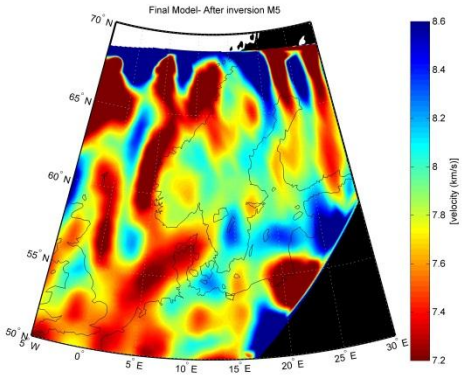

M5

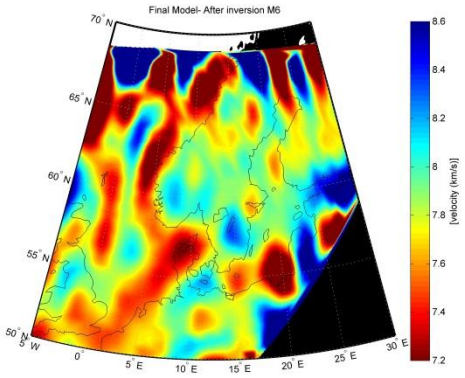

M6

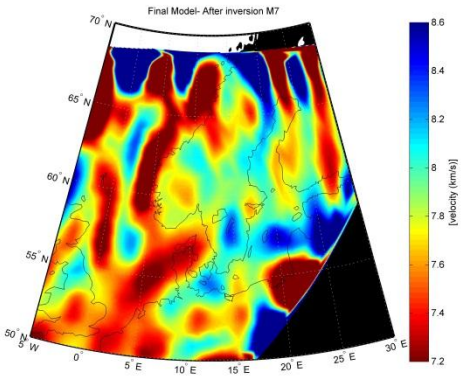

M8

- **Mantle velocity gradient below Moho**

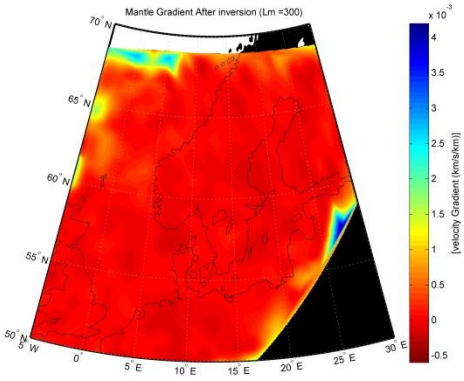

M1

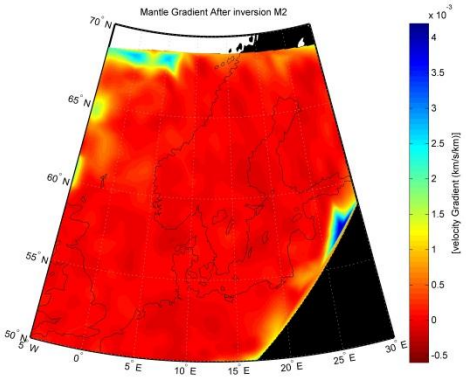

M2

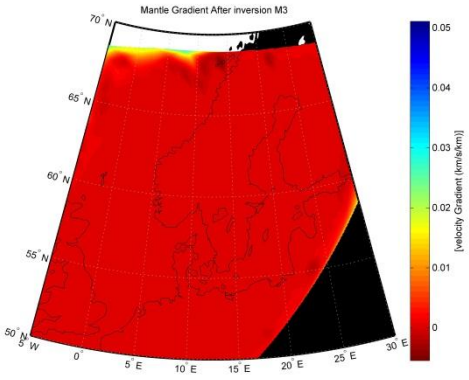
Mantle Gradient After inversion M3
[velocity Gradient (km/s/km)]

M3

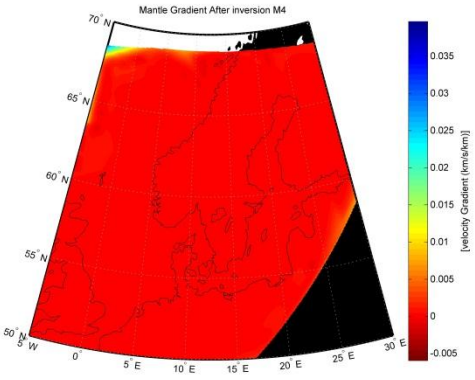
Mantle Gradient After inversion M4
[velocity Gradient (km/s/km)]

M4

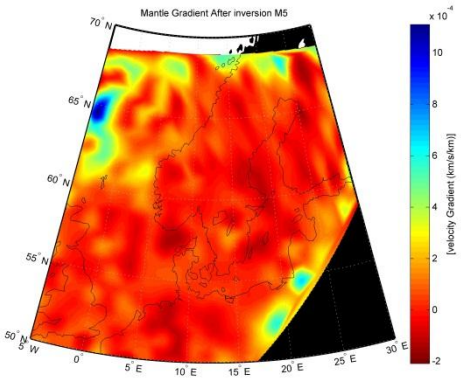
Mantle Gradient After inversion M5
[velocity Gradient (km/s/km)]

M5

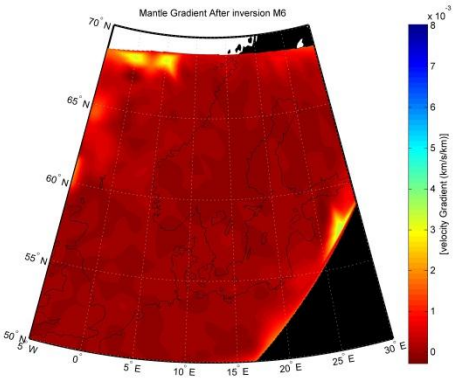
Mantle Gradient After inversion M6
[velocity Gradient (km/s/km)]

M6

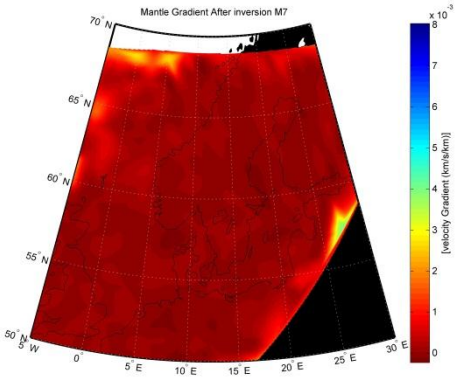
Mantle Gradient After inversion M7
[velocity Gradient (km/s/km)]

M7

- **Crustal modifier**

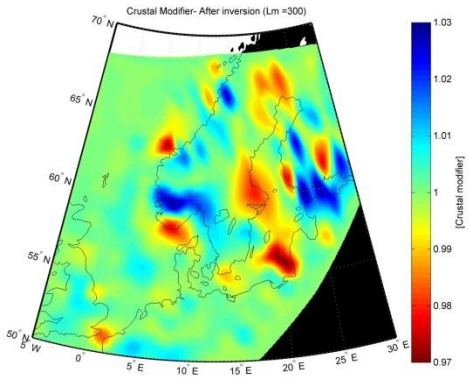

M1

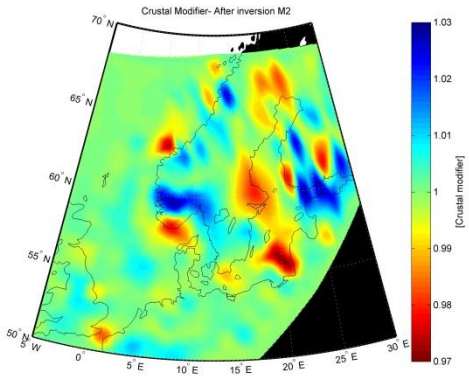

M2

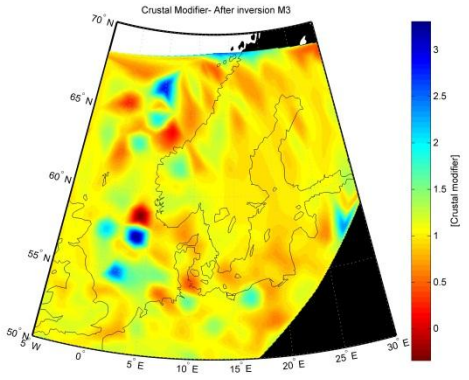

M3

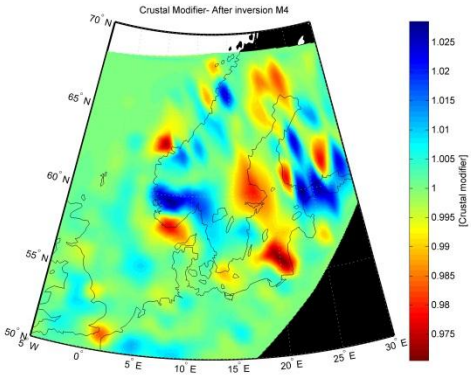

M4

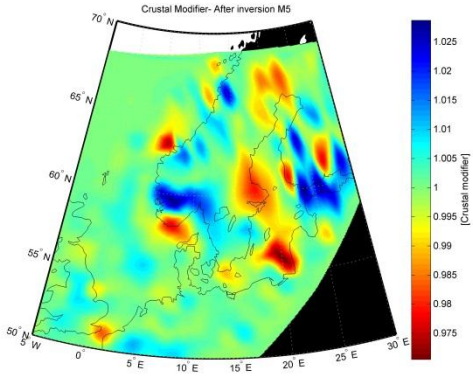

M5

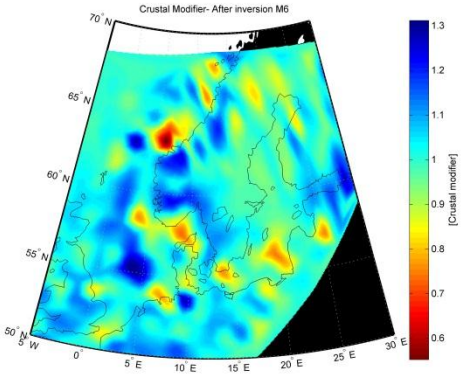

M6

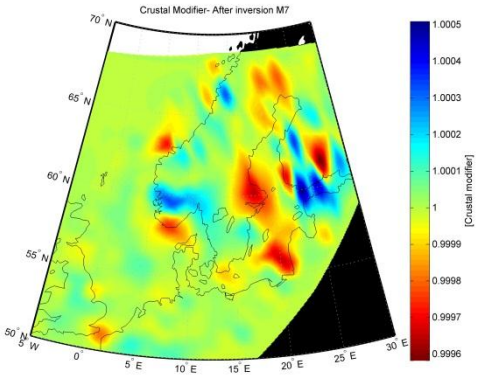

M7

- **Residuals before and after inversion**

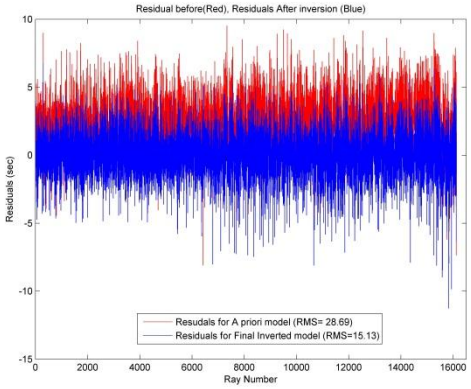

M1

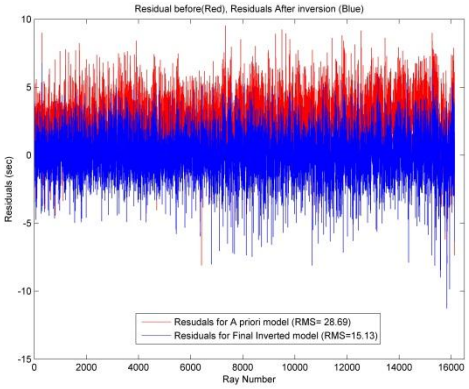

M2

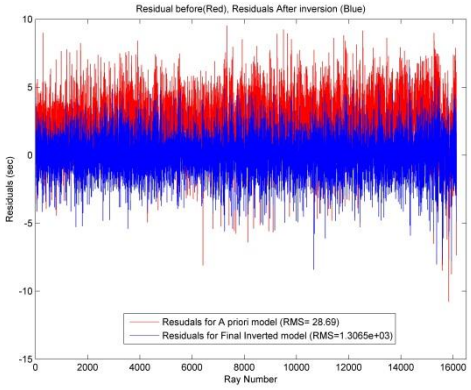

M3

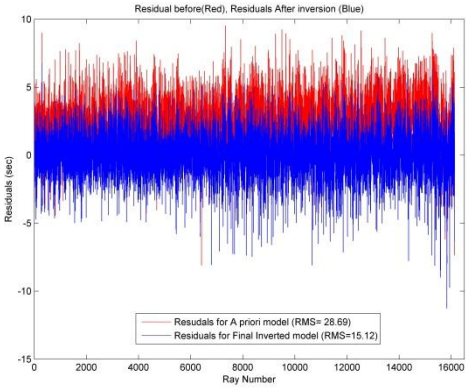

M4

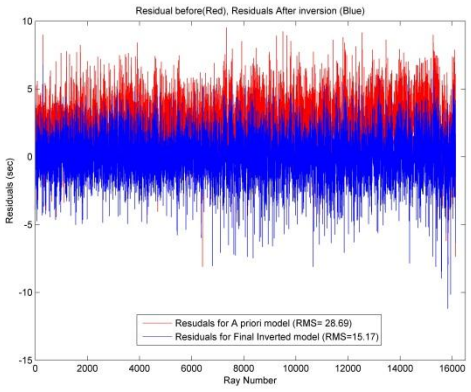

M5

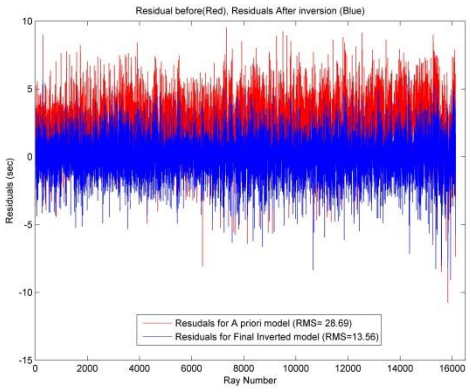

M6

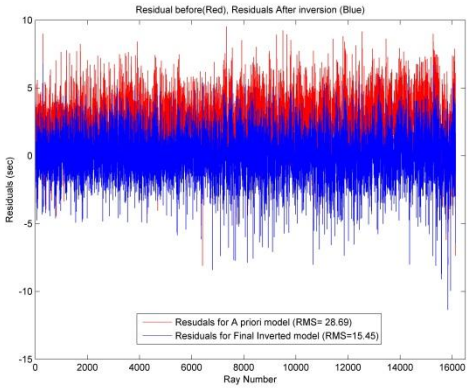

M7

- **Residual Distribution before and after inversion**

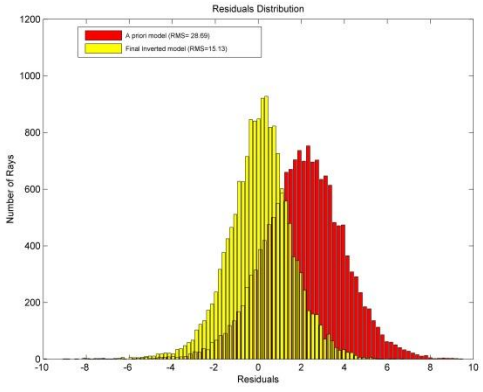

M1

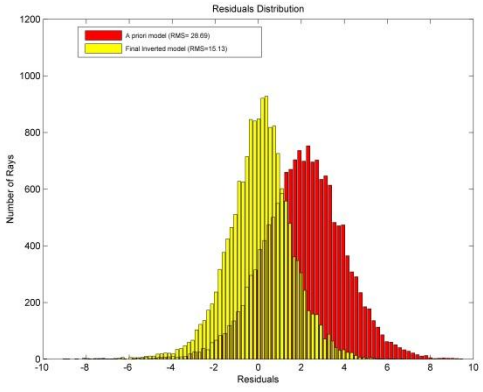

M2

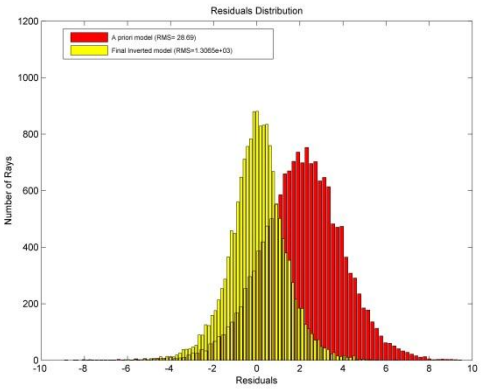
Residuals Distribution
A priori model (RMS= 28.69)
Final inverted model (RMS=1.3065e+03)
Number of Rays
Residuals

M3

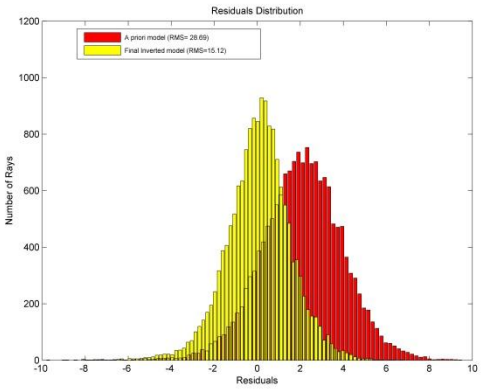
Residuals Distribution
A priori model (RMS= 28.69)
Final inverted model (RMS=15.12)
Number of Rays
Residuals

M4

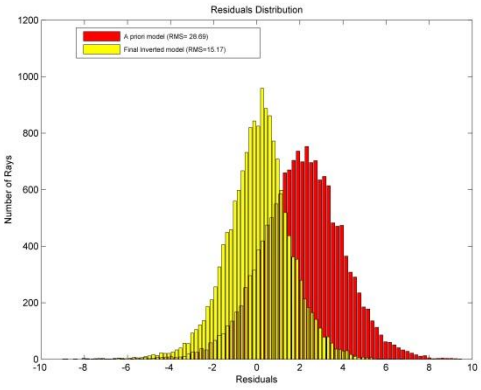
Residuals Distribution
A priori model (RMS= 28.69)
Final inverted model (RMS=15.17)
Number of Rays
Residuals

M5

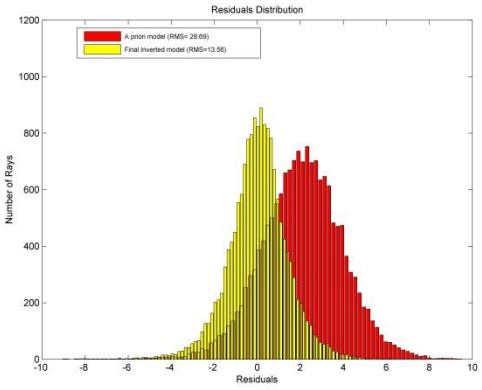
Residuals Distribution
A priori model (RMS= 28.69)
Final inverted model (RMS=13.56)
Number of Rays
Residuals

M6

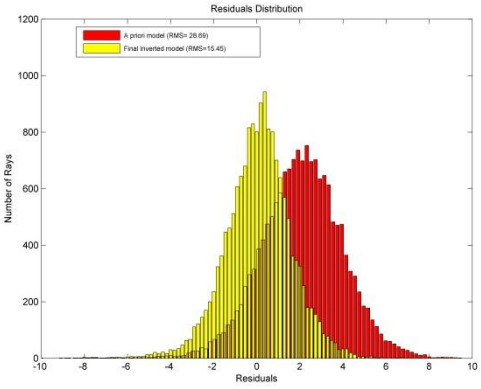
Residuals Distribution
A priori model (RMS= 28.69)
Final inverted model (RMS=15.45)
Number of Rays
Residuals

M7